Chapter 3
Geomagnetic methods

3.1 INTRODUCTION

It is thought that the Chinese first used lodestone (magnetite-rich rock) in primitive direction-finding as early as the second century BC. It was not until the twelfth century in Europe that reference was made to the use of a magnetic compass for navigation. The first scientific analysis of the Earth's magnetic field and associated phenomena was published by the English physicist William Gilbert in 1600 in his book *De Magnete*. Measurements of variations in the Earth's magnetic field were made in Sweden to locate iron ore deposits as early as 1640. In 1870, Thalén and Tiberg developed instruments to measure various components of the Earth's magnetic field accurately and quickly for routine prospecting.

In 1915, Adolf Schmidt made a balance magnetometer which enabled more widespread magnetic surveys to be undertaken. As with many geophysical methods, advances in technology were made during the Second World War which enabled more efficient, reliable and accurate measurements to be made thereafter. In the 1960s, optical absorption magnetometers were developed which provided the means for extremely rapid magnetic measurements with very high sensitivity, ideally suited to airborne magnetic surveys. Since the early 1970s, magnetic gradiometers have been used which measure not only the total Earth's magnetic field intensity but also the magnetic gradient between sensors. This provides extra information of sufficient resolution which can be invaluable in delimiting geological targets.

Geomagnetic methods can be used in a wide variety of applications (Table 3.1) and range from small-scale investigations to locate pipes and cables in the very near surface, and engineering site investigations, through to large-scale regional geological mapping to determine gross structure, such as in hydrocarbon exploration. Commonly in the larger exploration investigations, both magnetic and gravity methods are used to complement each other. Used together prior to seismic surveys, they can provide more information about the sub-surface, particularly the basement rocks, than either technique on its own. Subsequent seismic reflection surveys are then used to provide more detailed imaging of the

Table 3.1 Applications of geomagnetic surveys

Locating
■ Pipes, cables and metallic objects
■ Buried military ordnance (shells, bombs, etc.)
■ Buried metal drums of contaminated or toxic waste
■ Concealed mineshafts and adits
Mapping
■ Archaeological remains
■ Concealed basic igneous dykes
■ Metalliferous mineral lodes
■ Geological boundaries between magnetically contrasting lithologies, including faults
■ Large-scale geological structures

sub-surface, which is of more value to hydrocarbon exploration. The range of magnetic measurements which can now be made is extremely large, especially in the area of palaeomagnetism which will not be dealt with here. Palaeomagnetism is discussed in detail by Tarling (1983), for example.

3.2 BASIC CONCEPTS AND UNITS OF GEOMAGNETISM

3.2.1 Flux density, field strength and permeability

Around a bar magnet, a magnetic flux exists, as indicated by the flux lines in Figure 3.1, and converges near the ends of the magnet, which are known as the magnetic poles. If such a bar magnet is suspended in free air, the magnet will align itself with the Earth's magnetic field with one pole (the positive north-seeking) pointing towards the Earth's north pole and the other (the negative south-seeking) towards the south magnetic pole. Magnetic poles always exist in pairs of opposite sense to form a *dipole*. When one pole is sufficiently far removed from the other so that it no longer affects it, the single pole is referred to as a *monopole*.

If two magnetic poles of strength m_1 and m_2 are separated by a distance r, a force exists between them (Box 3.1). If the poles are of the same sort, the force will push the poles apart, and if they are of opposite polarity, the force is attractive and will draw the poles towards each other. Note the similarity of the form of the expression in Box 3.1 with that for the force of gravitational attraction in Box 2.1; both gravity and magnetism are *potential fields* and can be described by comparable potential field theory.

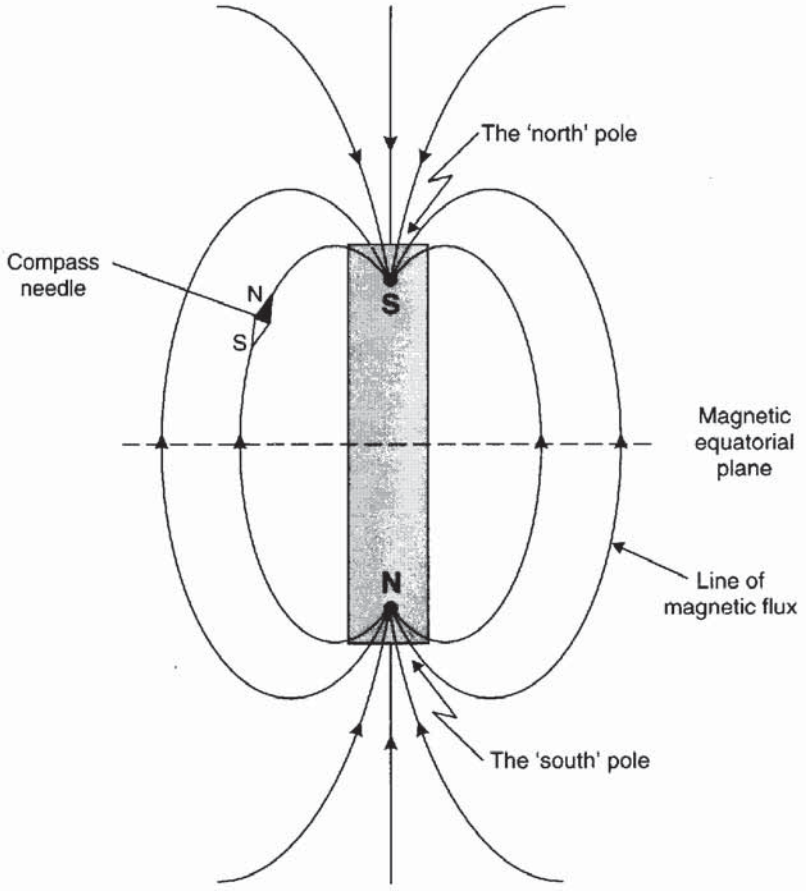

Figure 3.1 Lines of magnetic flux around a bar magnet

Box 3.1 Force between two magnetic poles

$$F = \frac{m_1 m_2}{4\pi\mu r^2}$$

where μ is the magnetic permeability of the medium separating the poles; m_1 and m_2 are pole strengths and r the distance between them.

The closeness of the flux lines shown in Figure 3.1, the flux per unit area, is the *flux density* $\boldsymbol{B}$ (and is measured in weber/m^2 = teslas). $\boldsymbol{B}$, which is also called the 'magnetic induction', is a vector quantity. (The former c.g.s. units of flux density were gauss, equivalent to 10^{-4} T.) The units of teslas are too large to be practical in geophysical work, so a sub-unit called the nanotesla (nT = 10^{-9} T) is used instead, where 1 nT is numerically equivalent to 1 gamma in c.g.s. units (1 nT is equivalent to 10^{-5} gauss).

The magnetic field can also be defined in terms of a force field which is produced by electric currents. This *magnetising field strength* $\boldsymbol{H}$ is defined, following Biot–Savart's Law, as being the field strength at the centre of a loop of wire of radius r through which a current $\boldsymbol{I}$ is flowing such that $\boldsymbol{H} = \boldsymbol{I}/2r$. Consequently the units of the magnetising field strength $\boldsymbol{H}$ are amperes per metre (A/m).

The ratio of the flux density $\boldsymbol{B}$ to the magnetising field strength $\boldsymbol{H}$ is a constant called the *absolute magnetic permeability* (μ). Practically, the magnetic permeability of water and air can be taken to be equal to the *magnetic permeability of free space* (a vacuum), denoted μ_0 which has the value $4\pi \times 10^{-7}$ Wb A^{-1} m^{-1}. For any medium other than a vacuum, the ratio of the permeabilities of a medium to that of free space is equal to the *relative permeability* μ_r, such that $\mu_r = \mu/\mu_0$ and, as it is a ratio, it has no units.

3.2.2 Susceptibility

It is possible to express the relationship between $\boldsymbol{B}$ and $\boldsymbol{H}$ in terms of a geologically diagnostic parameter, the *magnetic susceptibility* κ (see Box 3.2 and Section 3.3.1). Susceptibility is in essence a measure of how susceptible a material is to becoming magnetised. For a vacuum, $\mu_r = 1$ and $\kappa = 0$. Although susceptibility has no units, to rationalise its numerical value to be compatible with the SI or rationalised system of units, the value in c.g.s. equivalent units (e.g. unrationalised units such as e.m.u. – electromagnetic units) should be multiplied by 4π. Some materials have negative susceptibilities (see Section 3.3).

Box 3.2 Relationship between magnetic flux density $\boldsymbol{B}$, magnetising force $\boldsymbol{H}$, and susceptibility κ

Given:

$$\boldsymbol{B} = \mu \boldsymbol{H}$$

[units: μ(Wb/Am). $\boldsymbol{H}$(A/m) = Wb/m^2 = teslas]

Since $\mu = \mu_r \mu_0$:

$$\boldsymbol{B} = \mu_r \mu_0 \boldsymbol{H}.$$

Rearranging to introduce $k = \mu_r - 1$:

$$\begin{aligned} \boldsymbol{B} &= \mu_0 \boldsymbol{H} + \mu_0(\mu_r - 1)\boldsymbol{H} \\ &= \mu_0 \boldsymbol{H} + \mu_0 k \boldsymbol{H} = \mu_0 \boldsymbol{H} + \mu_0 \boldsymbol{J}. \end{aligned}$$

Hence:

$$\boldsymbol{B} = \mu_0 \boldsymbol{H}(1 + k) \quad \text{and} \quad \boldsymbol{J} = k\boldsymbol{H}.$$

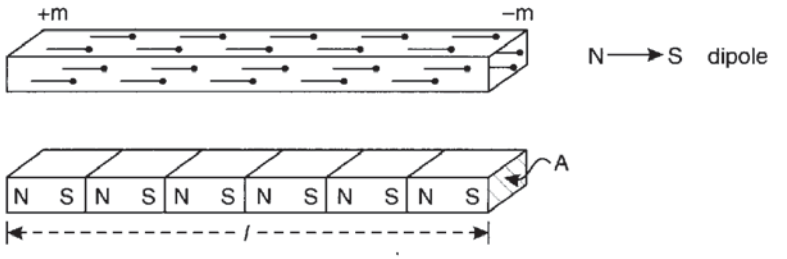

Figure 3.2 Schematic of a uniformly magnetised bar magnet as a collection of aligned dipoles producing a pole strength of $\pm \boldsymbol{m}$ and as a series of minor bar magnets

3.2.3 Intensity of magnetisation

From the last expressions given in Box 3.2, it is clear that for a vacuum, $\boldsymbol{B} = \mu_0 \boldsymbol{H}$ (as $k = 0$). The penultimate expression in Box 3.2 indicates that in a medium other than a vacuum, an extra magnetising field strength of $k\boldsymbol{H}$, called the *intensity of magnetisation* $\boldsymbol{J}$, is induced by the $\boldsymbol{H}$.

Another way of visualising the intensity of magnetisation is to examine a bar magnet of length l and cross-sectional area A which is uniformly magnetised in the direction of the long axis. The bar magnet can be thought of as consisting of a series of much smaller bar magnets or dipoles all aligned parallel to the long axis of the whole bar magnet (Figure 3.2). The magnetic intensities due to all the individual north and south poles will cancel out except at the end faces of the whole magnet, thus giving the whole magnet an overall magnetisation. The surface concentration of free poles, or pole strength m per unit area, is a measure of the intensity of magnetisation $\boldsymbol{J}$ (Box 3.3). The stronger the magnetisation, the greater will be the concentration of free poles. Furthermore, if a body of volume V is

Box 3.3 Intensity of magnetisation, $\boldsymbol{J}$ (amps/metre)

$$\boldsymbol{J} = \boldsymbol{m}/A$$

where $\boldsymbol{m}$ is the pole strength (amp.metre) and A is the cross-sectional area of the bar magnet (metre^2).
In terms of the *magnetic moment*, $\boldsymbol{M}$ (amp.metre^2):

$$\boldsymbol{J} = \boldsymbol{M}/V = \boldsymbol{m}.l/V$$

where l is the length of the dipole, V is the volume of the magnetised body, and $\boldsymbol{M} = \boldsymbol{m}.l$.

The intensity of the induced magnetisation, $\boldsymbol{J}_i$ in rock with susceptibility κ, caused by the Earth's magnetic field $\boldsymbol{F}$ (tesla) in the sense of the flux density, i.e. the B-field, is given by:

$$\boldsymbol{J}_i = k.\boldsymbol{F}/\mu_0$$

where μ_0 is the permeability of free space, and $\boldsymbol{F} = \mu_0 \boldsymbol{H}$, with $\boldsymbol{H}$ being the magnetising force.

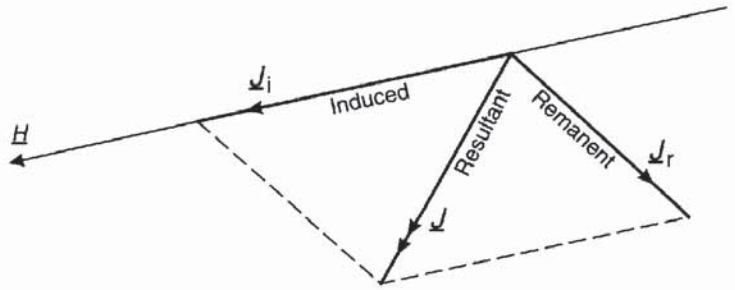

Figure 3.3 Vectorial summation of induced and remanent intensities of magnetisation

magnetised uniformly with intensity J, then that body is said to have a magnetic moment M which is defined as the product of the magnetic pole strength m and the length l separating the poles (Box 3.3). The intensity of magnetisation, which is thus the magnetic moment per unit volume, is of fundamental importance in describing the magnetic state of any rock mass.

3.2.4 Induced and remanent magnetisation

So far the discussion has centred upon a magnetisation that is induced by an applied field H where the induced intensity of magnetisation is denoted by J_i. In many cases, in the absence of an applied field (H), there is still a measurable intensity of magnetisation which is sustained by the internal field strength due to permanently magnetic particles. The intensity of this *permanent* or *remanent magnetisation* is denoted by J_r.

A rock mass containing magnetic minerals will have an induced as well as a remanent magnetisation. These magnetisations may have different directions and magnitudes of intensity (Figure 3.3). The magnitude and orientation of the resultant J dictate both the amplitude and shape of a magnetic anomaly, respectively. Consequently, interpretation of magnetic data is complicated by having greater degrees of freedom of the magnetic parameters and physical properties compared with gravity, which is largely dependent upon only rock density.

3.2.5 Diamagnetism, paramagnetism and ferromagnetism

All atoms have a magnetic moment as a result of the orbital motion of electrons around the nucleus and the spin of the electrons. According to quantum theory, two electrons can exist in the same electron shell (or state) as long as they spin in opposite directions. The magnetic moments of two such electrons, called *paired electrons*, will cancel out. In the majority of substances, when there is no external applied magnetic field, the spin magnetic moments of adjacent atoms are distributed randomly so there is no overall magnetisation. In a *diamagnetic* material, such as halite, all the electron shells are complete

and so there are no unpaired electrons. When an external magnetic field is applied, a magnetisation is induced. The electrons orbit in such a way so as to produce a magnetic field which opposes the applied field, giving rise to a weak, negative susceptibility.

Unpaired electrons in incomplete electron shells produce unbalanced spin magnetic moments and weak magnetic interactions between atoms in *paramagnetic* materials such as fayerite, amphiboles, pyroxenes, olivines, garnets and biotite. In an external applied field, the magnetic moments align themselves into the same direction, although this process is retarded by thermal agitation. The result is a weak positive susceptibility but one which decreases inversely with the absolute temperature according to the Curie–Weiss Law. Paramagnetism is generally at least an order of magnitude stronger than diamagnetism.

In *ferromagnetic* materials, the susceptibility is large but is dependent upon temperature and the strength of the applied magnetic field. The spin moments of unpaired electrons are coupled magnetically due to the very strong interaction between adjacent atoms and overlap of electron orbits. A small grain in which magnetic coupling occurs forms what is called a single *magnetic domain* and has dimensions of the order of one micron. This gives rise to a strong 'spontaneous magnetisation' which can exist even when there is no external applied field. The magnetic coupling can be such that the magnetic moments are aligned either parallel or antiparallel (Figure 3.4).

Truly ferromagnetic materials occur only rarely in nature but include substances such as cobalt, nickel and iron, all of which have parallel alignment of moments. Ferromagnetism disappears when the temperature of the material is raised above the *Curie temperature* T_C as inter-atomic magnetical coupling is severely restricted and the material thereafter exhibits paramagnetic behaviour. In *antiferromagnetic* materials, for example hematite, the moments are aligned in

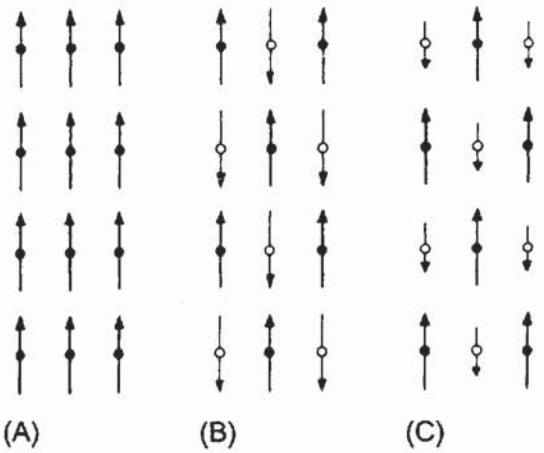

Figure 3.4 Schematic of magnetic moments in (A) ferromagnetic, (B) antiferromagnetic, and (C) ferrimagnetic crystals. After Nagata (1961), by permission

an antiparallel manner. Although the magnetic fields of the oppositely orientated dipoles cancel each other out, crystal lattice defects result in a net residual moment or *parasitic (anti)-ferromagnetism.* In ferrimagnetic materials, of which magnetite, titanomagnetite and ilmenite are prime examples, the sub-lattices are unequal and antiparallel. This results in a net magnetisation. Spontaneous magnetisation and large susceptibilities are characteristics of ferrimagnetic materials, such as in the case of pyrrhotite. Although the temperature dependence of ferrimagnetic behaviour is complex, ferrimagnetism disappears at temperatures above the Curie point. The majority of naturally occurring magnetic minerals exhibit either ferrimagnetic or imperfectly antiferromagnetic characteristics.

The Curie temperature varies with different minerals and will be different for whole rocks depending upon the composition of magnetic minerals present. In a granite rhyolite, for example, the Curie temperature for titanomagnetite is between 463 and 580°C, whereas for ilmenite–hematite series it is in the range 130–220°C. Oxidation of the iron–titanium oxides generally causes a rise in the Curie temperature. When low-temperature oxidation occurs, i.e. at temperatures lower than 300°C, in addition to increases in the Curie temperature, the intensity of magnetisation decreases. In order of increasing oxidation and decreasing intensity of magnetisation, titanomagnetite ($T_C = 100$–200°C) alters to titanomaghemite (150–450°C) then to magnetite (550–580°C) and ultimately to hematite (650–680°C) (Petersen 1990). Hematite has the lowest intensity of magnetisation. The alteration of magnetic minerals is important to remember when it comes to the interpretation of magnetic anomalies. Rocks which should display large susceptibilities and greatest intensities of magnetisation may exhibit much weaker magnetic properties owing to geochemical alteration of the magnetic minerals.

For a multidomain material in a field-free space ($\boldsymbol{H} = 0$), the spontaneous magnetisation of the magnetic domains within a crystal is related to the crystal axes (Figure 3.5). The magnetisation directions of all domains cancel each other out so there is no net magnetisation intensity ($\boldsymbol{J} = 0$). On increasing the applied magnetic field ($\boldsymbol{H}$), the domain walls can move easily and reversibly should $\boldsymbol{H}$ be reduced at this point. As $\boldsymbol{H}$ increases, so the various domains reorientate themselves parallel to the applied field, but in discrete steps called *Barkhausen jumps*, which are permanent. When there is no further increase in magnetisation intensity with increasing applied field strength, all the domains are orientated parallel to the applied field direction and the material is said to be magnetically *saturated.* On reducing $\boldsymbol{H}$ to zero following saturation, only some of the magnetic domains are able to return to their former orientation, which results in a remanent magnetisation $\boldsymbol{J}_r$.

If the magnetic permeability (μ) of a medium is independent of the magnetising force ($\boldsymbol{H}$), the material is said to be linear in its behaviour.

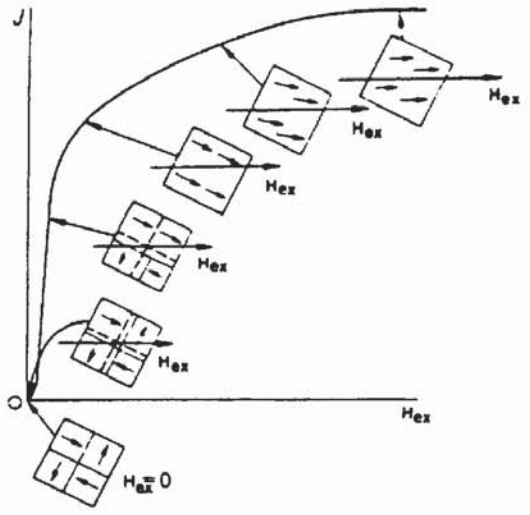

Figure 3.5 Process of magnetisation of a ferromagnetic substance according to domain theory. From Sharma (1986), by permission

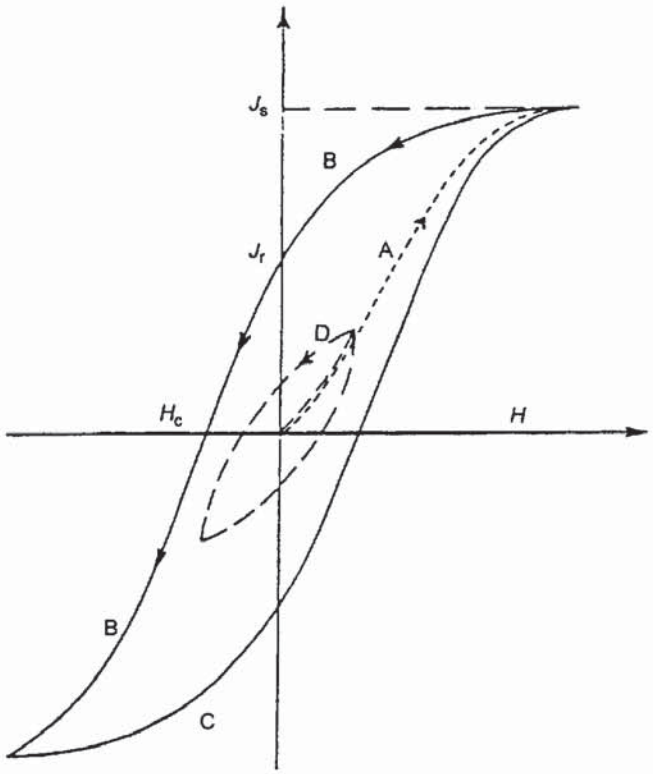

Figure 3.6 Hysteresis loop illustrating a cycle of magnetisation (curves A, B, C) of a ferromagnetic material. Small loop (D) shows the magnetisation cycle without saturation. From Sharma (1986), by permission

However, if a ferromagnetic or ferrimagnetic material, such as magnetite or pyrrhotite, with grains larger than 10 microns is placed in an increasing applied magnetic field, its magnetic intensity $\boldsymbol{J}$ increases to the point of saturation following a hysteresis loop (Figure 3.6). The physical processes by which this happens have already been described

in terms of domain theory. After reaching saturation, the applied field $\boldsymbol{H}$ is reduced to zero at which point the intensity of magnetisation is that attributed to the remanent magnetisation. To eliminate this magnetisation, a negative field, $-\boldsymbol{H}_c$, the *coercive force*, has to be applied. The *coercivity*, $\boldsymbol{H}_c$, is an indication as to the 'hardness' or permanence of the magnetisation. Consequently, larger magnetic grains, which thus contain more magnetic domains, are easier to magnetise (and therefore have a higher susceptibility), than fine grains which are magnetically hard as indicated by a relatively high coercivity and low susceptibility. On increasing the applied magnetic field to full saturation, the hysteresis loop is completed. It follows that, for minerals that exhibit a nonlinear behaviour, no unique value of susceptibility exists. Values cited for such materials are usually for weak values of $\boldsymbol{H}$ and prior to saturation ever having been reached. For much more detailed discussion of rock magnetism, see the monographs by Nagata (1961), Stacey and Banerjee (1973) and O'Reilly (1984).

3.3 MAGNETIC PROPERTIES OF ROCKS

3.3.1 Susceptibility of rocks and minerals

Magnetic susceptibility is an extremely important property of rocks and is to magnetic exploration methods what density is to gravity surveys. Rocks that have a significant concentration of ferro- and/or ferri-magnetic minerals tend to have the highest susceptibilities. Consequently, basic and ultrabasic rocks have the highest susceptibilities, acid igneous and metamorphic rocks have intermediate to low values, and sedimentary rocks have very small susceptibilities in general (Table 3.2 and Figure 3.7). In this compilation of data, specific details of rock types are not available and so the values cited should be taken only as a guide. Metamorphic rocks are dependent upon their parent material and metapsammites are likely to have different susceptibilities compared with metapelites, for example.

Whole rock susceptibilities can vary considerably owing to a number of factors in addition to mineralogical composition. Susceptibilities depend upon the alignment and shape of the magnetic grains dispersed throughout the rock. If there is a marked orientation of particles, such as in some sedimentary and metamorphic rocks, a strong physical anisotropy may exist. The variation of magnetic properties as a function of orientation and shape of mineral grains is known as the *magnetic fabric*. Magnetic fabric analysis provides a very sensitive indication as to the physical composition of a rock or sediment, which in turn can be important in interpreting physical processes affecting that rock. For example, it is possible to correlate magnetic fabric variation in estuarine sediments with sonograph

Table 3.2 Susceptibilities of rocks and minerals (rationalised SI units)

Mineral or rock type	Susceptibility*
Sedimentary	
Dolomite (pure)	−12.5 to +44
Dolomite (impure)	20000
Limestone	10 to 25000
Sandstone	0 to 21000
Shales	60 to 18600
Average for various	**0 to 360**
Metamorphic	
Schist	315 to 3000
Slate	0 to 38000
Gneiss	125 to 25000
Serpentenite	3100 to 75000
Average for various	**0 to 73000**
Igneous	
Granite	10 to 65
Granite (m)	20 to 50000
Rhyolite	250 to 37700
Pegmatite	3000 to 75000
Gabbro	800 to 76000
Basalts	500 to 182000
Oceanic basalts	300 to 36000
Peridotite	95500 to 196000
Average for acid igneous	**40 to 82000**
Average for basic igneous	**550 to 122000**
Minerals	
Ice (d)	−9
Rocksalt (d)	−10
Gypsum (d)	−13
Quartz (d)	−15
Graphite (d)	−80 to −200
Chalcopyrite	400
Pyrite (o)	50 to 5000
Hematite (o)	420 to 38000
Pyrrhotite (o)	1250 to 6.3×10^6
Ilmenite (o)	314000 to 3.8×10^6
Magnetite (o)	70000 to 2×10^7

(d) = diamagnetic material; (o) = ore; (m) = with magnetic
*$\kappa \times 10^6$ rationalised SI units; to convert to the unrationalised c.g.s. units, divide by 4π
Data from Parasnis (1986), Sharma (1986), Telford *et al.* (1990)

images of the estuary floor. In conjunction with Thematic Mapper images obtained from low-flying aircraft and simultaneous water sampling from boats, it is possible to establish a detailed model of estuarine sediment dynamic processes, as has been achieved for Plymouth Sound in south-west England (Fitzpatrick 1991). For further details of the magnetic fabric method, see the discussions by Lowrie (1990) and Tarling (1983), for example.

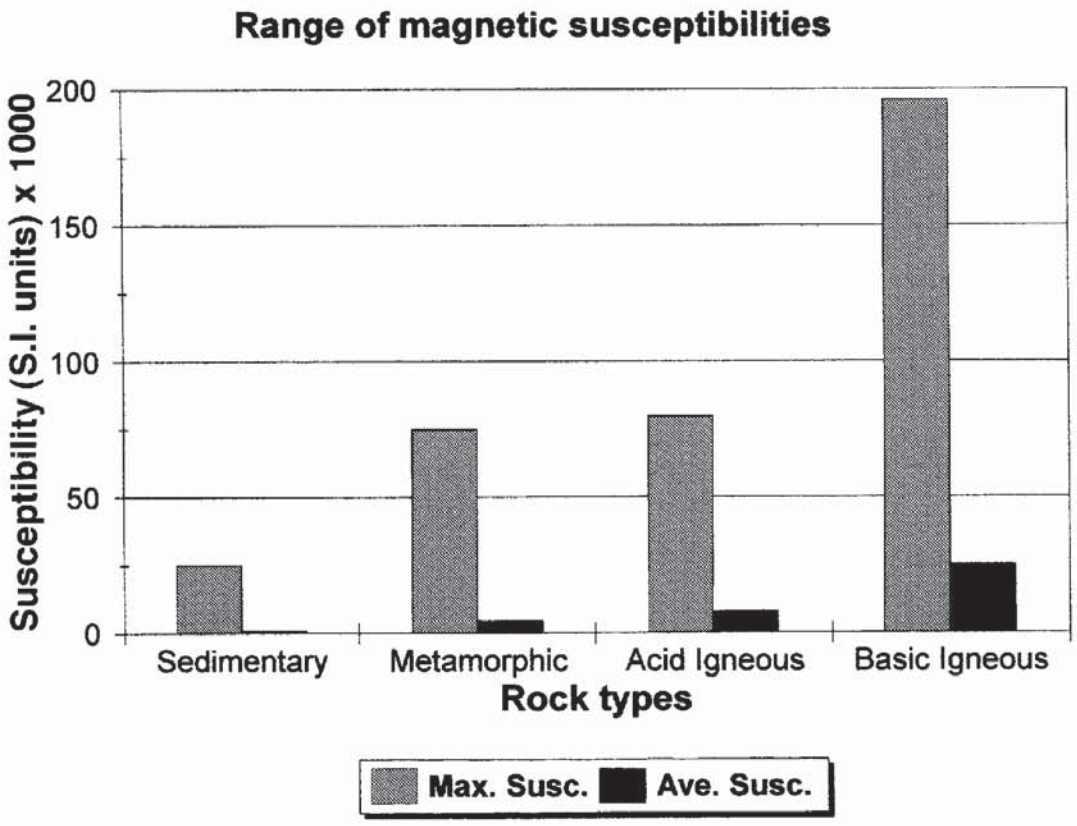

Figure 3.7 Susceptibilities of major rock types

For magnetic ore bodies with extremely high susceptibilities ($\kappa \geqslant 10^6$ SI), the measured susceptibility – more correctly referred to as the *apparent susceptibility* κ_a – can be reduced substantially by a shape demagnetisation effect (see Box 3.4). This involves a *demagnetisation factor* N_α which depends on a direction α. For a sphere, $N_\alpha = 1/3$ in all directions. In the case of a thin sheetlike body with a high true susceptibility ($\kappa \sim 10^6$ SI): $N_x \sim 1$ in the transverse direction, giving a susceptibility $\kappa_a \approx 0.5K$; and $N_\alpha \sim 0$ in the longitudinal direction, so that $\kappa_a \approx \kappa$. Demagnetisation factors are discussed further by Parasnis (1986) and Sharma (1986).

Box 3.4 Apparent susceptibility κ_a and the demagnetisation factor N_α

$$\kappa_a = \kappa/(1 + N_\alpha \kappa)$$

Susceptibilities can be measured either in the field using a hand-held susceptibility meter such as the kappameter, or on samples returned to a laboratory where they can be analysed more accurately.

3.3.2 Remanent magnetisation and Königsberger ratios

In addition to the induced magnetisation, many rocks and minerals exhibit a permanent or *natural remanent magnetisation* (NRM) of intensity J_r when the applied field H is zero. The various processes by which rocks can acquire a remanent magnetisation are listed in Table 3.3 and discussed in more detail by Merrill (1990), Sharma (1986) and Tarling (1983).

Table 3.3 Types of remanent magnetisation (RM). After Merrill (1990), by permission

Type of RM	Process
Natural (NRM)	Acquired by a rock or mineral under natural conditions
Thermal (TRM)	Acquired by a material during cooling from a temperature greater than the Curie temperature to room temperature (e.g. molten lava cooling after a volcanic eruption)
Isothermal (IRM)	Acquired over a short time (of the order of seconds) in a strong magnetic field at a constant temperature (e.g. such as by a lightning strike)
Chemical (CRM)	Also crystallisation RM; acquired at the time of nucleation and growth or crystallisation of fine magnetic grains far below the Curie point in an ambient field
Thermal–chemical (TCRM)	Acquired during chemical alteration and cooling
Detrital (DRM)	Also depositional RM; acquired by the settling out of previously magnetised particles to form ultimately consolidated sediments which then have a weak net magnetisation, but prior to any chemical alteration through diagenetic processes
Post-depositional (PDRM)	Acquired by a sediment by physical processes acting upon it after deposition (e.g. bioturbation and compaction)
Viscous VMR	Acquired after a lengthy exposure to an ambient field with all other factors being constant (e.g. chemistry and temperature)
Anhysteretic (ARM)	Acquired when a peak amplitude of an alternating magnetic field is decreased from a large value to zero in the presence of a weak but constant magnetic field

Primary remanent magnetisations are acquired by the cooling and solidification of an igneous rock from above the Curie temperature (of the constituent magnetic minerals) to normal surface temperature (TRM) or by detrital remanent magnetisation (DRM). Secondary remanent magnetisations, such as chemical, viscous or post-depositional remanent magnetisations, may be acquired later on in the rock's history. This is especially true of igneous rocks which have later undergone one or more periods of metamorphism, particularly thermal metamorphism.

The intensity of the remanent magnetisation $\boldsymbol{J}_r$ may swamp that of the induced magnetisation $\boldsymbol{J}_i$, particularly in igneous and thermally metamorphosed rocks. The ratio of the two intensities ($\boldsymbol{J}_r/\boldsymbol{J}_i$) is called the *Königsberger ratio*, Q, which can be expressed in terms of the Earth's magnetic field at a given locality and the susceptibility of the rocks (Box 3.5). Just as susceptibility can vary within a single rock type, so too can the Königsberger ratio. However, similar rock types have characteristic values of Q, some of which are listed in Table 3.4. Nagata (1961) has made four broad generalizations on the basis of Q:

- $Q \sim 1$ for slowly crystallised igneous and thermally metamorphosed rocks in continental areas;
- $Q \sim 10$ for volcanic rocks;

Table 3.4 Examples of values of the Königsberger ratio

Rock type	Location	Q
Basalt	Mihare volcano, Japan	99–118
Oceanic basalts	Northeast Pacific	15–105
Oceanic basalts	Mid-Atlantic Ridge	1–160
Sea-mount basalts	North Pacific	8–57
Cainozoic basalts	Victoria, Australia	5
Early tertiary basalts	Disko, West Greenland	1–39
Tholeiite dykes	England	0.6–1.6
Dolerite sills	North England	2–3.5
Dolerite	Sutherland, Scotland	0.48–0.51
Quartz dolerite	Whin Sill, England	2–2.9
Gabbro	Småland, Sweden	9.5
Gabbro	Minnesota, USA	1–8
Gabbro	Cuillin Hills, Scotland	29
Andesite	Taga, Japan	4.9
Granite	Madagascar	0.3–10
Granite plutons	California, USA	0.2–0.9
Granodiorite	Nevada, USA	0.1–0.2
Diabase	Astano Ticino, Switzerland	1.5
Diabase dykes	Canadian Shield	0.2–4
Magnetite ore	Sweden	1–10
Magnetite ore	South India	1–5

- $Q \sim 30$–50 for many rapidly quenched basaltic rocks;
- $Q < 1$ in sedimentary and metamorphic rocks, except when iron ore is involved.

Box 3.5 Königsberger ratio, Q

$$Q = \boldsymbol{J}_r/\kappa(\boldsymbol{F}/\mu_0)$$

where $\boldsymbol{J}_r$ is the intensity of remanent (NRM) magnetisation, κ is the susceptibility, μ_0 is the permeability of free space and $\boldsymbol{F}$ is the magnitude of the Earth's magnetic field (in tesla) at a given location in the same sense as the B-field (flux density).

It is also very important to consider that not only may $\boldsymbol{J}_r$ exceed $\boldsymbol{J}_i$, but the direction of remanent magnetisation may be quite different from that of the ambient induced field at a location. Consequently, the resultant magnetisation (i.e. the vectorial sum of the remanent and induced magnetisations) will give rise to characteristic magnetic anomalies (refer back to Figure 3.3) when reversely magnetised rocks are present.

3.4 THE EARTH'S MAGNETIC FIELD

3.4.1 Components of the Earth's magnetic field

The geomagnetic field at or near the surface of the Earth originates largely from within and around the Earth's core. Currents external to the Earth in the ionosphere and magnetosphere associated with the Van Allen radiation belts (Figure 3.8), currents induced in the Earth by external field variations and the permanent (remanent) and steady-state induced magnetisations of crustal rocks, also contribute to the overall geomagnetic field. The magnetosphere is vital for the survival of life on Earth as it forms the primary force field which protects the planet from harmful radiation from the Sun. The various components of the geomagnetic field affect exploration surveys in a variety of ways which will be discussed in turn.

3.4.1.1 The main dipole field

The main component of the geomagnetic field is called the *dipolar field* as it behaves, to a first-order approximation, like a dipolar electromagnet located at the centre of the Earth but inclined at 11.5° to the rotational axis (Figure 3.9).

The *geomagnetic poles*, the positions on the Earth's surface through which the axis of the best-fitting dipole passes – which are located in Hayes Peninsula in northern Greenland and near the Russian Vostok research station in Greater Antarctica – are not the same as the

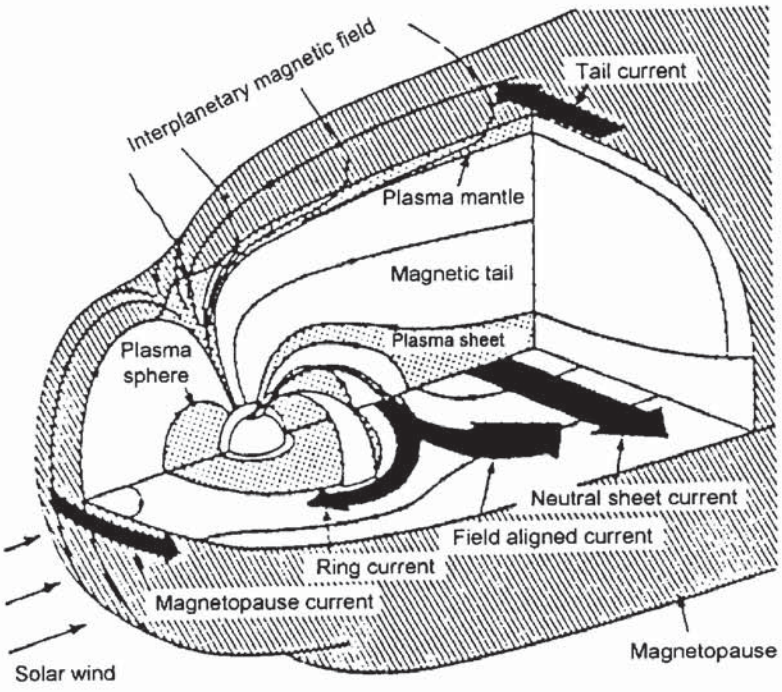

Figure 3.8 The geomagnetic field showing the magnetosphere, magnetopause and Van Allen radiation belts. From James (1990), by permission

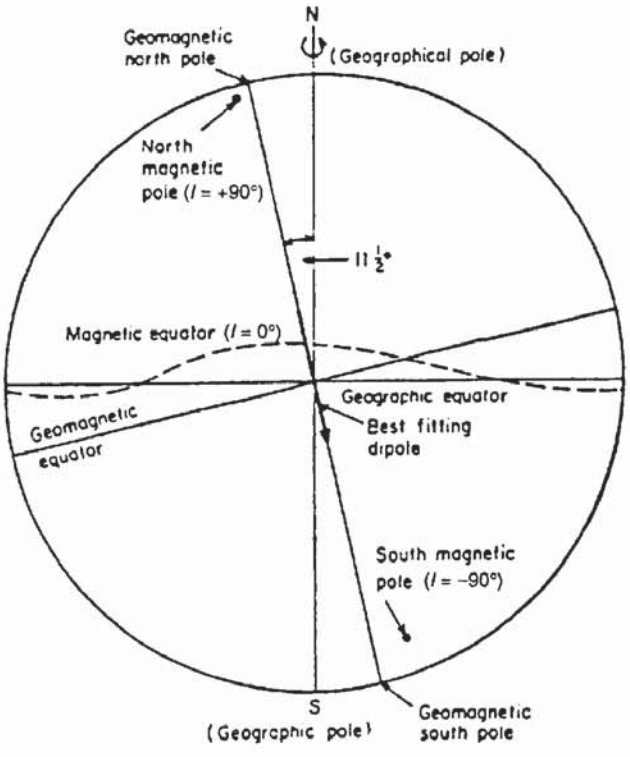

Figure 3.9 The field due to an inclined geocentric dipole. From McElhinny (1973), by permission

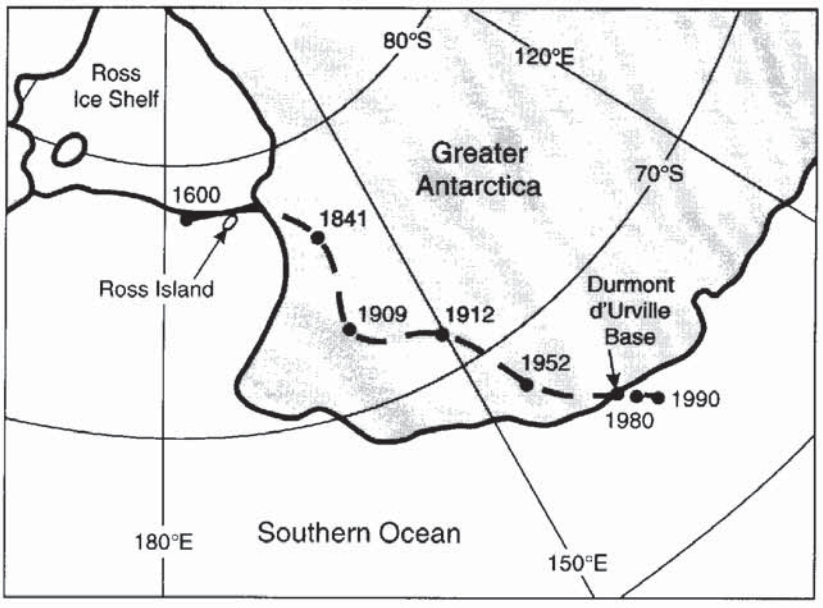

Figure 3.10 Location of the south magnetic pole and its drift since the year 1600

magnetic or *dip poles*. These are located where the magnetic field is directed vertically. The north magnetic pole is currently just north of Bathurst Island in the Canadian Arctic Archipelago and was discovered on 1 June 1831 by James Clark Ross and his uncle Sir John Ross. The south magnetic pole is currently about 150 km offshore from the French Research Station Durmont d'Urville on the Adélie Coast of Greater Antarctica. James Ross came extremely close to locating the south magnetic pole in 1841 but as it was then inland (Figure 3.10) he was thwarted by icebergs and the land ice. It was only on 15 January 1909 that Alistair Mackay, Edgeworth David and Douglas Mawson reached the south magnetic pole after an epic sledge journey from their base on Ross Island.

The geomagnetic field is produced by electric currents induced within the conductive liquid outer core as a result of slow convective movements within it (Figure 3.11). It is for this reason that the analogy of the Earth's field to that induced by an electromagnet is preferred to that of a permanently magnetised bar magnet. The liquid core behaves as a geodynamo but the precise nature of the processes involved has yet to be resolved. Models to explain the disposition of the magnetic field must also account for the slow but progressive change in field intensity and westward drift in direction known as the *secular variation*. Furthermore, the model must also explain how the Earth's magnetic field goes through reversals of magnetic polarity. The study of how the Earth's magnetic field has changed through geological time is known as *palaeomagnetism*. The use of magnetic reversals to provide global chronometric calibration of geological events is known as *magnetostratigraphy* (Tauxe, 1990).

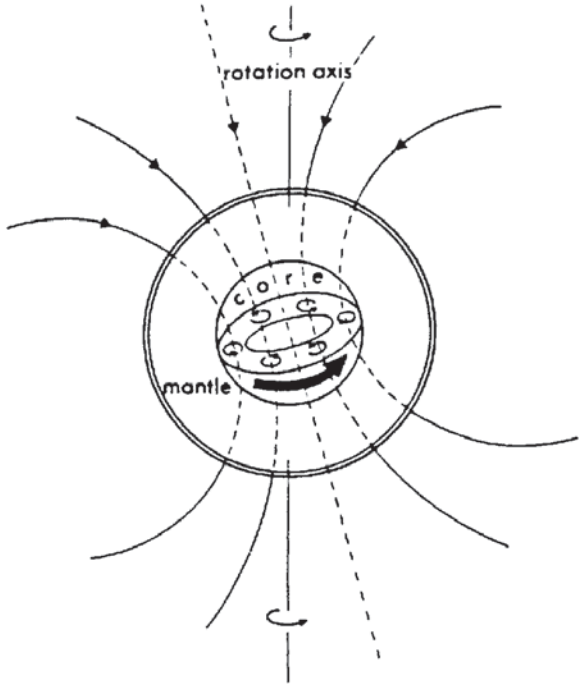

Figure 3.11 Schematic of the cause of the majority of the Earth's magnetic field. From Sharma (1986), by permission

The geomagnetic field can be described in terms of the declination, D, inclination, I, and the total force vector $\boldsymbol{F}$ (Figure 3.12). A freely suspended magnetised needle will align itself along the $\boldsymbol{F}$ vector so that at the magnetic (dip) north, the inclination is 90°; i.e. the needle will point vertically downwards. At the south magnetic (dip) pole, the needle will point vertically upwards. At the magnetic equator, the needle will lie horizontally (Figure 3.13). Furthermore, the vertical component of the magnetic intensity of the Earth's magnetic field varies with latitude, from a minimum of around 30 000 nT at the magnetic equator to 60 000 nT at the magnetic poles.

3.4.1.2 The non-dipolar field

While the single dipole field approximates to the Earth's observed magnetic field, there is a significant difference between them, which is known as the *non-dipole field*. The total intensity for the non-dipole field is shown in Figure 3.14, from which several large-scale features can be seen with dimensions of the order of several thousand kilometres and with amplitudes up to 20 000 nT, about one-third of the Earth's total field. Using the method of spherical harmonic analysis, it can be demonstrated that the non-dipole field and the associated large-scale features can be represented by a fictitious set of 8–12 small dipoles radially located close to the liquid core. These dipoles serve to simulate the eddy currents associated with the processes within the liquid core.

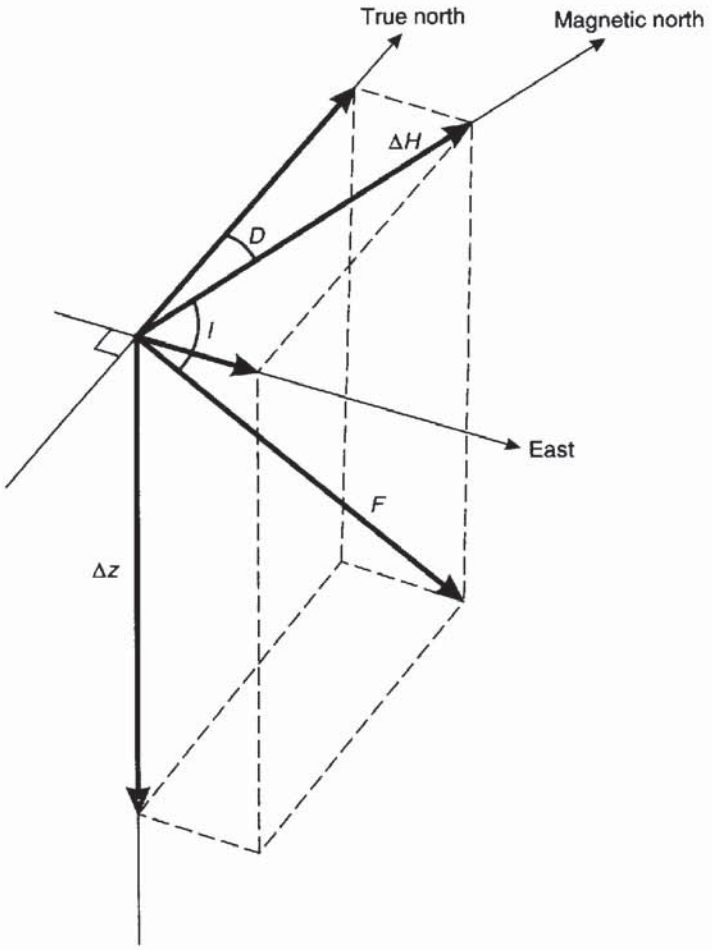

Figure 3.12 Elements of the magnetic field: inclination ***I***, declination ***D***, and total magnetic force ***F***

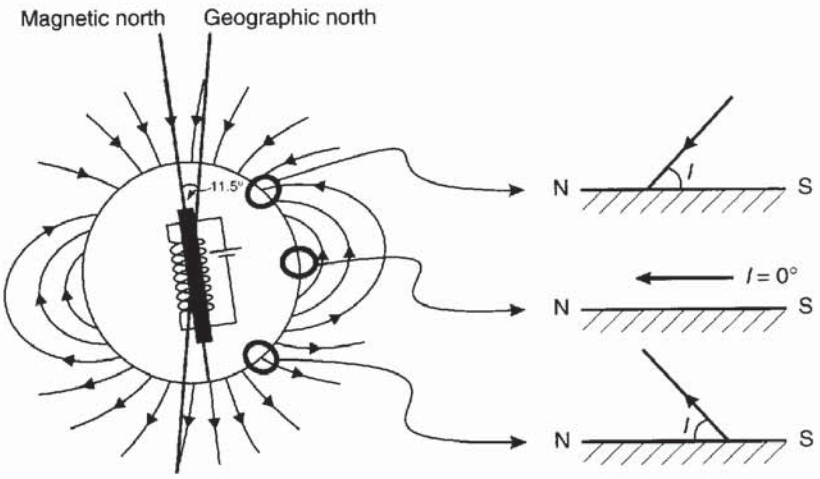

Figure 3.13 Variation of inclination with latitude

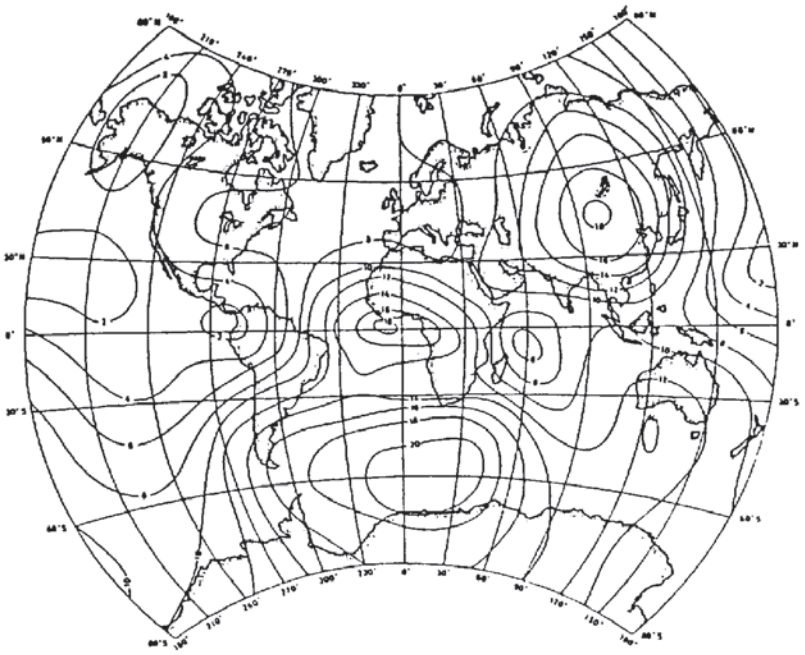

Figure 3.14 Variation in the intensity of the non-dipole field for epoch 1980. From Sharma (1986), by permission

A further use of the spherical harmonic analysis is that it provides a means whereby the spatial distribution and intensity of the total magnetic field can be calculated for the whole globe. The total field, which is calculated every five years, is called the *International Geomagnetic Reference Field* (IGRF) and the year of calculation is known as the *epoch*. It has to be recalculated regularly because of the secular variation (see, for example, IAGA (1987) and Peddie (1982)). Consequently, it is possible to obtain a theoretical value for the field strength of the Earth's magnetic field for any location on Earth (Figure 3.15). It can be seen from this figure that instead of the anticipated two maxima consistent with a truly dipolar field, there are in fact four maxima. The significance of the IGRF in processing magnetic data is discussed in Section 3.6.3.

Data used in the computation of revisions of the International Geomagnetic Reference Field have been obtained by satellite (e.g. during 1965–71, Polar Orbiting Geophysical Observatory series, POGO; October 1979 to June 1980, MAGSAT). However, at satellite orbit ranges, perturbations in the earth's magnetic field caused by magnetic materials in the crust are not resolvable. Surface or airborne measurements can detect considerable high-amplitude small-scale features within the crust down to a depth of 25–30 km where the Curie isotherm is reached. These features may be caused by induction due to the Earth's field or remanent magnetisation or a mixture of both.

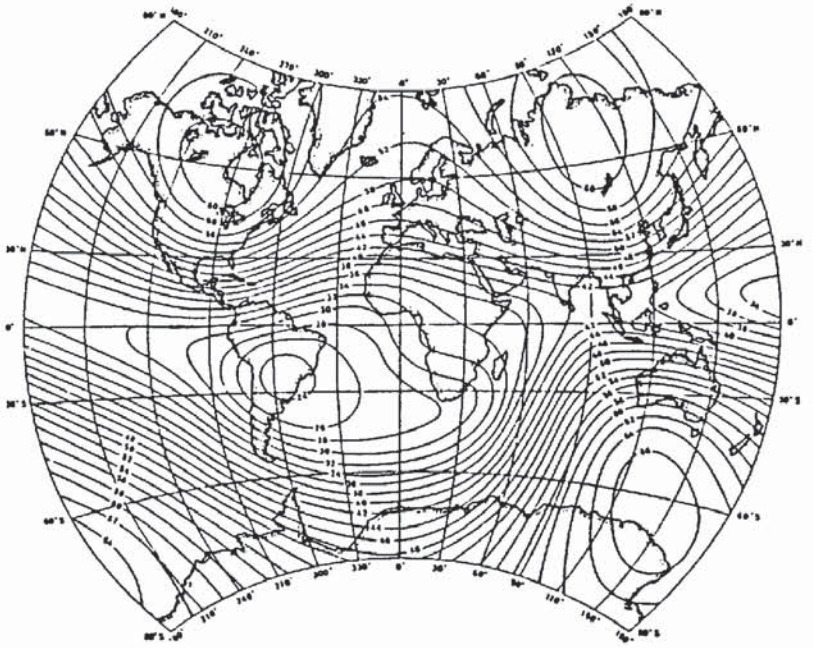

Figure 3.15 Total field intensity derived using the IGRF epoch 1980. From Sharma (1986), by permission

3.4.2 Time variable field

Observations of the Earth's magnetic field have been made for over four centuries at London and Paris. From these data, it is clear that the geomagnetic and magnetic pole positions drift with time, known as the secular variation in the magnetic field (Figure 3.16). In addition, the intensity of the main magnetic field is decreasing at about 5% per century. These rates of change, although very significant on a geological time scale, do not affect data acquisition on a typical exploration survey unless it covers large geographical areas and takes many months to complete, or if such surveys are being used to compare with historical data.

The Earth's magnetic field changes over a daily period, the *diurnal variations*. These are caused by changes in the strength and direction of currents in the ionosphere. On a magnetically 'quiet' (Q) day, the changes are smooth and are on average around 50 nT but with maximum amplitudes up to 200 nT at the geomagnetic equator. The changes are least during the night when the background is almost constant, and decrease in amplitude from dawn to midday whereupon they increase to the daily maximum about mid-late afternoon before settling down to the night-time value.

Magnetically disturbed (D) days are marked by a rapid onset of fluctuations of the order of hundreds of nanoteslas followed by slower but still erratic fluctuations with decreasing amplitude. These

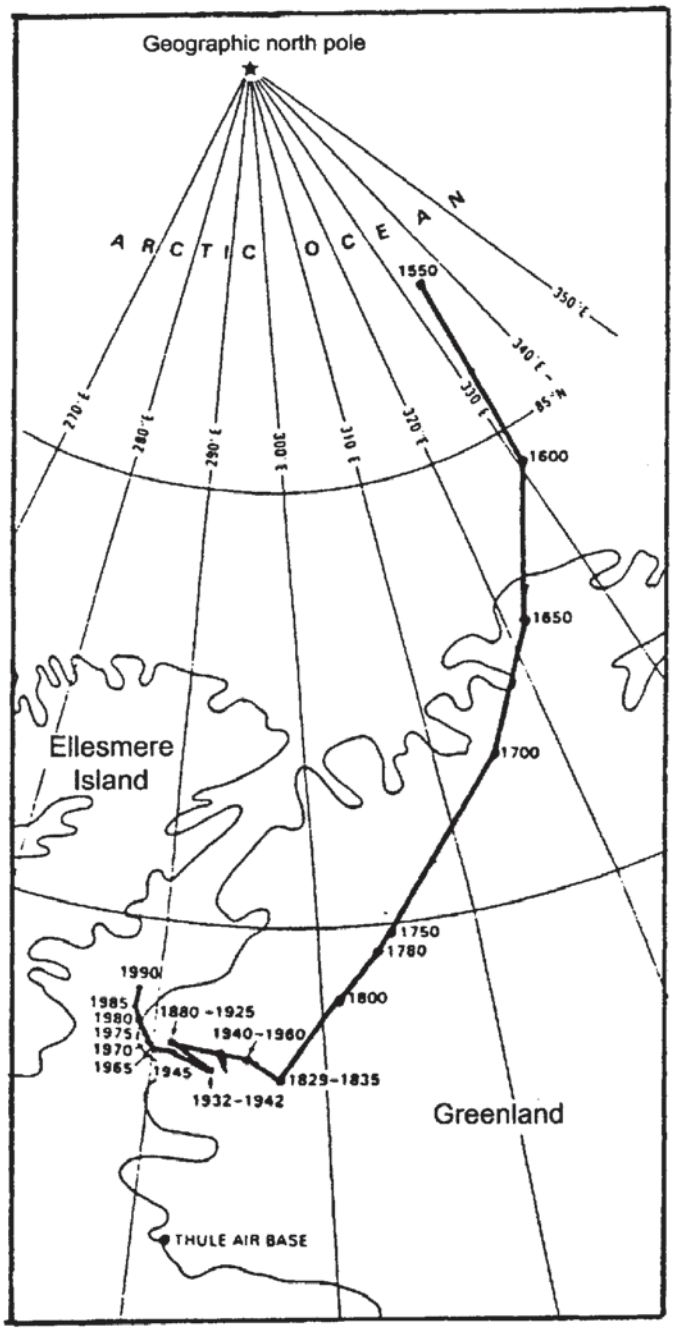

Figure 3.16 Drift of the north magnetic pole position from 1550 to 1990. From James (1990), by permission

disturbances, which are called *magnetic storms*, may persist for several hours or even days. Such frenetic magnetic activity is caused by sunspot and solar activity resulting in solar-charged particles entering the ionosphere. This may happen on fine sunny days and not necessarily in stormy weather. Magnetic observatories around the

world provide an advance warning service to advise of the probability of magnetic storm activity. In severe storms, all magnetic surveying has to stop as it is not practicable to correct for such extreme fluctuations. In minor disturbances, if a continuous-reading base station magnetometer is used, the diurnal variations can be corrected. In aeromagnetic surveys, it is necessary to specify contractually what constitutes a magnetic storm. Survey data adversely affected by magnetic disturbances may have to be reflown and this obviously has cost implications. Practical details of how to correct for diurnal variations are given in Section 3.6.2.

3.5 MAGNETIC INSTRUMENTS

The earliest known device which responded to the Earth's magnetic field was a magnetised spoon used by Chinese geomancers (diviners) in the first century AD. Compass needles were introduced for navigation around the year 1000 in China and in Europe about 200 years later. The first accurate measurement of the inclination of the Earth's field was made at Radcliffe in London in 1576 by Robert Norman. He described his instruments and collected data in his book *The Newe Attractive* (1581), which was the first book ever to be devoted to geomagnetism.

Magnetometers used specifically in geophysical exploration can be classified into three groups: the torsion (and balance), fluxgate and resonance types, of which the last two have now completely superseded the first. Torsion magnetometers are still in use at 75% of geomagnetic observatories, particularly for the measurement of declination. Magnetometers measure horizontal and/or vertical components of the magnetic field (F_h and F_z respectively) or the total field $\boldsymbol{F}_t$ (see Figure 3.12).

3.5.1 Torsion and balance magnetometers

Historically the first to be devised (1640), these comprise in essence a magnetic needle suspended on a wire (torsion type) or balanced on a pivot. In the Earth's magnetic field the magnet adopts an equilibrium position. If the device is taken to another location where the Earth's magnetic field is different from that at the base station, or if the magnetic field changes at the base station, the magnet will align itself to the new field and the deflection from the rest position is taken as a measure of the Earth's magnetic field. The Swedish mine compass, Hotchkiss superdip, and Thalén-Tiberg magnetometer are all early examples of this type of device. In 1915, Adolf Schmidt devised his variometer in which a magnetic beam was asymmetrically balanced on an agate knife edge (Figure 3.17) and zeroed at a base station.

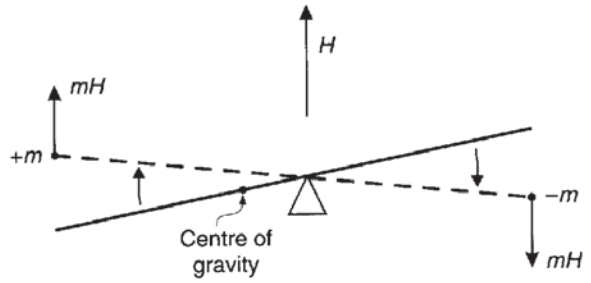

Figure 3.17 Basic principle of operation of a torsion or balance-type magnetometer

Deflections from the rest position at other locations were then read using a collimating telescope. To be used it had to be orientated at right-angles to the magnetic meridian so as to remove the horizontal component of the Earth's field. The device was calibrated using Helmholtz coils so that the magnitude of the deflection was a measure of the vertical component of the field strength.

A development of the Schmidt variometer was the compensation variometer. This measured the force required to restore the beam to the rest position. In exploration work, the greatest precision with a balance magnetometer was only 10 nT at best. For further details of these devices, see the descriptions by Telford *et al.* (1990).

3.5.2 Fluxgate magnetometers

The fluxgate magnetometer was developed during the Second World War to detect submarines. It consists of two parallel cores made out of high-permeability ferromagnetic material. Primary coils are wound around these cores in series but in opposite directions (Figure 3.18). Secondary coils are also wound around the cores but in the opposite sense to the respective primary coil. A current alternating at 50–

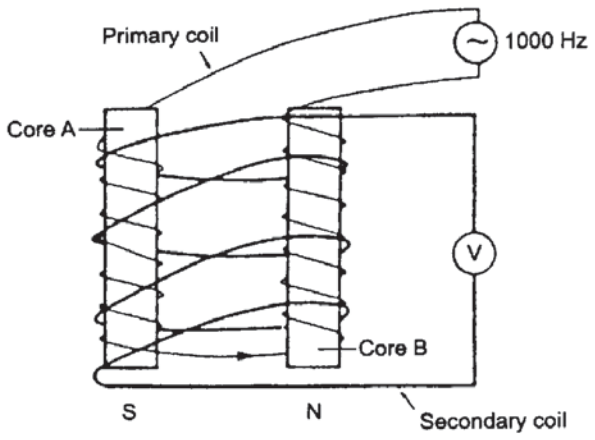

Figure 3.18 Basic operating principle of the fluxgate magnetometer

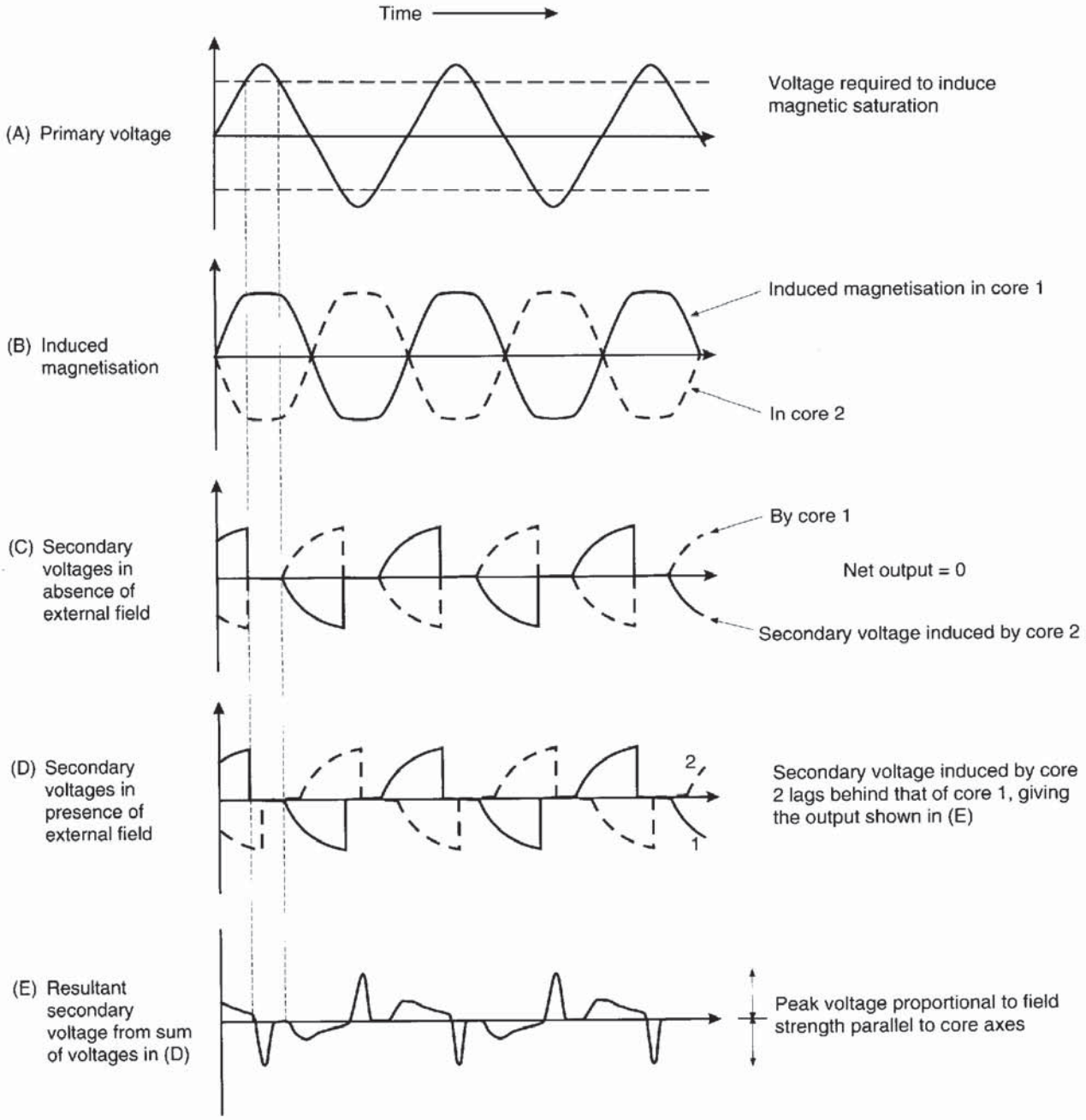

Figure 3.19 Response characteristics of primary and secondary circuits in a fluxgate magnetometer

1000 Hz (Figure 3.19A) is passed through the primary coils which drives each core through a B–H hysteresis loop (cf. Figure 3.6) to saturation at every half-cycle (Figure 3.19B) in the absence of an external field, so inducing a magnetic field in each core. The generated alternating magnetic field induces an in-phase voltage within the secondary coils. This voltage reaches its maximum when the rate of

change of the magnetic field is fastest (Figure 3.19C). As the coils are wound in opposing directions around the two cores, the secondary voltages are in phase but have opposite polarity (Figure 3.19C) so that the sum of the two voltages is at all times zero. However, when the cores are placed in the Earth's magnetic field, a component of that field will be parallel to the orientation of the cores. Consequently, the core whose primary field is reinforced by the ambient external field will reach saturation earlier than the other core whose magnetic field is opposed by the external field. This has the effect of shifting the phases of the secondary voltages (Figure 3.19D) so that the sum of the two secondary voltages is now non-zero (Figure 3.19E). The peak amplitude of the pulsed output of the combined secondary coils is proportional to the magnitude of the external field component (Primdahl 1979).

The fluxgate magnetometer can be used to measure specific magnetic components with the same attitude as the sensor cores. As the fluxgate magnetometer is relatively insensitive to magnetic field gradients, it has the advantage that it can be used in areas where very steep gradients would militate against the use of resonance-type devices which are affected. Some portable fluxgate magnetometers suffer from temperature effects owing to inadequate thermal insulation, which can reduce the resolution to only ± 10 to 20 nT, this being inadequate for ground exploration surveys. They are used quite widely in airborne surveys where better thermal insulation can be ensured and additional devices can be used to aid the consistent orientation of the sensor cores. In such cases, an accuracy to within ± 1 nT can be achieved. In addition, fluxgate instruments can provide a continuous output which is another advantage for airborne applications. Fluxgate magnetometers can also be used in down-hole logging applications in mineral exploration.

3.5.3 Resonance magnetometers

There are two main types of resonance magnetometer: the *proton free-precession magnetometer*, which is the best known, and the *alkali vapour magnetometer*. Both types monitor the precession of atomic particles in an ambient magnetic field to provide an absolute measure of the total magnetic field, $\boldsymbol{F}$.

The proton magnetometer has a sensor which consists of a bottle containing a proton-rich liquid, usually water or kerosene, around which a coil is wrapped, connected to the measuring apparatus (Figure 3.20). Each proton has a magnetic moment $\boldsymbol{M}$ and, as it is always in motion, it also possesses an angular momentum $\boldsymbol{G}$, rather like a spinning top. In an ambient magnetic field such as the Earth's ($\boldsymbol{F}$), the majority of the protons align themselves parallel with this field with the remainder orientated antiparallel (Figure 3.21A). Consequently, the volume of proton-rich liquid

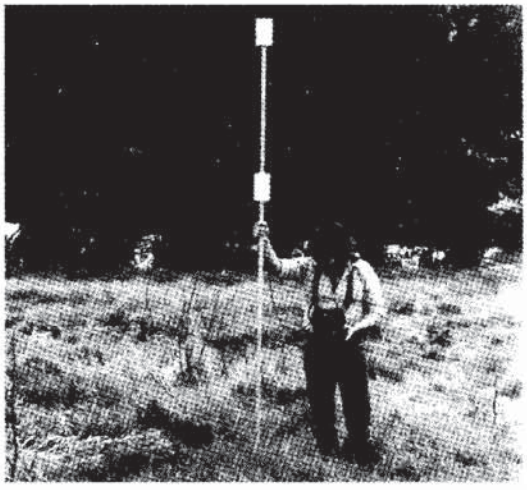

(A)

(B)

Figure 3.20 (A) A nuclear proton precession magnetometer in use, and (B) a caesium vapour magnetometer. Courtesy of Geometrics

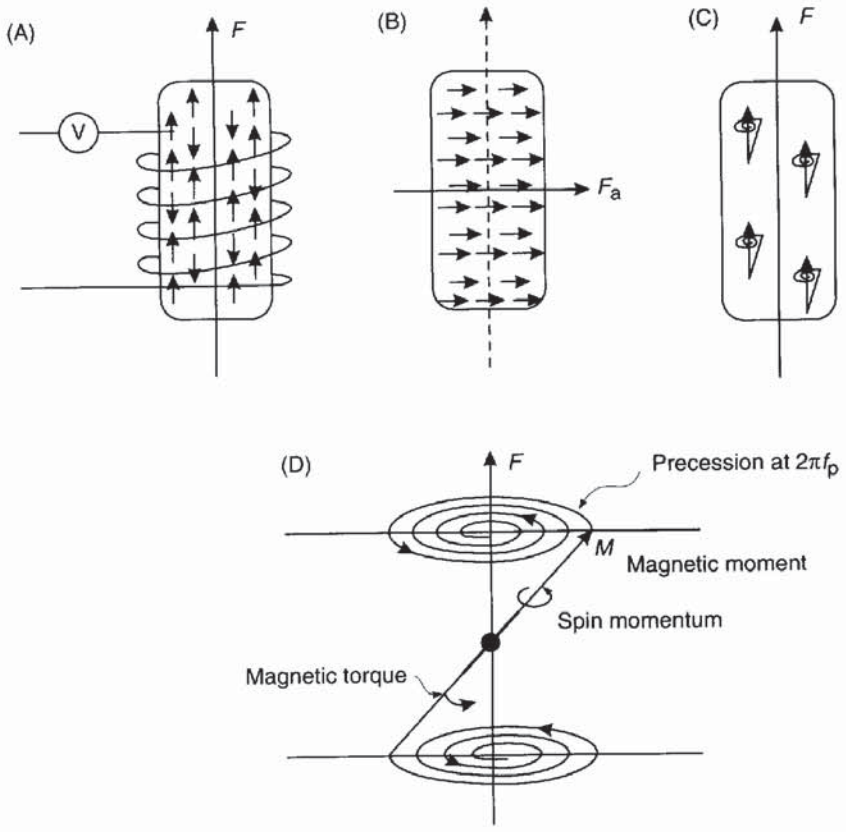

Figure 3.21 Basic operating principles of a proton magnetometer. After Kearey and Brooks (1991), by permission

acquires a net magnetic moment in the direction of the ambient field (***F***).

A current is applied to the coil surrounding the liquid, generating a magnetic field about 50 to 100 times stronger than, and at right-angles to, the Earth's field. The protons align themselves to the new magnetic direction (Figure 3.21B). When the applied field is switched off, the protons precess around the pre-existent ambient field ***F*** (Figure 3.21C) at the *Larmor precession frequency* (f_p) which is proportional to the magnetic field strength ***F*** (Box 3.6). As protons are charged particles, as they precess they induce an alternating voltage at the same frequency as f_p into the coil surrounding the sensor bottle. Interaction between adjacent protons causes the precession to decay within 2–3 seconds, which is sufficient time to measure the precession frequency. To obtain a value of ***F*** to within ± 0.1 nT, frequency must be measured to within ± 0.004 Hz, which is quite easily achieved. This resolution is equivalent to 1 part in 10^6, which is 100 times less sensitive than in gravity measurements.

Box 3.6 Magnetic field strength, F, and precession frequency, f_P

$$F = 2\pi f_P/\Phi_P$$

where Φ_P is the gyromagnetic ratio of the proton, which is the ratio of the magnetic moment and spin angular momentum (see Figure 3.21); and

$$\Phi_P = 0.26753 \text{ Hz/nT and } 2\pi/\Phi_P = 23.4859 \text{ nT/Hz.}$$

Thus:

$$F = 23.4859 f_P.$$

For example, for $F = 50\,000$ nT, $f_P = 2128.94$ Hz.

One of the limiting factors of the proton magnetometer is that its accuracy is reduced in areas of high magnetic gradient. As the sensor bottle is of the order of 15 cm long, a strong field gradient of 500 nT/m, for example, means that there is a 75 nT difference in field strength between the top and bottom of the sensor and the rate of damping is increased. The accuracy of measurement of the precession frequency is thus reduced. As a guide, if the gradient is 400 nT/m, the precision is at best 1 nT; for 200 nT/m it is 0.5 nT.

As the precession frequency is only a function of field strength, there is no need to orientate the field sensor. Modern proton magnetometers give a direct readout of the field strength in nanoteslas and data can be automatically output into a datalogger for subsequent downloading into a computer.

Proton magnetometers are used extensively not only in land surveys but also at sea and in airborne investigations. In marine surveys, the magnetometer sensor bottle, which is located in a sealed unit called a 'fish', is deployed two or three ship's lengths astern so as to be sufficiently removed from magnetic interference from the ship. In the case of aircraft, two techniques are used. One is to tow the sensor bottle at least 30 m below and behind the aircraft in what is called a 'bird', or place it in a non-magnetic boom called a 'stinger' on the nose, on the tail fin or on a wingtip of the aircraft. In the fixed mode, special magnetic compensation measures can be taken to annul the magnetisation of the aircraft; the excellence of the compensation is called the *figure of merit* (FOM) rating. The fitting of active compensation systems in modern aircraft has improved FOM values and reduced the time taken for compensation, and so helped to improve the cost-effectiveness of airborne surveys. In addition to ground, marine and airborne applications, proton magnetometers can be deployed down boreholes, and can be particularly useful in mineral exploration programmes.

A limitation on proton magnetometers, particularly in airborne surveys, is the rate at which measurements can be made. As the proton

precession and measurement take a finite time (of the order of a second or longer), continuous readings are not possible and this can be restricting in some situations.

One manufacturer (GEM Systems Inc.) has produced a modified precession instrument that utilises the Overhauser Effect. An electron-rich fluid containing free radicals is added to a standard hydrogen-rich liquid. The combination increases the polarisation by a factor of 5000 in comparison with standard liquids. Overhauser proton precession uses a radio-frequency (RF) magnetic field and so needs only minimal power, in contrast with high-power direct current fields used in traditional proton precession magnetometers. Polarisation and magnetisation can occur simultaneously and thus rapid sampling of the total field strength (two readings per second) can be achieved.

The second type of resonance magnetometer is the *alkali vapour magnetometer* or *optical absorption magnetometer*, which utilises the optical pumping technique (Bloom 1962). The principle on which this method is based is illustrated in Figure 3.22. Under normal conditions of temperature and pressure, electrons exist at certain energy states (A and B) around the nucleus of the atom. According to quantum physics, it is only possible to transfer an electron from a lower energy state (A) to one with higher energy (B) in discrete jumps. If a vapour of an element such as rubidium or caesium is illuminated by a light whose filament is made of the same element, the light emitted is at the correct wavelength for incident photons to be absorbed by the vapour and the low-energy state electrons excited up to higher levels. If the incident light is circularly polarised, only electrons in the A_1 orbit will be excited or 'optically pumped' up to the B orbit. At this point, the excess photons will be transmitted through the excited vapour and will be detected by the photocell as an increase in light intensity.

A small alternating current is passed through a coil at a frequency of between 90 and 300 kHz to induce a magnetic field around the

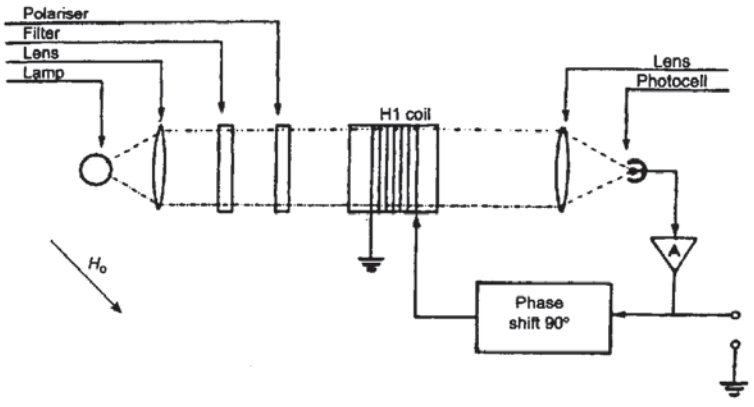

Figure 3.22 Optical pumping – principle of the alkali vapour magnetometer. From James (1990), by permission

alkali vapour cell. The frequency is tuned until it is locked into the Larmor frequency for the alkali vapour concerned. This small magnetic field energises some electrons back into their vacant A ground states. The consequence of this is that the light intensity at the photocell diminishes as photons are absorbed by the alkali vapour in the cell until saturation is reached again. Photons will continue to be absorbed until all the available electrons have been excited to the B state, when the light at the photocell will again be at its most intense. Consequently, the cycled optical pumping produces a light at the photocell that flickers at the Larmor precession frequency, which can easily be measured. As the precession frequency is dependent upon the ambient field strength of the Earth (see Box 3.6), the total field strength can be determined from a measurement of the precession frequency. The factor $2\pi/\Phi_p$ is approximately equal to 0.2141 and 0.1429 nT/Hz for rubidium and sodium respectively, which give corresponding precession frequencies of 233.5 and 350 kHz in a field of 50 000 nT. As long as the light beam axis is not parallel or antiparallel to the Earth's magnetic field (when no signals would be produced), the precession frequency can be measured with sufficient accuracy so that the magnetic field strength can be determined to within ± 0.01 nT. The measurement time is extremely small, and so alkali vapour magnetometers can be used as virtually continuous reading instruments, which makes them ideally suited to airborne surveys.

For land-based archaeological or environmental geophysical applications, self-oscillating split-beam caesium vapour magnetometers have been developed, largely from military ordnance detection instruments (e.g. the Geometrics G-822L magnetometer). Sampling rates of up to 10 readings per second are possible with a sensitivity of 0.1 nT.

3.5.4 Cryogenic (SQUID) magnetometers

The most sensitive magnetometer available is the cryogenic magnetometer which operates using processes associated with superconductivity, details of which have been given by Goree and Fuller (1976). These magnetometers are perhaps better known as *SQUID* (Superconducting QUantum Interference Device) magnetometers. Used extensively in palaeomagnetic laboratories, the SQUID magnetometer has also been developed for use in aeromagnetic surveying since the early 1980s, particularly as a gradiometer. SQUIDs can have a measurement sensitivity of 10^{-5} nT/m; this means that two sensors need only be placed 25 cm or less apart, thus making it possible to have the entire sensor system in a very small space. This has great advantages in mounting the equipment in aircraft, in borehole probes and in submarine devices where space is at a premium. Measurement accuracy of the total field strength is within ± 0.01 nT.

Technical difficulties over the use of liquid helium, which has to be maintained at a temperature of 4.2 K for superconductivity to occur, limit the widespread deployment of SQUID magnetometers. They are rarely, if ever, used in surface magnetic measurements.

3.5.5 Gradiometers

A gradiometer measures the difference in the total magnetic field strength between two identical magnetometers separated by a small distance. In airborne work, typical separations between sensors is 2 m to 5 m for stingers (Figure 3.23) and up to 30 m for birds. In ground instruments, a separation of 0.5 m is common. The magnetic field gradient is expressed in units of nT/m and taken to apply at the mid-point between the sensors. A major advantage of gradiometers is that because they take differential measurements, no correction for diurnal variation is necessary as both sensors will be equally affected. As gradiometers measure the vertical magnetic gradient, noise effects from long-wavelength features are suppressed and anomalies from shallow sources are emphasised. For detailed high-resolution surveys exploring for mineral targets, magnetic gradiometry is the preferred method (Hood 1981).

Fluxgate and resonance-type magnetometers are commonly used in ground surveys. Where continuous-reading devices are required, such as when automatic datalogging is being used, fluxgate gradiometers are preferable (e.g. Sowerbutts and Mason 1984). A detailed although dated comparison of the different types of gradiometers and magnetometers has been made by Hood *et al.* (1979).

Self-oscillating split-beam caesium vapour gradiometers have also been developed for small-scale land-based surveys, such as Geomet-

Figure 3.23 Eurocopter AS315 about to lift a 3-axis magnetic gradiometer system. Courtesy of Aerodat Inc., Canada

rics Inc.'s G-858 instrument. These instruments can sample at up to 10 readings per second with a sensitivity of 0.05 nT. An additional feature of this particular instrument is that it can be connected to a Differential Global Positioning System for the simultaneous logging of position and magnetic data. The system was first tested at Stanford University, USA, in March 1993. As with any geophysical instruments, it is always best to check with equipment manufacturers for the latest technical specifications.

3.6 MAGNETIC SURVEYING

3.6.1 Field survey procedures

As with every geophysical survey, the keeping of detailed and accurate field notes cannot be emphasised too strongly, even if dataloggers or memory-magnetometers are used. Orderly record-keeping permits more efficient and accurate data processing. Practical details of how magnetic surveys should be undertaken have been given by Milsom (1989).

In the vast majority of cases where the magnetic targets have a substantial strike length, survey profiles should, where possible, be conducted across strike with tie-lines along strike. In cases such as some archeological and engineering site investigations where the targets are more equidimensional, such as the ruins of a Roman villa or a brick-lined mineshaft, north–south and east–west orientations are commonly used.

In ground-based surveys, it is important to establish a local base station in an area away from suspected magnetic targets or magnetic noise and where the local field gradient is relatively flat. A base station should be quick and easy to relocate and re-occupy. The precise approach to the survey will depend on the type of equipment. If a manual push-button proton magnetometer is deployed, the exact time of occupation of each station is needed and at least three readings of the total field strength should be recorded. Each of the three values should be within ± 1 or 2 nanoteslas; an average of these three readings is then calculated. As the survey progresses, the base station must be re-occupied every half or three-quarters of an hour in order to compile a diurnal variation curve for later correction (see next section). Next to each data entry, where required, should be any comments about the terrain or other factors that may be considered to be important or relevant to subsequent data processing and interpretation.

If a continuous-reading base-station magnetometer is used to measure the diurnal variation, it is still worth returning to base every 2–3 hours, just in case the base magnetometer fails.

When dataloggers or memory magnetometers are used, regular checks on the recording of data are vital. It is all very well occupying

hundreds of stations and taking perhaps several thousand measurements only to find that the logger is not functioning or the memory has been corrupted.

One golden rule is always to check your data as they are collected and at the end of each survey day. This serves two purposes. First, it provides a data quality check and allows the operator to alter the survey in response to the magnetic values measured. For example, if a 50 m station interval was selected at the outset and the field values indicate a rapid change over a much shorter interval, the separation between stations must be reduced in order to collect enough data to image the magnetic anomaly. Secondly, it provides a check on the consistency of the data. Odd anomalous values may indicate something of geologic interest which may need to be followed up, or may highlight human error. In either case, the next day's survey can take this into account and measurements can be made to check out the oddball values.

In the case of aeromagnetic or ship-borne surveys, the specifications are often agreed contractually before an investigation begins. Even so, there are guidelines as to what constitutes an adequate line separation or flying height, orientation of survey line, and so on. As an example, Reid (1980) compiled a set of criteria based on avoidance of spatial aliasing (Tables 3.5 and 3.6). For example, if a mean flying height over magnetic basement (h) of 500 m is used with a flight line spacing (δx) of 2 km, then $h/\delta x = 0.5/2 = 0.25$, which would indicate that 21% aliasing would occur in measurements of the total field and

Table 3.5 Degree of aliasing (Reid 1980)

$h/\delta x$	F_T	F_G
0.25	21	79
0.5	4.3	39
1	0.19	5
2	0.0003	0.03
4	0	0

F_T and F_G are the aliased power fraction (per cent) expected from surveys of total field and vertical gradient respectively

Table 3.6 Maximum line spacings (Reid 1980)

Survey type	Intended use	δx_{max}
Total field	Contour map	$2h$
Total field	Computation of gradient, etc., maps	h
Vertical gradient	Gradient contour maps	h
Total field	Modelling of single anomalies	$h/2$

as much as 79% if the vertical magnetic gradient were being measured (Table 3.5). Neither value is acceptable. The larger the value of $h/\delta x$, the less aliasing will occur; a survey is considered reasonably designed if $h/\delta x \geqslant 0.5$, depending on survey type. At this minimum value, about 5% maximum aliasing is acceptable if contouring is to be undertaken on total field data. Other maximum flight line spacings are given in Table 3.6. There have been examples of commercially flown surveys in Egypt, for instance, where the flying height was 400 m above ground, but with 1 km thickness of sedimentary cover over magnetic basement (hence $h = 1.4$ km) and the line spacing was 21 km. This gives a value of $h/\delta x \approx 0.07$, resulting in more than 65% aliasing. The contour maps of these surveys, which covered thousands of square kilometers, are virtually useless. To have been contoured adequately, the flight line spacing for data acquired at a flying height of 1.4 km above basement should have been no more than 2.8 km; i.e. from Table 3.6, $\delta x \leqslant 2h$.

The choice of survey parameters will also affect the success (or otherwise) of subsequent computer contouring. These guidelines can also apply to surface surveys using a proton magnetometer where $h = 3$ m (1 m of overburden over a magnetic target, plus 2 m for the magnetometer sensor pole) for example. In this case, an acceptable maximum line spacing would be 6 m if a contour map of the total field were required. Survey design parameters and automated contouring have been described briefly in Chapter 1 and in detail by Hood *et al.* (1979) and by Reid (1980).

3.6.2 Noise and corrections

All magnetic data sets contain elements of noise and will require some form of correction to the raw data to remove all contributions to the observed magnetic field other than those caused by sub-surface magnetic sources. In ground magnetometer surveys, it is always advisable to keep any magnetic objects (keys, penknives, some wristwatches, etc.), which may cause *magnetic noise*, away from the sensor. Geological hammers put next to the sensor bottle of a proton magnetometer will have a significant effect, as demonstrated by students trying to simulate a magnetic storm so that they could abandon the survey and retire to the nearest hostelry! It is also essential to keep the sensor away from obviously magnetic objects such as cars, metal sheds, power lines, metal pipes, electrified railway lines, walls made of mafic rocks, etc.

The most significant correction is for the *diurnal variation* in the Earth's magnetic field. Base station readings taken over the period of a survey facilitate the compilation of the diurnal 'drift' as illustrated in Figure 3.24. Measurements of the total field made at other stations can easily be adjusted by the variation in the diurnal curve. For example, at point A in Figure 3.24, the ambient field has increased by

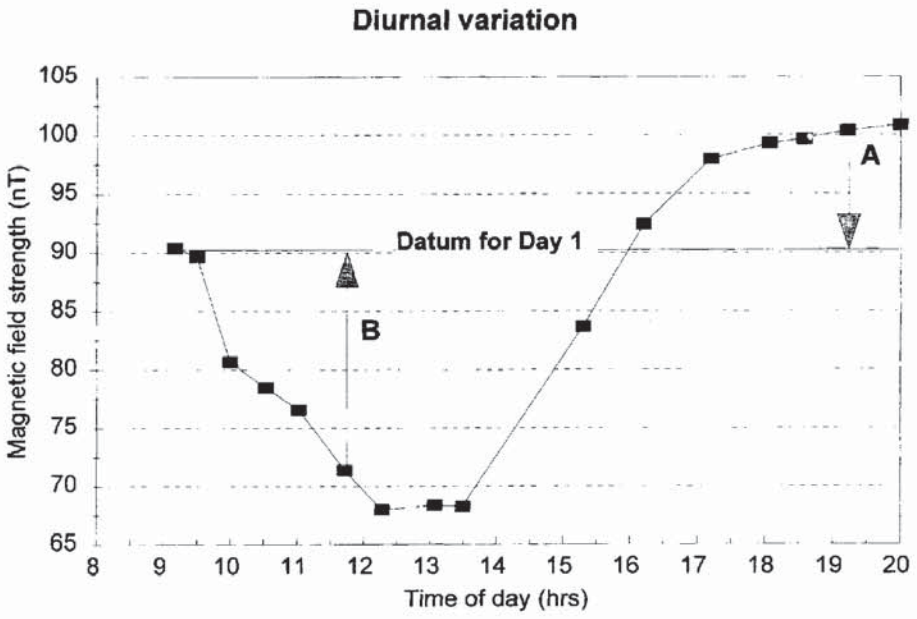

Figure 3.24 Diurnal drift curve measured using a proton magnetometer

10 nT and thus the value measured at A should be reduced by 10 nT. Similarly, at B, the ambient field has fallen by 19 nT and so the value at B should be increased by 19 nT. Further details of diurnal corrections have been given by Milsom (1989). Gradiometer data do not need to be adjusted as both sensors are affected simultaneously and the gradient remains the same between them.

In airborne and shipborne surveys, it is obviously not possible to return to a base station frequently. By designing the survey so that the track lines intersect (Figure 3.25), the dataset can be appropriately corrected. Some surveys use profiles and tie-lines at the same spacing to give a regular grid. Other surveys have tie-lines at 10 times the inter-profile line spacing. In addition to checking on diurnal variations, tie-lines also serve as a useful control on navigational and measurement accuracy. A flow chart depicting the reduction of aeromagnetic data is given in Figure 3.26. In regional surveys, a further tie is to a local Geomagnetic Observatory, if there is one within 150 km, at which all the magnetic components are measured and which can provide diurnal variations. It would then have to be demonstrated that the curve obtained from the observatory applied in the survey area.

The degree of data processing is dependent upon the resolution required in the final dataset. For a broad reconnaissance survey, a coarser survey with lower resolution, say several nanoteslas, may be

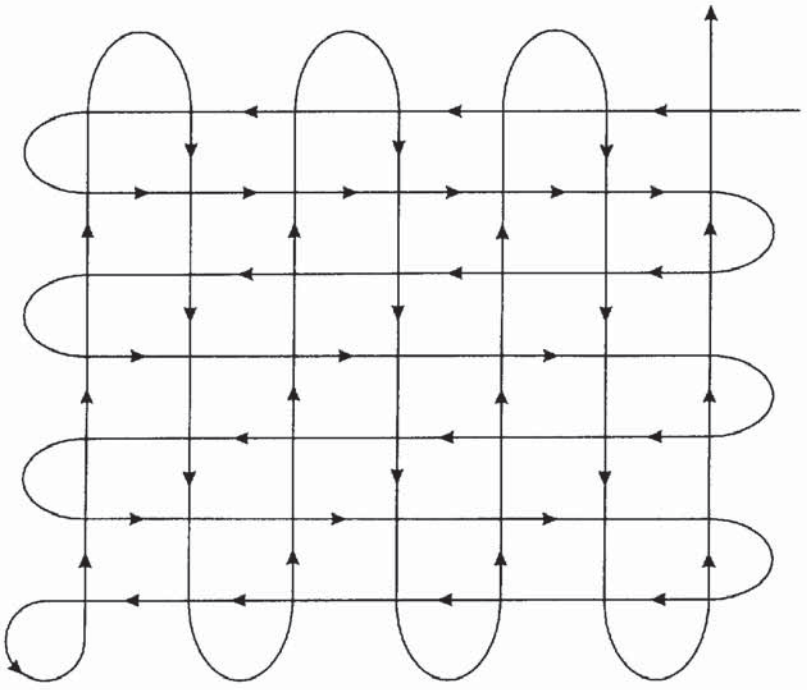

Figure 3.25 Tracks of a shipborne or airborne magnetic survey. Some surveys, rather than having equal spacings between all tracks, have tie-lines at 10 times the normal interline spacing

all that is required. In detailed surveys, however, an accuracy to within 0.1 nT will need a finer survey grid, more accurate position-fixing and diurnal drift corrections.

Rarely, a *terrain correction* may need to be applied when the ground over which a survey is conducted is both magnetic and topographically rough. Unlike the gravity case where terrain corrections, though laborious, are relatively easy to calculate, corrections for terrain for magnetic data are extremely complex. If the rough terrain is made up largely of low-susceptibility sedimentary rocks, there will be little or no distortion of the Earth's magnetic field. However, if the rocks have a significant susceptibility, a terrain factor may have to be applied. Anomalous readings as large as 700 nT have been reported by Gupta and Fitzpatrick (1971) for a 10 m high ridge of material with susceptibility $\kappa \approx 0.01$ (SI). Furthermore, magnetic readings taken in a gulley whose walls are made of basic igneous rocks will be anomalous owing to the magnetic effects of the rocks above the magnetic sensor. Considerable computational effort (see Sharma, 1986, appendix C) then has to be applied to correct the data so that they are interpretable. Similar geometric effects can also occur in radiometric surveys.

Another way of correcting for the effect of topography, or of reducing the data to a different reference plane, is by *upward continuation*. This permits data acquired at a lower level (e.g. on the ground) to be processed so that they can be compared with airborne surveys. The effect of this is to lessen the effects of short-wavelength high-

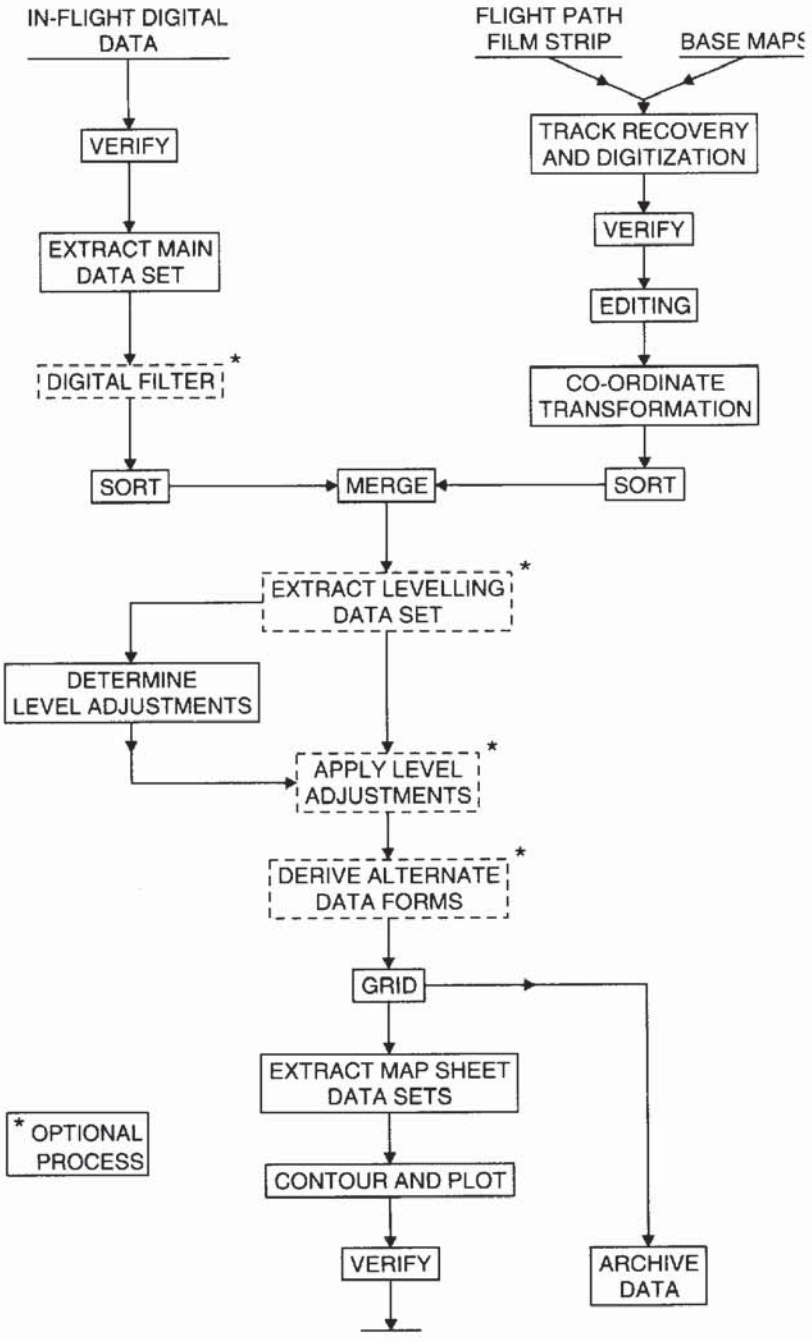

Figure 3.26 Flow chart of reduction processes on aeromagnetic data. From Hood *et al.* (1979), by permission

amplitude features as the magnetic force is indirectly proportional to the square of the distance between source and sensor (see Box 3.1). The rate of change of the field with elevation (akin to the gravitational free-air correction) is between 1.5 and 3.5 nT/100 m, with the maximum gradient being at the poles. In areas where the range of

elevations of the ground surface is large, such as in the Rockies or Andes, and Himalayas, maintaining a constant terrain clearance is not practicable (or safe!). Indeed, in areas of extreme altitude, airborne surveys are not possible as the ground can be higher than the flying ceiling of available aircraft owing to the rarified atmosphere. Different flying heights can be specified for particular areas within a survey region and the various datasets processed to the same flying height or alternative datum.

In some regions, metal pipes can become inductively magnetised by currents in the atmosphere (Campbell 1986) or are cathodically protected by passing a large direct current (1–7 amps) through them to reduce internal corrosion. The presence of such pipes can contribute a significant anomaly on high-resolution aeromagnetic data (Gay 1986). In hydrocarbon exploration over sedimentary basins up to 6 km depth, basement faulting, which affects basement-controlled traps and reservoirs, can be identified from their respective magnetic anomalies which can have amplitudes of only several nanoteslas. There is then a problem over differentiating between a geologically significant fault and a cathodically protected pipe as their respective magnetic anomalies may appear to be similar.

Iron pipes have a permanent magnetisation acquired at the foundry at the time of manufacture. Being magnetisable, they also acquire a magnetisation induced by the Earth's magnetic field. Current injected into the pipes will also generate a magnetic field according to the right-hand rule. This states that a conductor carrying electrical current, indicated by the thumb on the right hand, will generate a magnetic field in the direction indicated by the coiled fingers of the right hand (Figure 3.27A). The injection of current at specific points along a pipe has one marked effect (Figures 3.27B and C). The polarity of the magnetic anomaly will be reversed either side of the injection point as the current is flowing in opposite directions away from it and into the ground. The point at which the polarity reverses (Figure 3.27B) indicates the position of current injection. The figure shows the magnitudes and senses of the western and eastern anomaly peaks for each survey line. Lines 9–13 have a positive western peak and corresponding negative eastern peak while lines 14–17 south of the injection point have a negative western peak and positive eastern peak (Figure 3.27C). The magnitude of the anomaly will also decrease away from the injection point. The magnitudes determined for survey lines south of the injection point are slightly larger than those for northern lines as the flying height was 40 m lower to the south. Mean flying height was 257 m. These characteristics are diagnostic of cathodically protected pipes and can be used to tell them apart from linear fault structures whose polarity does not switch along its length, although its magnitude may vary along the strike of the fault. Having identified a linear anomaly as being due to a cathodically protected pipe, the anomaly can be filtered out of the dataset.

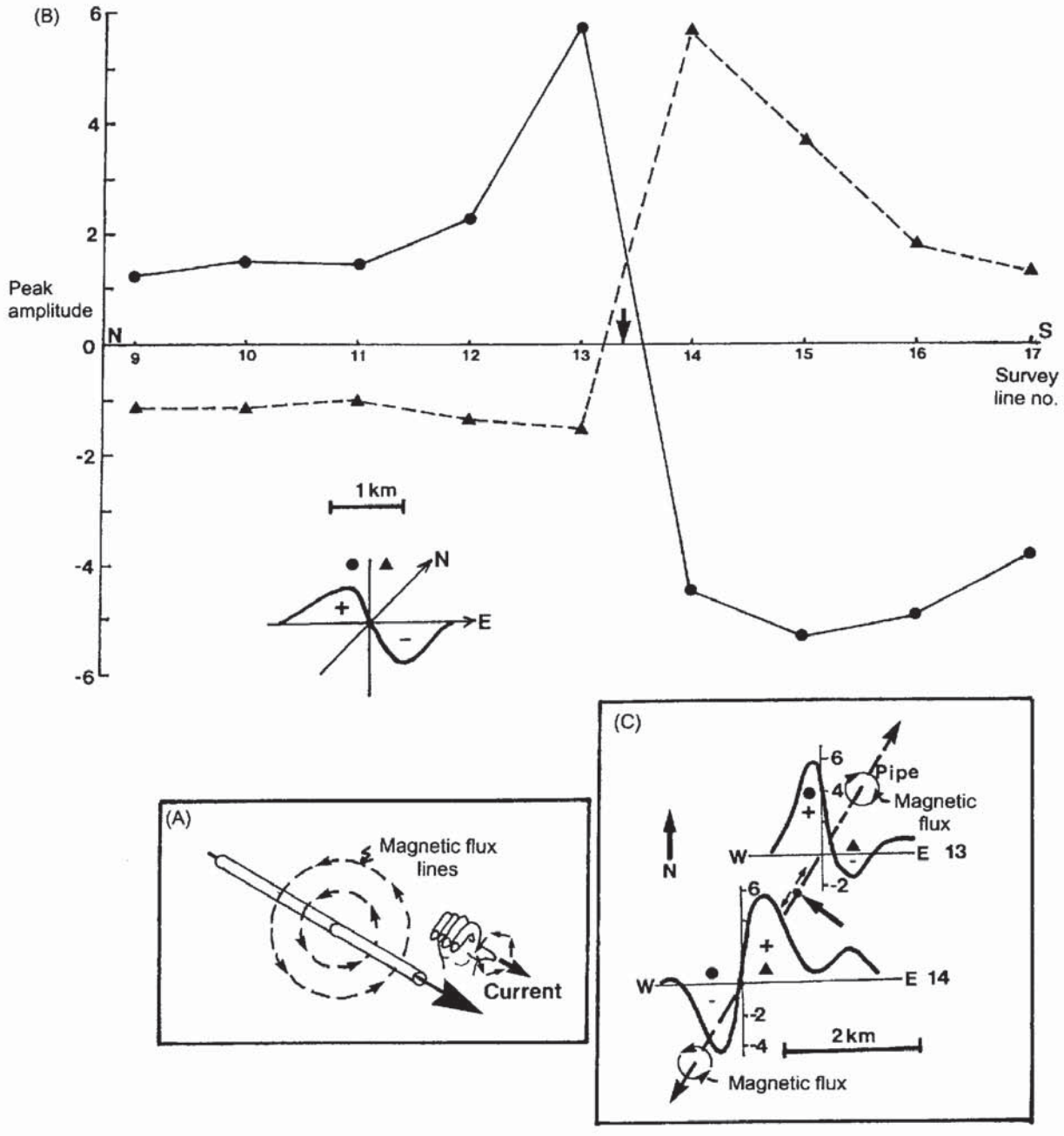

3.6.3 Data reduction

In order to produce a magnetic anomaly map of a region, the data have to be corrected to take into account the effect of latitude and, to a lesser extent, longitude. As the Earth's magnetic field strength varies from 25 000 nT at the magnetic equator to 69 000 nT at the poles, the

increase in magnitude with latitude needs to be taken into account. Survey data at any given location can be corrected by subtracting the theoretical field value F_{th}, obtained from the International Geomagnetic Reference Field, from the measured value, F_{obs}. This works well in areas where the IGRF is tied-in at or near to Geomagnetic Observatories, but in many places the IGRF is too crude. Instead, it is better to use a local correction which can be considered to vary linearly over the magnetic survey area. Regional latitudinal (ϕ) and longitudinal (θ) gradients can be determined for areas concerned and tied to a base value (F_0), for example, at the south-east corner of the survey area. Gradients northwards ($\delta F/\delta\phi$) and westwards ($\delta F/\delta\theta$) are expressed in nT/km and can easily be calculated for any location within the survey area. For example, in Great Britain, gradients of 2.13 nT/km north and 0.26 nT/km west are used. Consequently, the anomalous value of the total field (δF) can be calculated arithmetically, as demonstrated by the example in Box 3.7.

Another method of calculating the anomalous field δF is to determine statistically the trend of a regional field to isolate the higher-frequency anomalies, which are then residualised in the same way that gravity residuals are calculated. The regional field is subtracted from the observed field to produce a residual field (δF) (Figure 3.28A). If the survey is so laterally restricted, as in the case of small-scale archaeological, engineering or detailed mineral prospecting surveys (e.g. $< 500\,\text{m} \times 500\,\text{m}$ in area), the use of regional gradients is not practicable. Instead, profile data can be referred to a local base station (F_b) which is remote from any suspected magnetic sources. In this case, the anomalous field δF is obtained by subtracting the base value (F_b) from every diurnally corrected observed value F_{obs} along the profile ($\delta F = F_{obs} - F_b$), as illustrated in Figure 3.28B.

Box 3.7 Anomalous total field strength δF

$$\delta F = F_{obs} - (F_0 + \delta F/\delta\phi + \delta F/\delta\theta) \quad (\text{nT})$$

where F_{obs} is the measured value of F at a point within the survey area with coordinates (x, y); F_0 is the value at a reference point ($x = 0$; $y = 0$); $\delta F/\delta\phi$ and $\delta F/\delta\theta$ are the latitudinal and longitudinal gradients respectively (in units of nT/km).

Example: For a station 15 km north and 18 km west of a reference station at which $F_0 = 49\,500$ nT with gradients $\delta F/\delta\phi = 2.13$ nT/km north, and $\delta F/\delta\theta = 0.26$ nT/km west, and the actual observed field $F_{obs} = 50\,248$ nT, the magnetic anomaly δF is:

$$\delta F = 50\,248 - (49\,500 + 2.13 \times 15 + 0.26 \times 18)\,\text{nT}$$
$$= 711\,\text{nT}$$

Figure 3.27 (*opposite*) Variation in magnetic anomalies associated with a cathodically protected pipe in north-east Oklahoma, USA. (A) Right-hand rule applied to a pipe through which a current is passed to show direction of magnetic flux lines. (B) Peak amplitudes for western and eastern parts of profile anomalies, of which two for lines 13 and 14 are shown in (C). Note the relative amplitudes of the anomalies on lines 13 and 14 either side of the current injection point (arrowed). Data from Gay (1986), by permission

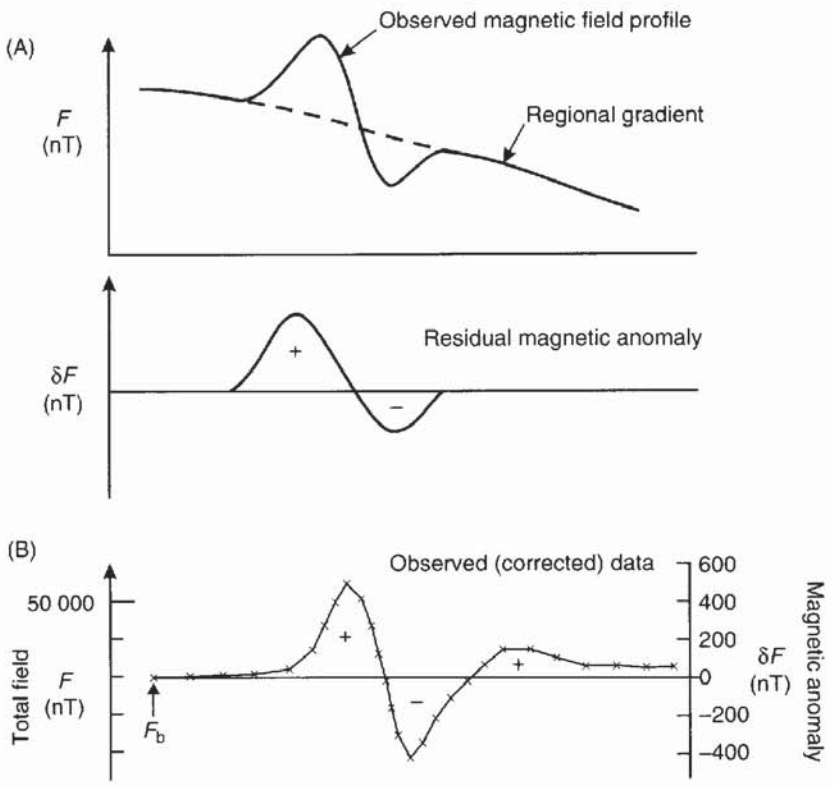

Figure 3.28 Magnetic residuals (A) Subtraction of a regional field gradient, and (B) reference to a local arbitrary base station

3.7 QUALITATIVE INTERPRETATION

Once magnetic data have been fully corrected and reduced to their final form, they are usually displayed either as profiles (Section 3.7.1) or as maps (Section 3.7.2) and the interpretation procedures are different for the two cases. However, it must always be borne in mind that, although the techniques used are similar to those for gravity surveys, there are two important complications. First, the Earth's magnetic field is dipolar, which means that a single anomaly can have the form of a positive peak only, a negative peak only or a doublet consisting of both positive and negative peaks. Secondly, the single largest unknown is whether there is any remanent magnetisation and, if there is, its intensity and direction ($\boldsymbol{J}_r$) need to be ascertained. It must also be remembered that many geophysical interpretations may fit the observed data and that a given interpretation may not be unique (see Chapter 1, and Figure 1.1 in particular). For this reason, it is always useful to use other geophysical methods in the same area to help constrain the interpretations. If some geological information already exists for the area, then this should be used to help with the

geophysical interpretations. However, a word of warning: be careful that some geological information may itself be an interpretation and should not be considered to be the only solution. The geophysics may disprove the geological hypothesis!

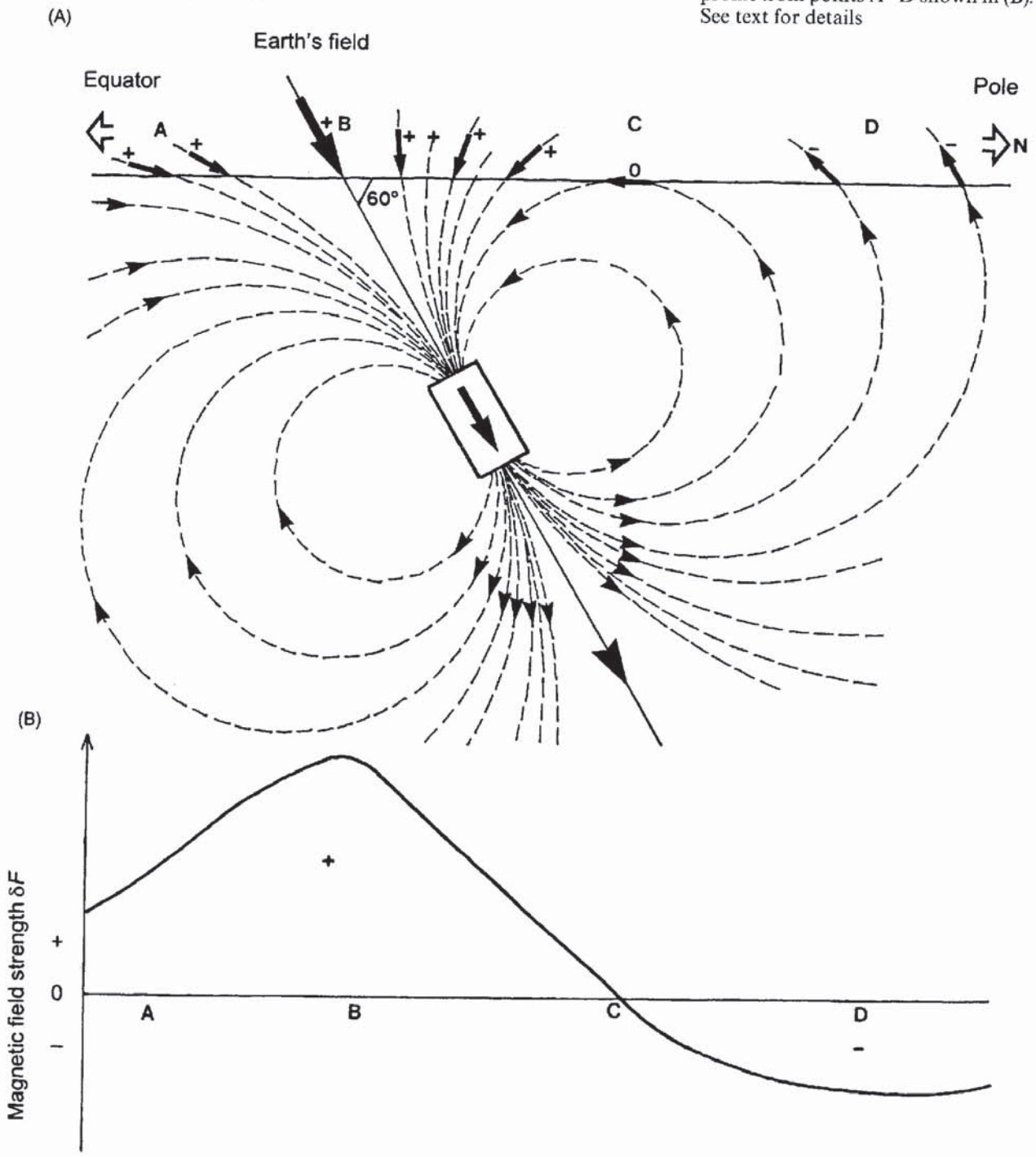

Figure 3.29 The magnetic field generated by a magnetised body inclined at 60° parallel to the Earth's field (A) would produce the magnetic anomaly profile from points A–D shown in (B). See text for details

A magnetisable body will have a magnetisation induced within it by the Earth's magnetic field (Figure 3.29A). As magnetisation is a vector quantity, the anomaly shape will depend on the summation of the vectors of the Earth's field $\boldsymbol{F}$ (with intensity $\boldsymbol{J}$) and the induced field ($\boldsymbol{J}_i$) from the sub-surface body and from any remanent magnetisation ($\boldsymbol{J}_r$). It can be seen from Figure 3.29 (A and B) how any magnetic anomaly is produced. The maximum occurs when the induced field is parallel to the Earth's field; the anomaly goes negative when the induced field vector is orientated upwards as at D. As the magnetic data have been corrected to remove the effect of the Earth's magnetic

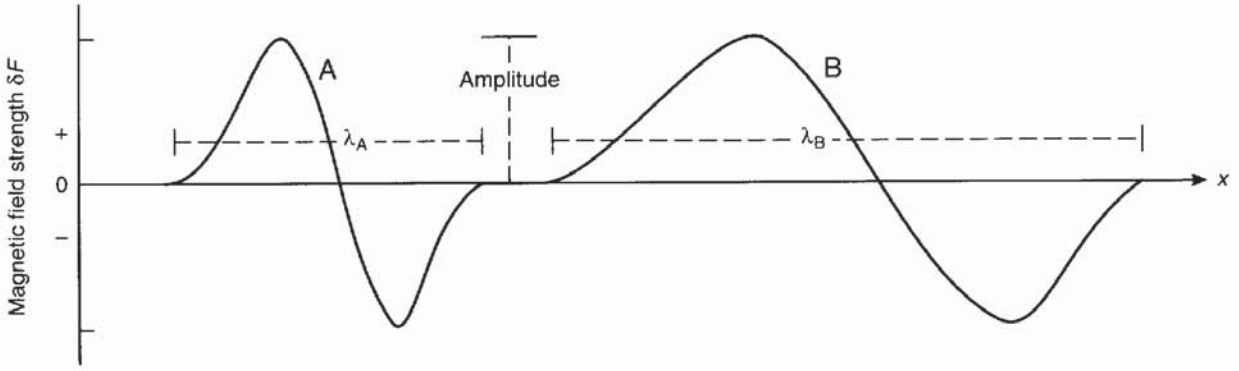

Figure 3.30 Two magnetic anomalies arising from buried magnetised bodies (see text for details)

Table 3.7 Guidelines to qualitative interpretation of magnetic profiles and maps

Applies to:	Magnetic character	Possible cause
Segments of a profile and areas of maps	Magnetically quiet Magnetically noisy	Low κ rocks near surface Moderate–high κ rocks near surface
Anomaly	Wavelength	Short ⇒ near-surface feature Long ⇒ deep-seated feature
	± amplitude	Indicative of intensity of magnetisation
Profile*	Anomaly structure† and shape	Indicates possible dip and dip direction Induced magnetisation indicated by negative to north and positive to south in northern hemisphere and vice versa in southern hemisphere; if the guideline does not hold, it implies significant remanent magnetisation present
Profile and maps	Magnetic gradient	Possible contrast in κ and/or magnetisation direction
Maps	Linearity in anomaly	Indicates possible strike of magnetic feature
Maps	Dislocation of contours	Lateral offset by fault
Maps	Broadening of contour interval	Downthrow of magnetic rocks

* Can be determined from maps also; † Structure = composition of anomaly, i.e. positive peak only, negative peak only or doublet of positive and negative peaks; κ = magnetic susceptibility

field, the anomaly will be due to the vectors associated with the source body. The sign convention is positive downwards, negative upwards. Where there is no remanent magnetisation, a magnetised body in the northern hemisphere will always have a negative anomaly on its northern side and a positive anomaly on its southern side. The opposite is true for the southern hemisphere.

For the two anomalies shown in Figure 3.30, anomaly A has a short wavelength compared with anomaly B, indicating that the magnetic body causing anomaly A is shallower than the body causing B. As the amplitude of anomaly B is identical to that of anomaly A, despite the causative body being deeper, this must suggest that the magnetisation of body B is much greater than for body A, as amplitude decreases with increasing separation of the sensor from the magnetised object.

Some general guidelines for the qualitative interpretation of magnetic profiles and maps are listed in Table 3.7, and an example in Figure 3.31. The list of guidelines should be used like a menu from which various combinations of parameters apply to specific anomalies. For instance, a short-wavelength high-amplitude doublet anomaly with negative to the north, and positive to the south, with an

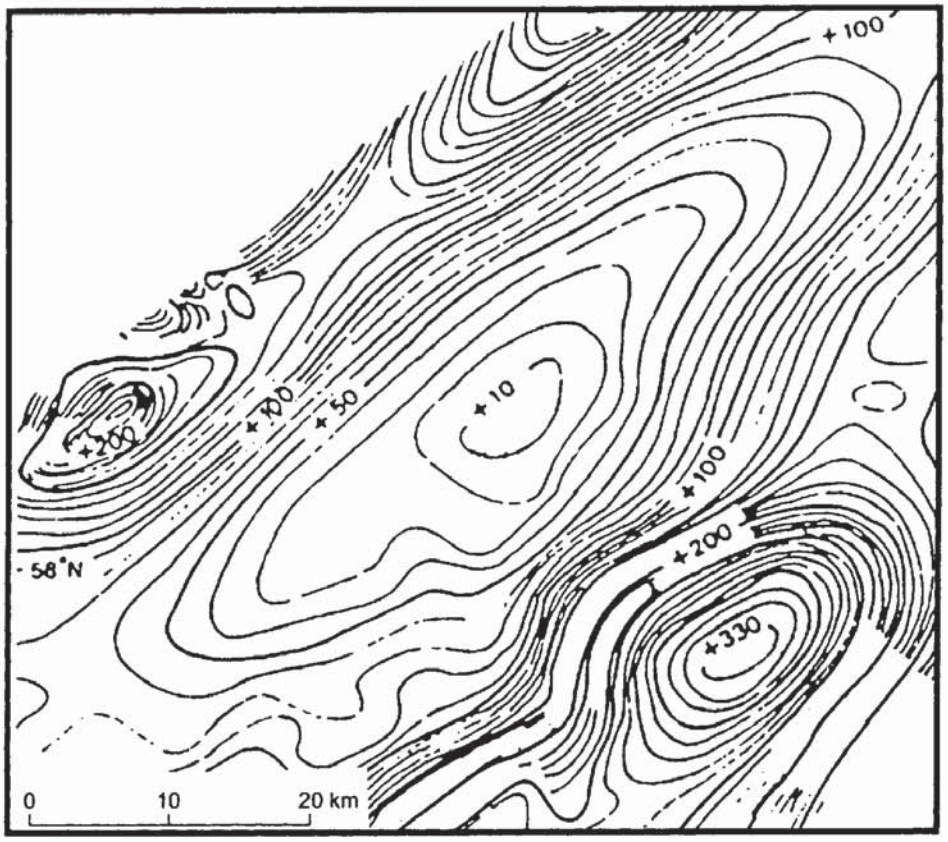

Figure 3.31 Magnetic anomaly map associated with a fault-bounded sedimentary basin with upthrown horst block to south-east – Inner Moray Firth, Scotland. After McQuillin *et al.* (1984), by permission

elongation in the east–west direction in the mid-latitudes of the northern hemisphere, suggests a near-surface, moderate-to-high susceptibility magnetic feature with induced magnetisation in a sheet-like body with an east–west strike and northerly dip.

3.7.1 Profiles

The simplest interpretation technique is to identify zones with different magnetic characteristics. Segments of the profile with little variation are termed magnetically 'quiet' and are associated with rocks with low susceptibilities. Segments showing considerable variation are called magnetically 'noisy' and indicate magnetic sources in the sub-surface. The relative amplitudes of any magnetic anomalies (both

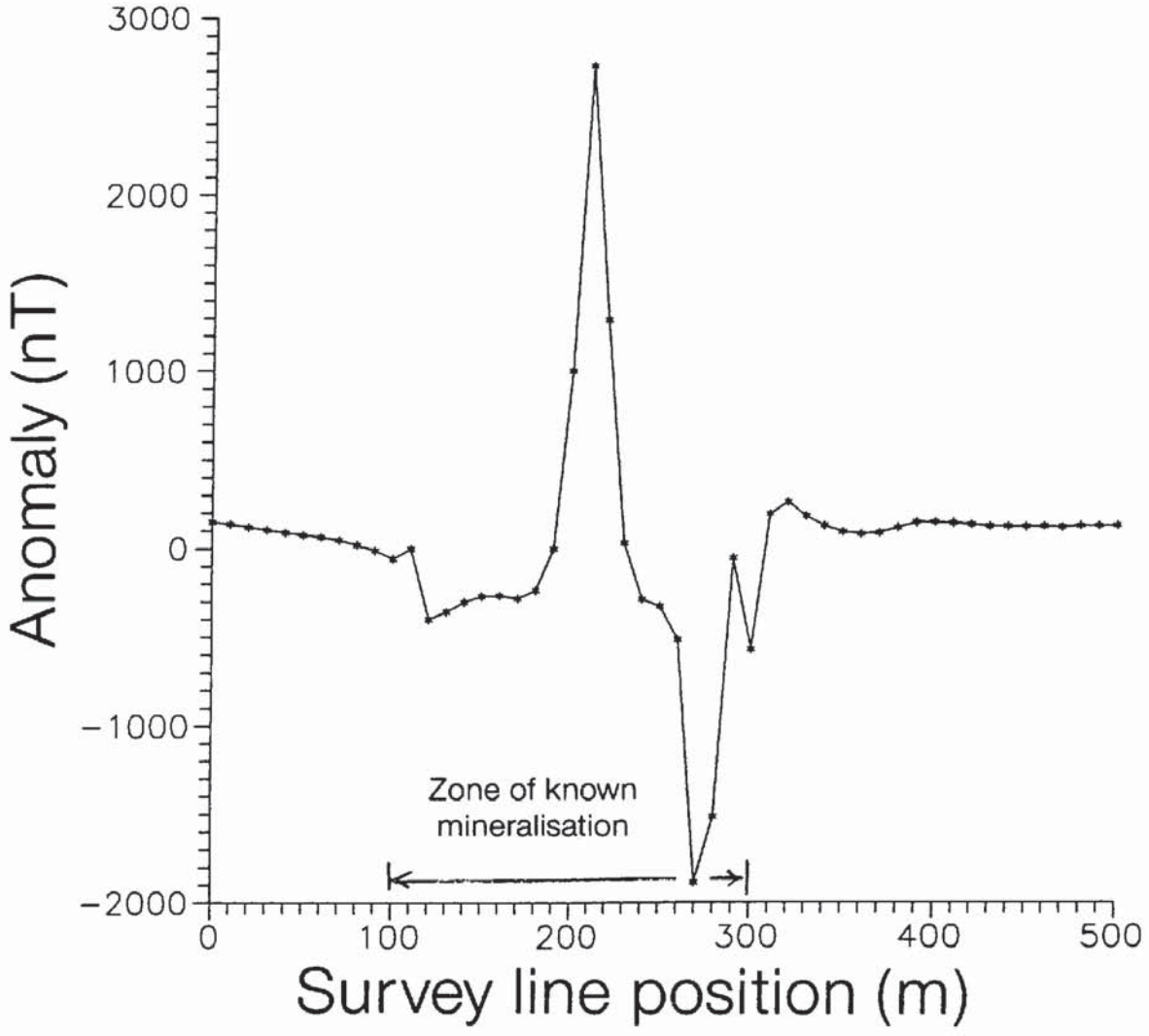

Figure 3.32 Magnetic zonation of a proton magnetiometer profile across Sourton Common, north Dartmoor, England

positive and negative) and the local magnetic gradients can all help to provide an indication of the sub-surface.

Figure 3.32 illustrates the differences between noisy and quiet zones in a profile over Sourton Tors, north Dartmoor, England, where the magnetically noisy segments indicate metalliferous mineralisation. The negative occurring as the northern part of the doublet indicates that there is little remanent magnetisation and that the anomaly is due largely to induction ($J_i \gg J_r$).

Figure 3.33 shows a profile measured at Kildonnan, Isle of Arran, Scotland, across a beach section over a series of vertical dolerite dykes. Two of the three dykes (A and B) give rise to large positive anomalies, while a third dyke (C) produces a broader low. All the dykes have virtually identical geochemistry and petrology and hence

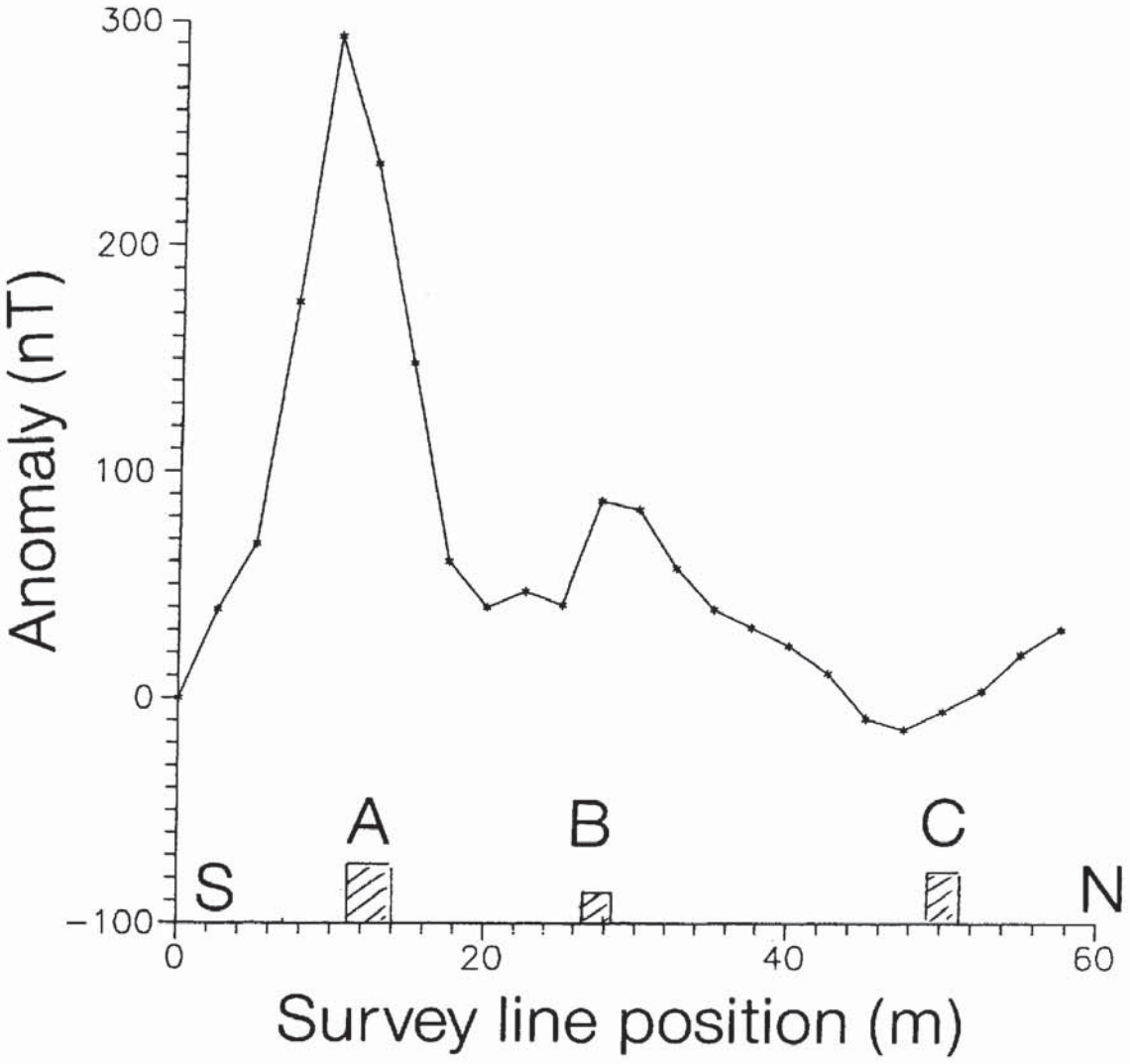

Figure 3.33 Proton magnetometer profile across three vertical dolerite dykes at Kildonnan, Isle of Arran, Scotland, which have been intruded during a period when the Earth's magnetic polarity changed

similar susceptibilities. The difference in magnetic character associated with dyke C compared with dykes A and B is attributed to there having been a magnetic reversal between the intrusion of dyke C relative to the other two. It is well known that in the British Tertiary Igneous Province, which includes the western isles of Scotland, a phase of doleritic intrusion occurred which lasted 10 million years and straddled a magnetic reversal (Dagley *et al.* 1978). Some dykes are normally magnetised and others have a reversed polarity. The different magnetic characters therefore provide a means of identifying which dykes were associated with which phase of the intrusion episode, whereas it is virtually impossible to make such an identification in the field on the basis of rock descriptions.

Having identified zones with magnetic sources, and possibly having gained an indication of direction of dip (if any) of magnetic

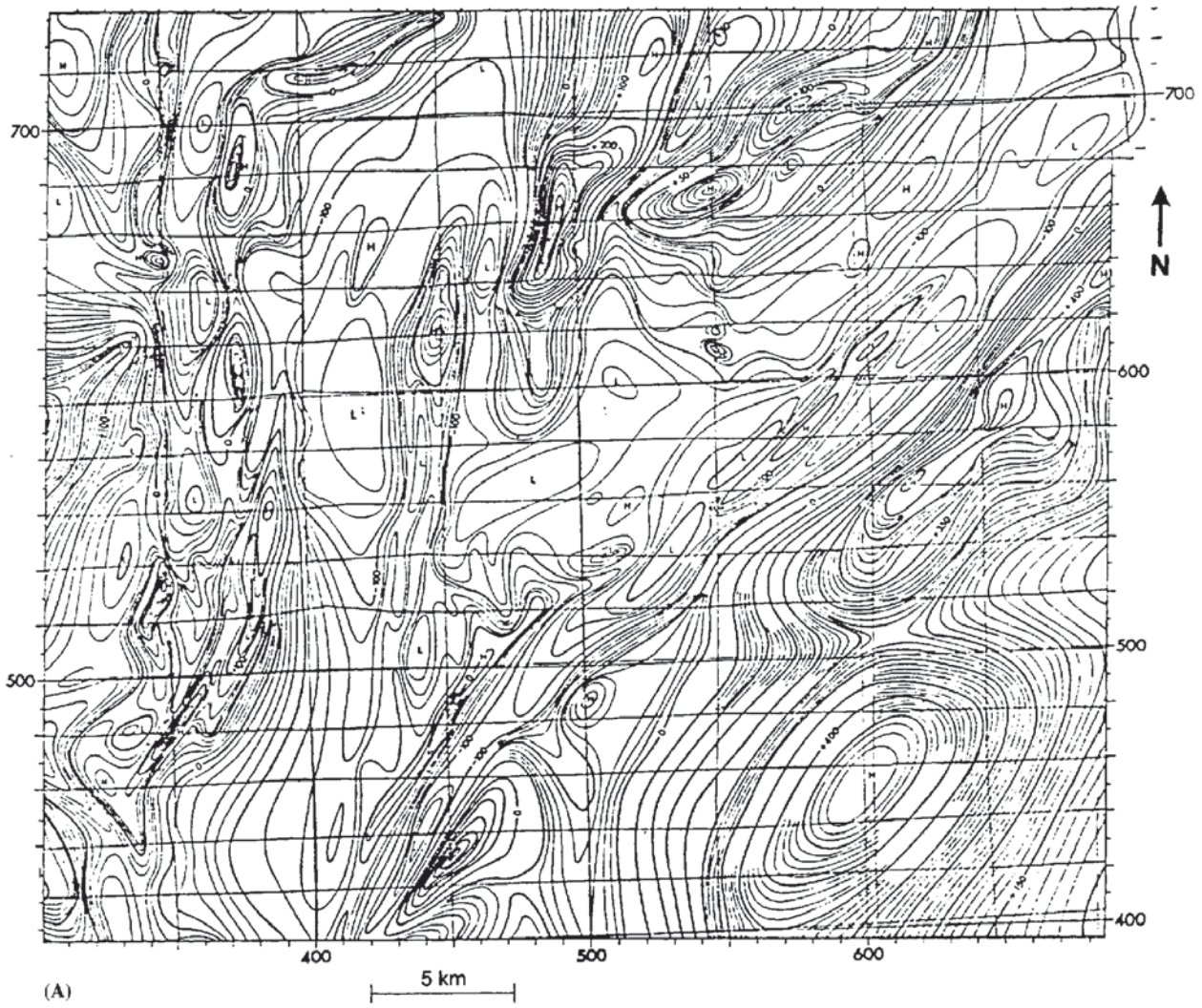

Figure 3.34 (A) Aeromagnetic map of the south-east part of the Shetland Islands, Scotland (Flinn 1977); (B) (*opposite*) zonation of (A) in terms of magnetic characteristics

targets and relative intensities, either more detailed fieldwork can be undertaken to obtain more information and/or the existing data can be interpreted using quantitative methods (see Section 3.8).

3.7.2 Pattern analysis on aeromagnetic maps

Magnetic data acquired over a grid with no spatial aliasing are displayed as contoured maps, as three-dimensional isometric projections, or as image-processed displays (see Section 3.8.3). The various displays can be interpreted in terms of the guidelines in Table 3.7. Commonly, even such a basic level of interpretation can yield important information about the sub-surface geology very quickly. One major advantage of airborne surveys is that they can provide information about the geology in areas covered by water.

An aeromagnetic survey was acquired over the south-eastern part of the Shetland Islands, north-east Scotland, and described in detail by Flinn (1977). The original aeromagnetic data were extracted from part of a British Geological Survey map and are shown in Figure 3.34A. The corresponding pattern analysis for the same area is shown in Figure 3.34B and compares very well with Flinn's

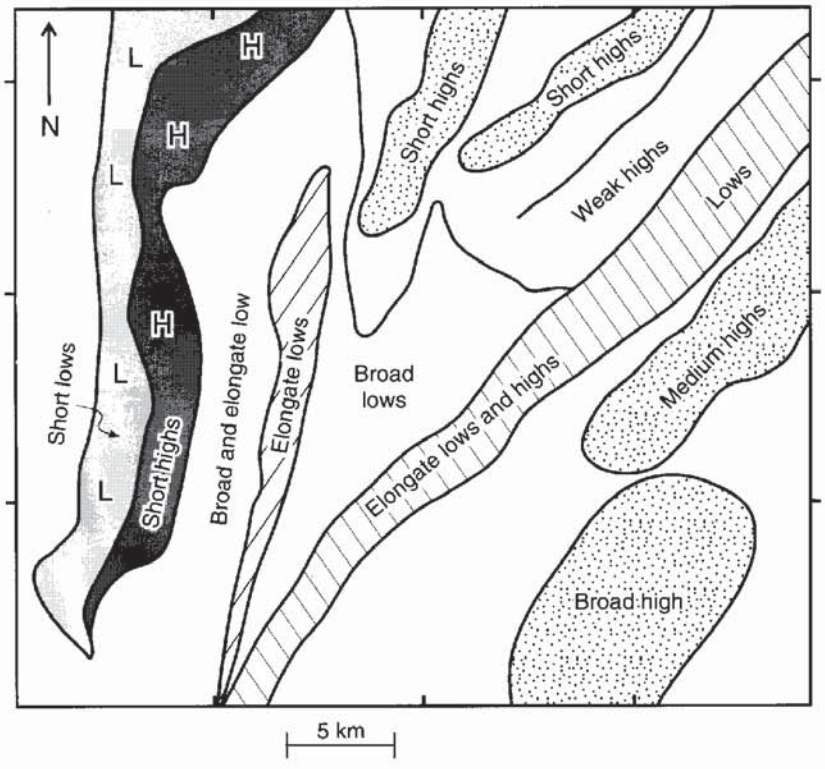

(B)

interpretation (Figure 3.35). Magnetic lows in band A are associated with psammites and migmatised psammites which have been heavily injected by pegmatite. The lows in band B correspond to gneissified semipelites and psammites intruded by granites and pegmatites. The short-wavelength but large-amplitude highs just east of band A are attributed to the magnetic pelitic schist and gneiss. In the central part of Figure 3.34A, truncation of NE–SW trending contours can be seen to be associated with the Whalsay Sound Fault. Other faults, such as the Lunning Sound Fault and the Nesting Fault, separate zones of differing magnetic character and lie parallel to the local aeromagnetic contours. A series of three localised positive highs in the south-east corner (h, i and j along the thrust beneath the Quarff Nappe;

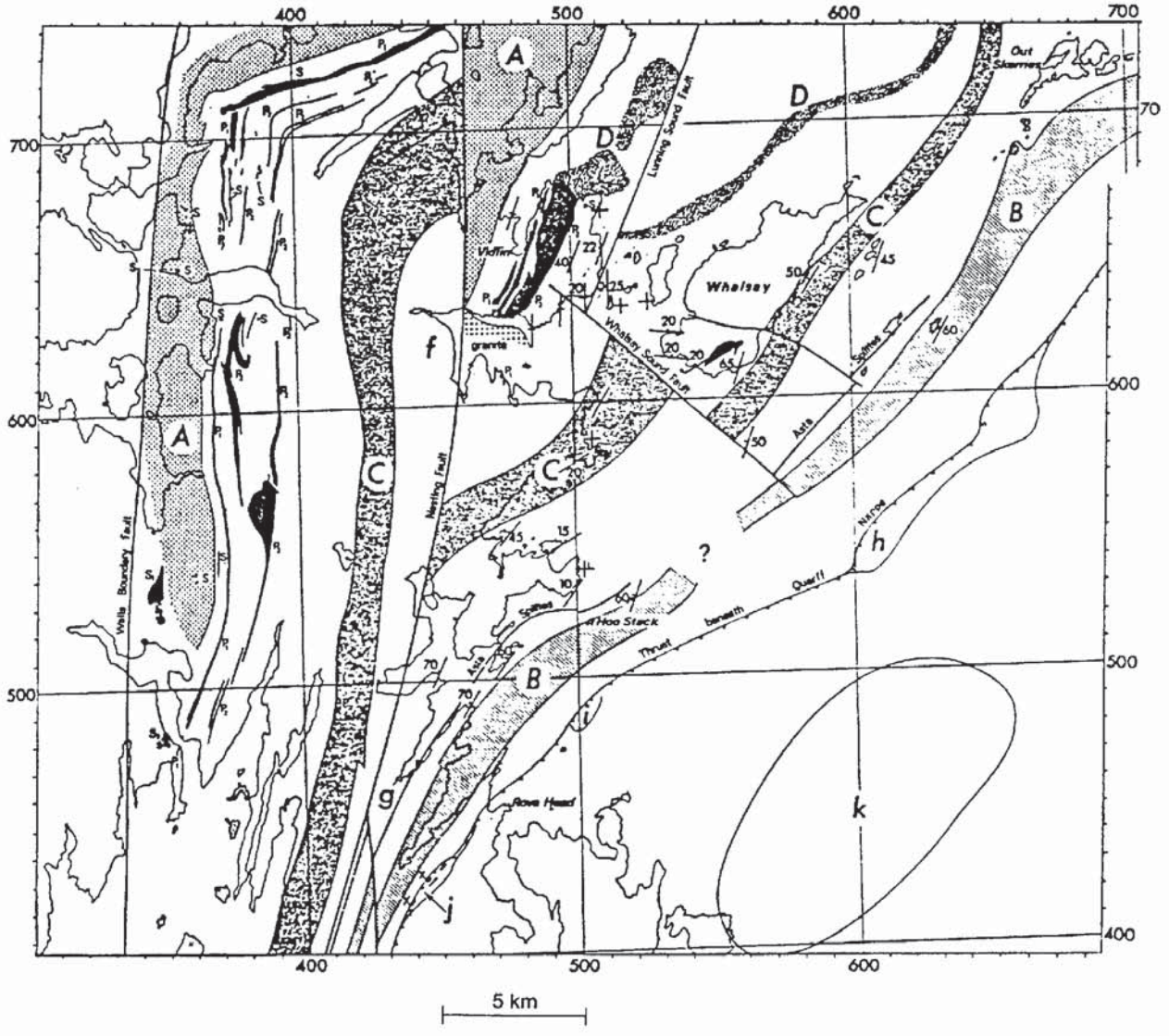

Figure 3.35 Geological interpretation of the aeromagnetic map shown in Figure 3.34 of the south-east part of the Shetland Islands, Scotland. From Flinn (1977), by permission

Figure 3.35) is thought to be due to phyllites with 4% hematite which in itself cannot explain the anomaly amplitudes. However, suitably orientated remanent magnetisation could account for these magnetic features. The large-amplitude anomaly (k) in the south-east corner is attributed to a large buried intrusive which is also evident on gravity data. However, this and similar anomalies in the vicinity with similar character all occur over sea and have not been sampled and so the exact nature of the rock remains unknown.

More detailed discussions on the interpretation of aeromagnetic maps have been given, for example, by Vacquier *et al.* (1951), Nettleton (1976) and Hinze (1985).

3.8 QUANTITATIVE INTERPRETATION

The essence of quantitative interpretation is to obtain information about the depth to a particular magnetic body, its shape and size, and details about its magnetisation in two possible ways. One is direct, where the field data are interpreted to yield a physical model. The other is the inverse method, where models are generated from which synthetic magnetic anomalies are generated and fitted statistically against the observed data. The degree of detail is limited by the quality and amount of available data and by the sophistication of either the manual methods or the computer software that can be used.

3.8.1 Anomalies due to different geometric forms

Just as with gravity data, magnetic data can be interpreted in terms of specific geometric forms which approximate to the shapes of sub-surface magnetised bodies. This tends to be true where profiles are to be interpreted only in terms of two dimensions. Three-dimensional models are far more complex and can be used to approximate to irregularly shaped bodies (see Section 3.8.3). Detailed mathematical treatments of the interpretation of magnetic data have been given by Grant and West (1965), Telford *et al.* (1990) and Parasnis (1986), among others.

The commonest shapes used are the sphere and the dipping sheet, both of which are assumed to be uniformly magnetised and, in the simplest cases, have no remanence. Total field anomalies (δF) for various types of model are illustrated in Figures 3.36–3.39; except where otherwise stated, the field strength is 50 000 nT, inclination $I = 60°$, declination $D = 0°$, and susceptibility $\kappa = 0.05$ (SI).

In the example of a uniformly magnetised sphere (Figure 3.36), the horizontal and vertical components are shown in addition to the total field anomaly. The anomalies associated with vertical bodies of various thicknesses are shown in Figure 3.37. The anomaly produced by a 50 m thick vertical dyke (Figure 3.37A) is both wider and has

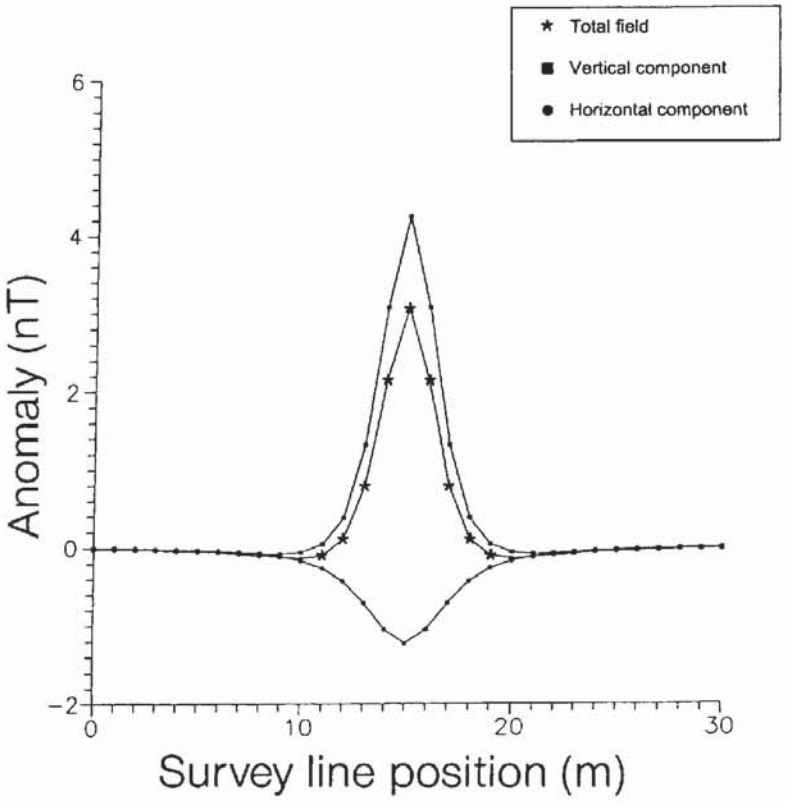

Figure 3.36 Horizontal and vertical components and the total field over a uniformly magnetised sphere with a radius of 1 m and whose centre lies at 3 m depth at position $x = 15$ m

a significantly larger amplitude (830 nT) than that of the 5 m thick dyke (peak amplitude 135 nT). Notice also that the anomaly shape changes considerably with strike direction, from being a positive–negative doublet when the dyke is striking east–west (with the negative on the northern side) to being a single symmetric positive peak when the dyke strikes north–south. In all cases, when an inductively magnetised body of regular shape is orientated north–south, its anomaly is symmetric. For a 70 m thick, 400 m long magnetised slab with its top 30 m below ground, a symmetric M-shaped anomaly is produced with the strike in a north–south direction (Figure 3.37B). When striking east–west, the positive–negative doublet is stretched to form an inflection in the middle; again the negative is on the northern side.

The effects on anomaly shape caused by changing the depth to the top of a vertical magnetised dyke are illustrated in Figure 3.38. With increasing depth, the anomaly decreases in amplitude and widens. At any given latitude, the anomaly shape will also be affected by any dip (α) of a sheet-like body, such as the inductively magnetised sheet (5 m thick) striking east–west (dip direction is towards the north) indicated in Figure 3.39. With zero dip, the body behaves like a thin horizontal slab with its northern edge off the scale of the figure.

If one end of a thick horizontal slab is sufficiently far enough away from the other, the model effectively becomes a vertical boundary separating two contrasting magnetic media (Figure 3.40A). The anomaly produced when the boundary strikes east–west has a significantly larger field strength (peaking around 1870 nT) than when in the other orientation. Furthermore, the single peak is effectively the positive peak of Figure 3.37C isolated from its negative partner.

The direction and degree of dip of a fault plane in a magnetised body also has a distinctive anomaly shape (Figure 3.40B). The negative anomaly is associated with the downthrown side. The anomaly shape is very similar to half of the M-shaped anomaly in Figure 3.37B.

Anomalies produced over a near-semicylindrical low-susceptibility body within magnetised basement, to simulate a buried rock valley

(A)

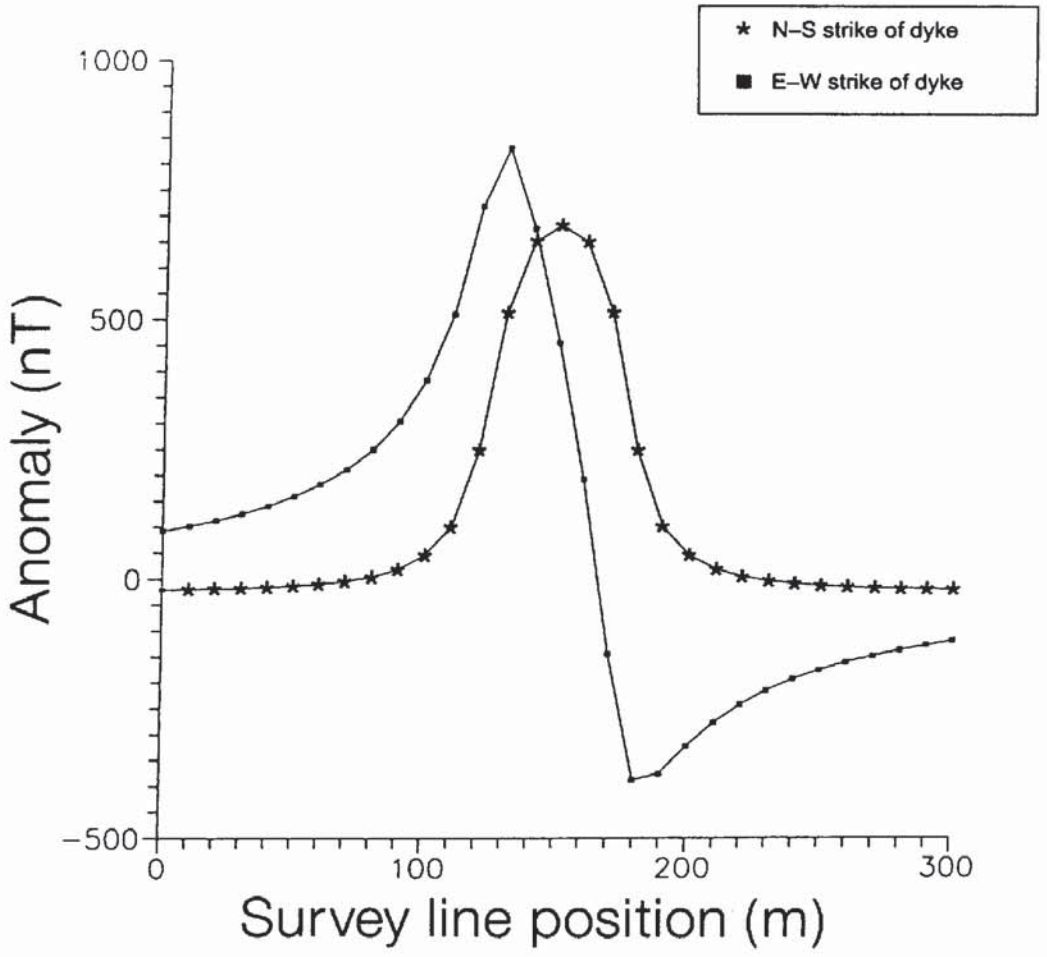

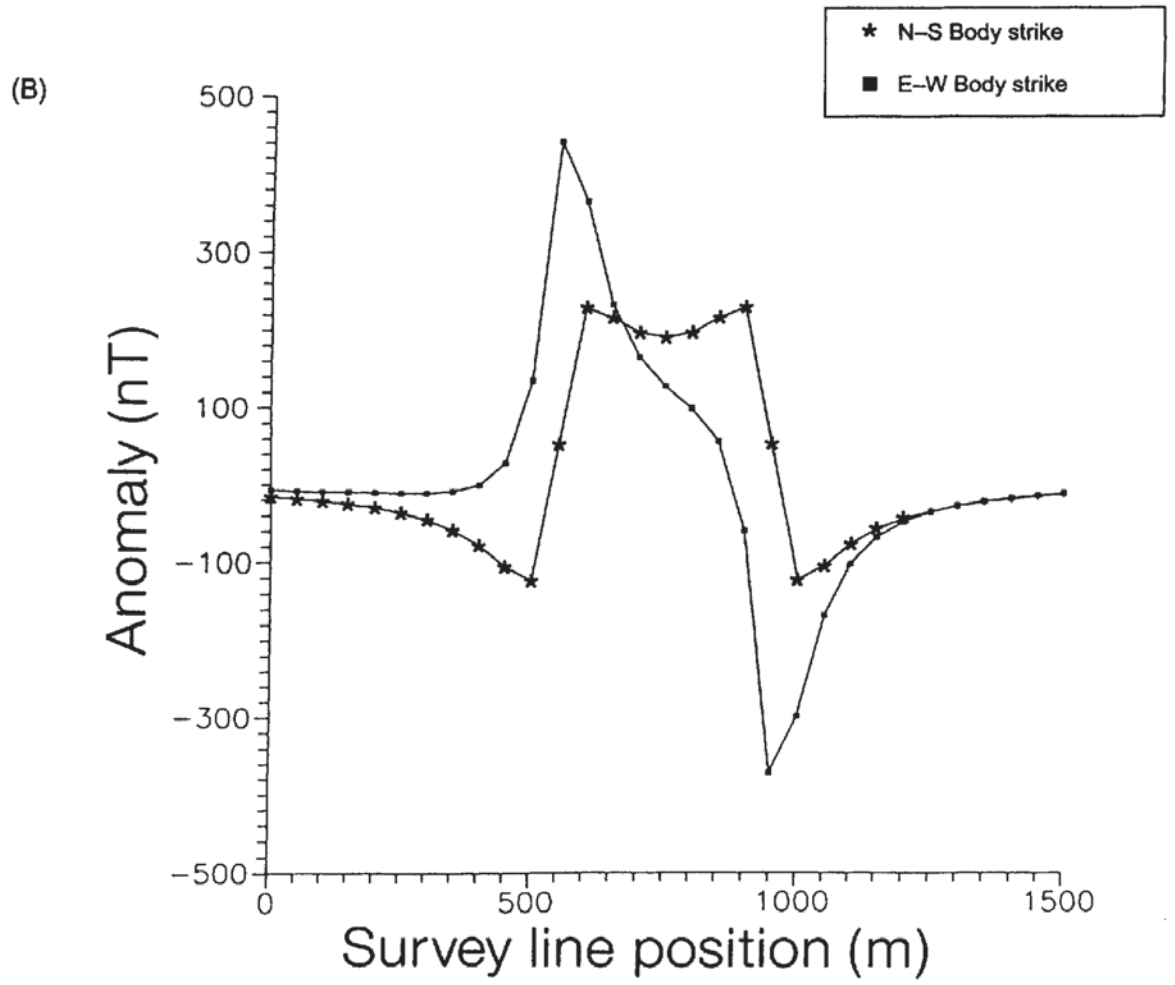

Figure 3.37 Total field anomalies over a vertical sheet-like body. (A) (*previous page*) 50 m and (B) 400 m wide. In (A), the magnetic anomaly arising from a 5 m wide body is given for comparison

infilled by sediments in magnetic bedrock, are shown in Figure 3.41. The symmetric anomaly is obtained when the semicylinder is orientated north–south. When this body is orientated north–south, the negative anomaly is on the southern side and so can be distinguished from the anomaly over a thin vertical dyke. Furthermore, the minimum anomaly amplitude is far greater in the case of the low-susceptibility semicylinder than for a vertical dyke.

One of the largest effects on anomaly shape for a given geological structure is latitude. Anomalies in the northern hemisphere over a 5 m thick dyke dipping at 45° to the north decrease in amplitude (partly a function of the reduced field strength towards the magnetic equator) and the negative minimum becomes more pronounced (Figure 3.42A). If the same geological structure exists at different latitudes in the southern hemisphere, this trend continues (Figure 3.42B) but with the slight growth of the now northern positive anomaly. These curves

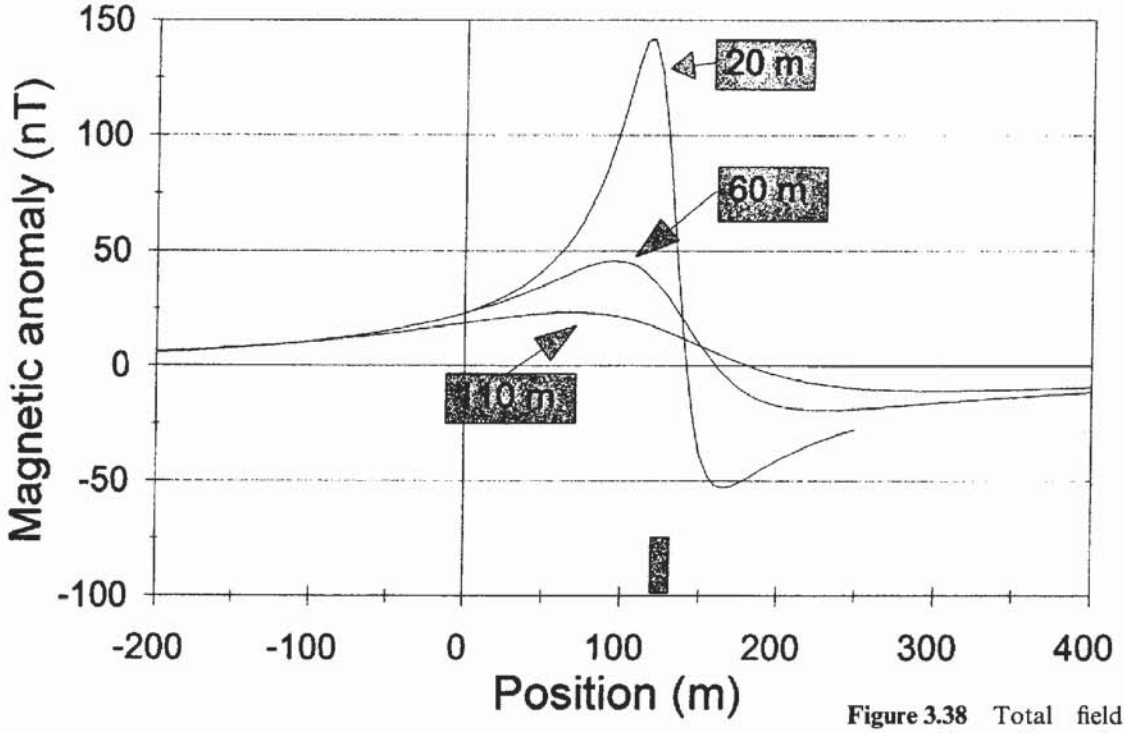

Figure 3.38 Total field anomalies over a 10 m wide vertical sheet-like body orientated east–west and buried at depths of 20 m, 60 m and 110 m; the position of the magnetised body is indicated

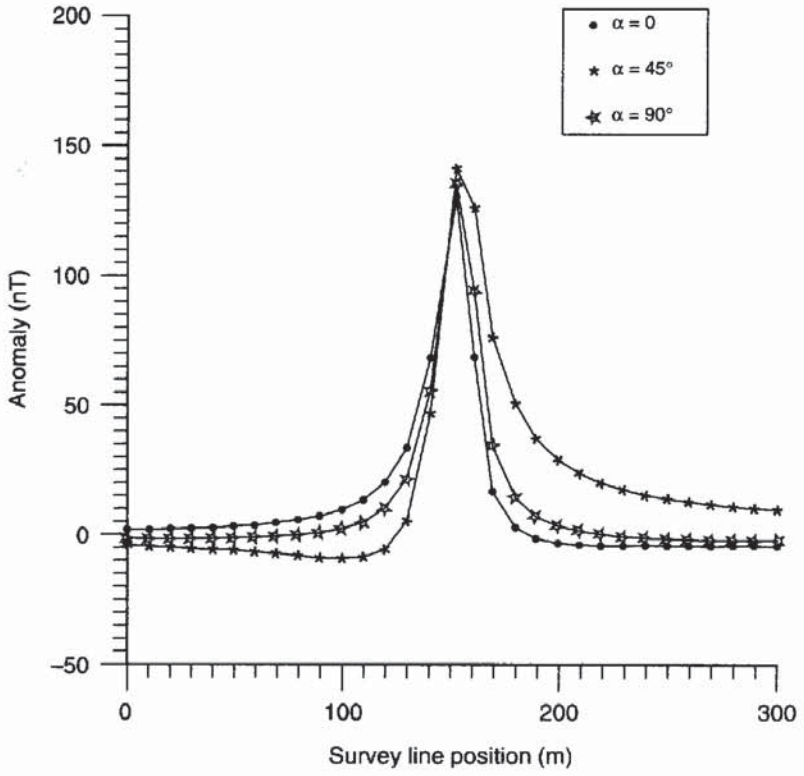

Figure 3.39 Total field anomalies over a thin dyke (5 m wide) dipping to the north at angles from $\alpha = 90°$ to $\alpha = 0°$; body strike is east–west

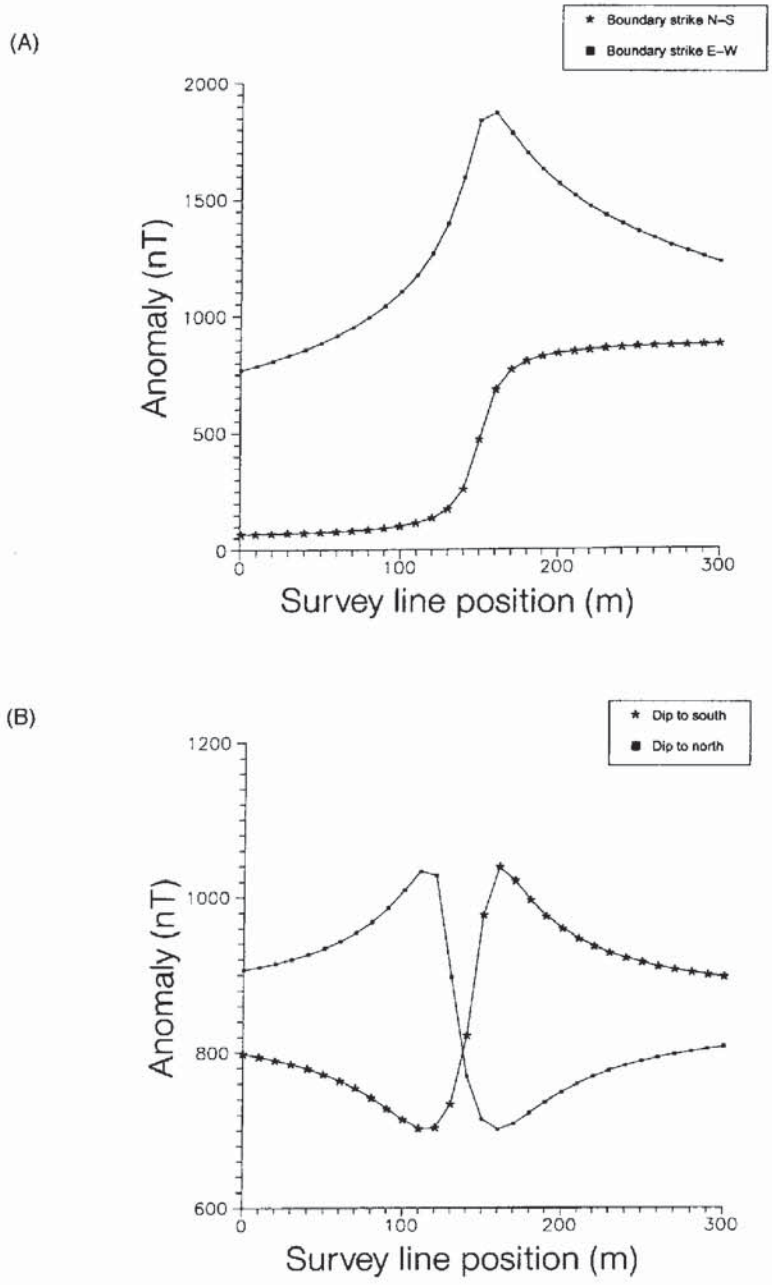

Figure 3.40 Total field anomalies over (A) a vertical contact between contrasting magnetised bodies, and (B) over a fault plane dipping at 45° to the south and to the north for a north–south fault strike direction

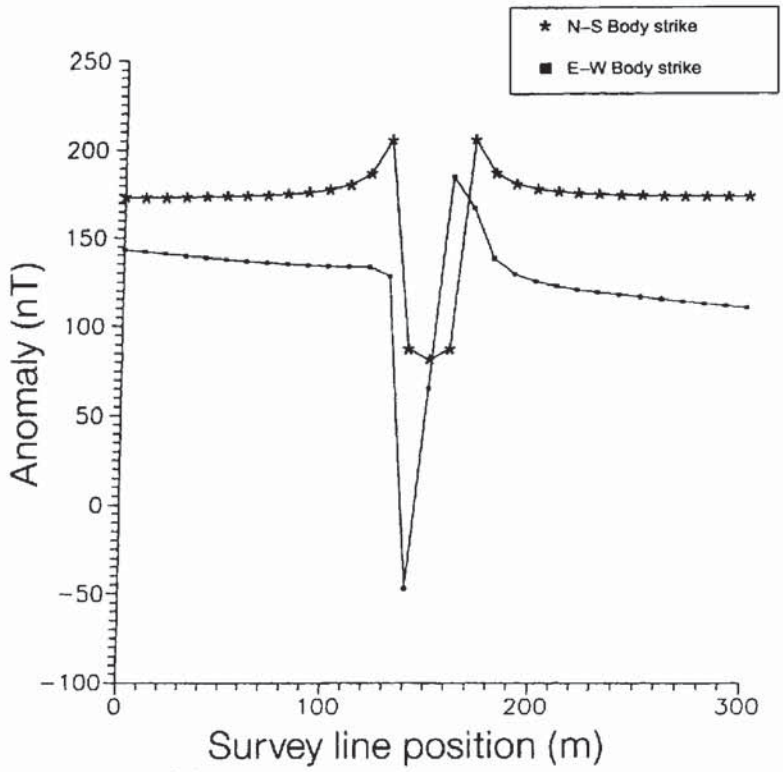

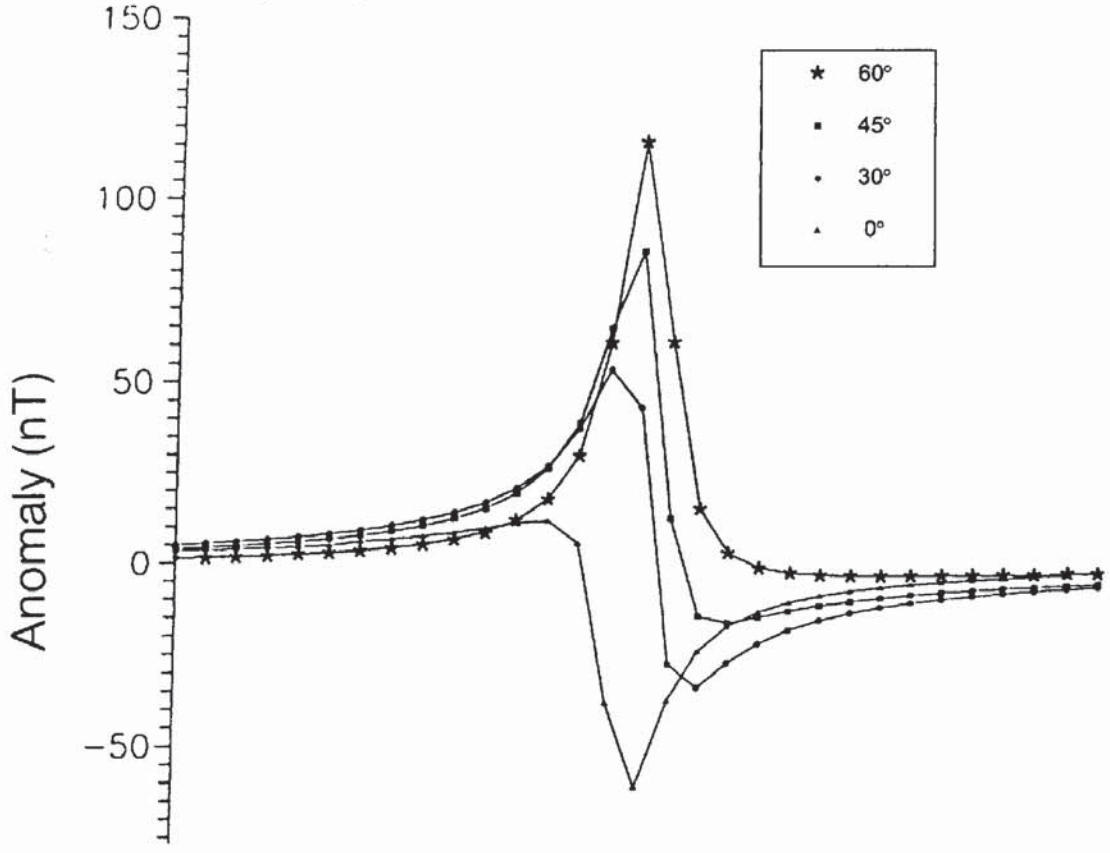

Figure 3.41 Total field anomalies over a semicylindrical body of low susceptibility within a magnetised basement

were calculated along the 0° Greenwich meridian where the field strengths in the southern hemisphere are significantly less than at equivalent latitudes in the northern hemisphere. Profiles along other lines of longitude would produce anomalies of similar shapes but with different amplitudes. It is also worth remembering that a given geological model, which produces a significant magnetic anomaly at one latitude and strike direction, may produce only a negligible anomaly at a different latitude and strike (Figure 3.42B) and so could be overlooked.

Figure 3.42 Total field anomalies over a 5 m thick dyke dipping at 45° to the north with an east–west strike direction but with different magnetic inclinations along the 0° Greenwich Meridian, with (A) (*previous page*) the northern hemisphere, and (B) (*below*) the southern hemisphere, taking into account changes in magnetic field strengh with latitude. (C) (*next page*) The total field anomaly for a vertical dyke but at two different magnetic latitudes and directions to illustrate how the magnetic anomaly over a magnetised body can become insignificant by only changing the magnetic latitude (inclination) and strike direction

(B)

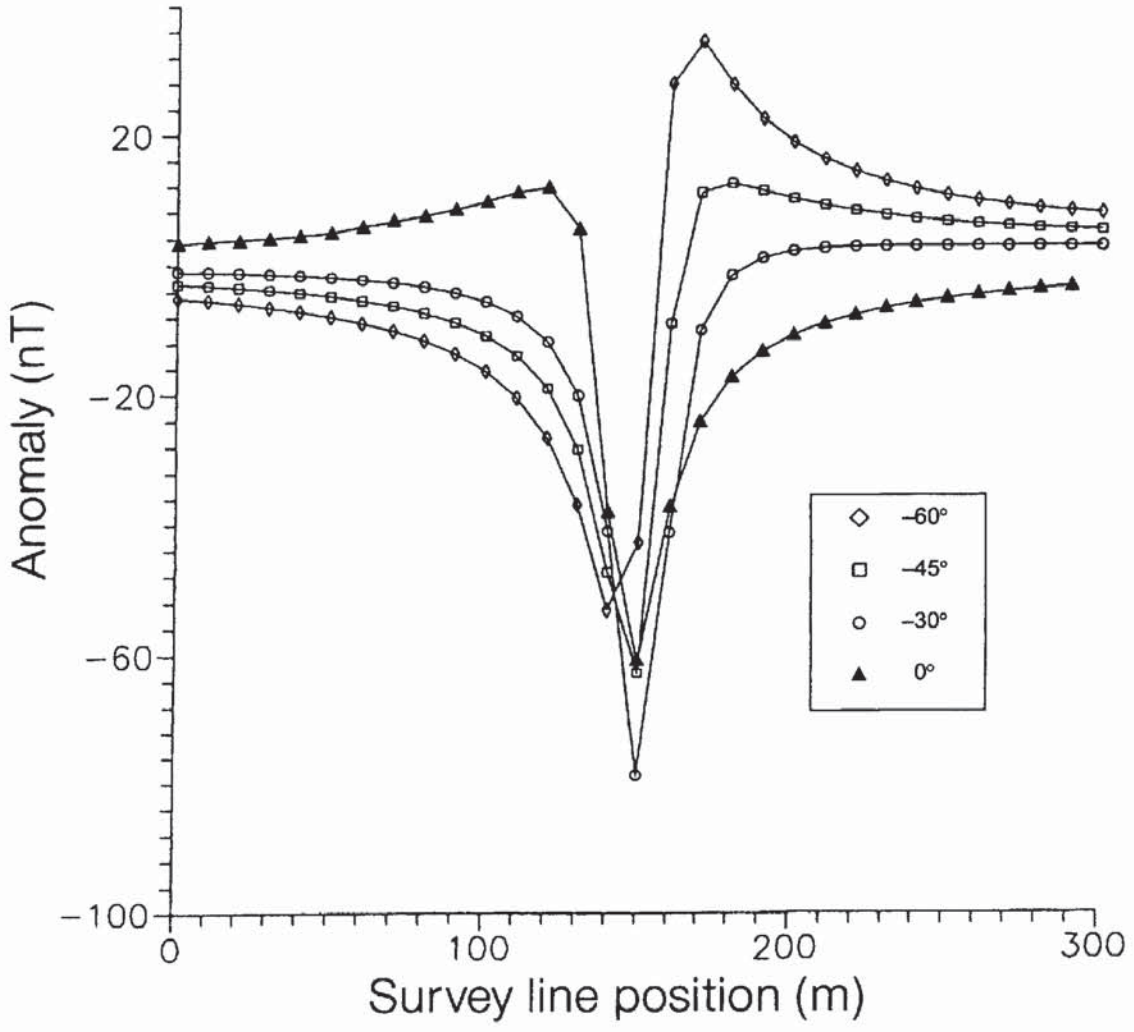

(C)

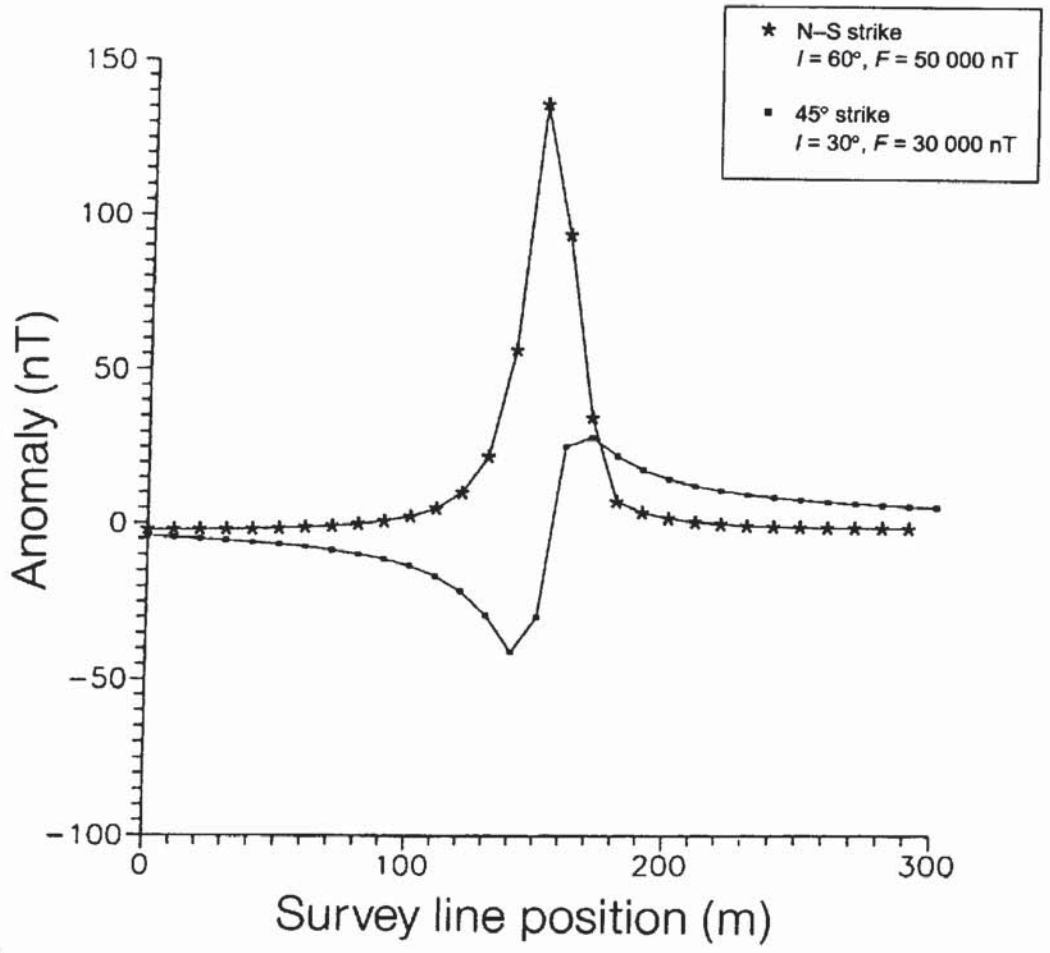

In all the above cases, it was assumed that there was no remanent magnetisation, yet if present, it can affect the shape of an anomaly significantly (Green 1960). In Figure 3.43, four profiles are illustrated, one where there is no remanent magnetisation, and three others where the intensity of remanent magnetisation is constant at 0.12 A/m (giving a strength of 150 nT). A schematic vector diagram is shown to illustrate the effects of remanence and the significance of the vertical component in high magnetic latitudes ($>45°$). When the direction of permanent magnetisation is antiparallel to the Earth's field (A), the resultant amplitude is $F'_a (\ll F)$, so the anomaly amplitude is substantially reduced. In the case B, where the remanent magnetisation is at right-angles to the Earth's field, the resultant F'_b ($<F$) has a smaller vertical component than F and so the amplitude is slightly reduced. In

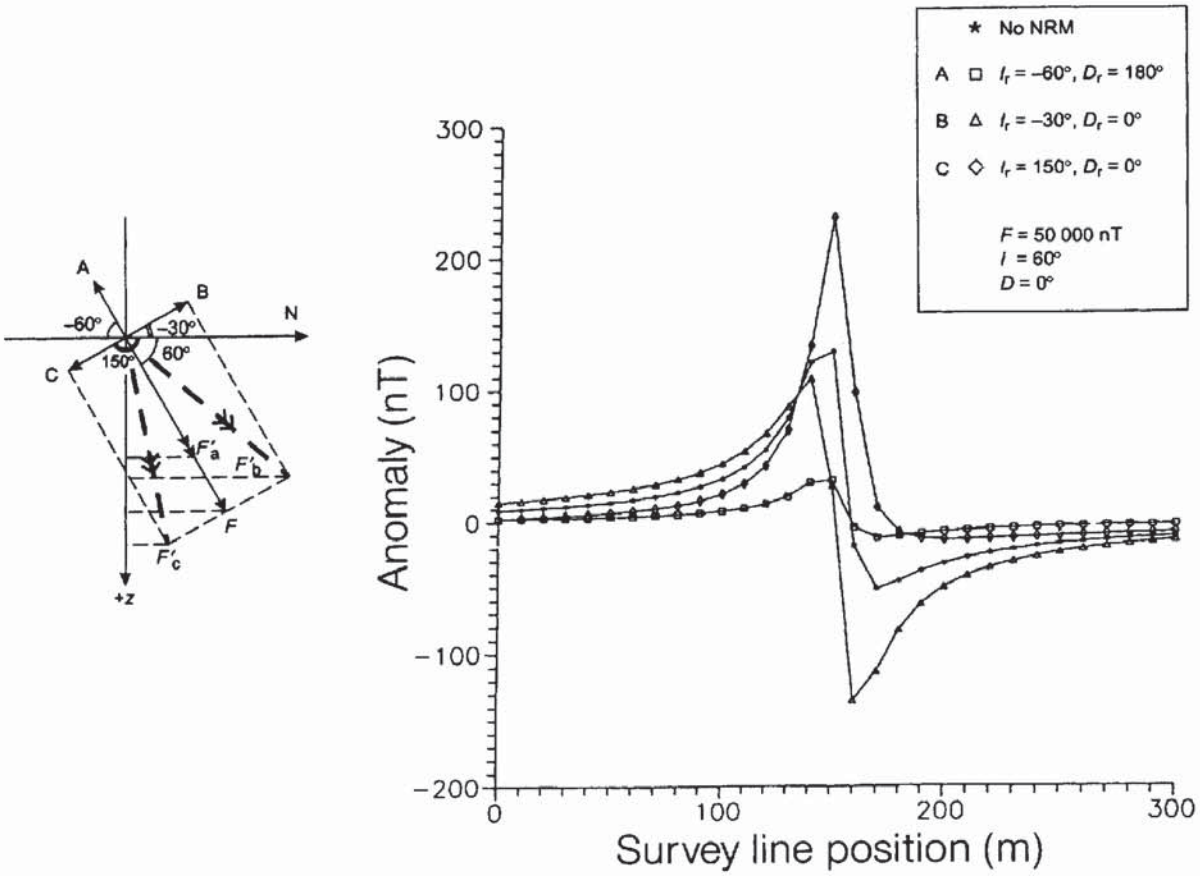

Figure 3.43 Total field anomalies over a vertical dyke striking east-west with either no remanent magnetisation (*), or remanent magnetisation of 150 nT in three directions as indicated by the schematic vector diagram

case C, where the remanent magnetisation is also at right-angles to the Earth's field but has the same positive downwards sense, F'_c, although the same magnitude as F'_b, has a larger vertical component than even the Earth's field and so the anomaly amplitude is increased substantially. In low magnetic latitudes ($<45°$), the horizontal vector component becomes more important than the vertical component when considering remanent magnetisation.

A range of different anomaly shapes demonstrating the effects of strike, latitude, dip, depth and body size has been provided above for comparison. When a field profile is to be interpreted, there is usually some background information available about the local geology (how else was the survey designed?). Consequently, many of the variables can be constrained so that a reasonable interpretation can be produced. The biggest unknown in many cases is the presence or otherwise of any remanance. Commonly it is assumed to have no effect unless found otherwise from measurements of remanence of

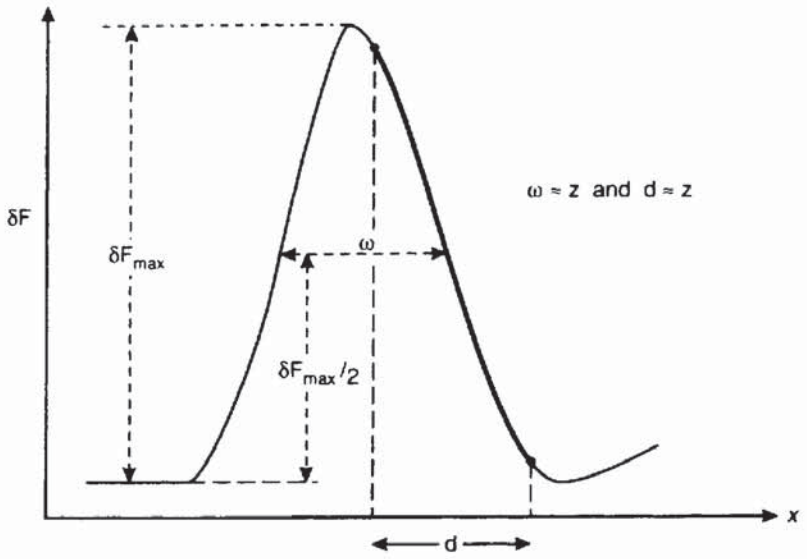

Figure 3.44 Simple graphical methods to estimate the depth to the top of a magnetised body

retrieved rock samples. However, to obtain a more exact interpretation it is necessary to model the observed data using computer methods (see Section 3.8.3).

3.8.2 Simple depth determinations

It is possible to obtain a very approximate estimate of depth to a magnetic body using the shape of the anomaly. By referring to either a simple sphere or horizontal cylinder, the width of the main peak at half its maximum value ($\delta F_{max}/2$) is very crudely equal to the depth to the centre of the magnetic body (Figure 3.44). In the case of a dipping sheet or prism, it is better to use a gradient method where the depth to the top of the body can be estimated. The simplest rule of thumb to determine depth is to measure the horizontal extent, d, of the approximately linear segment of the main peak (Figure 3.44). This distance is approximately equal to the depth (to within $\pm 20\%$).

A more theoretically based graphical method was devised by Peters (1949) and is known as Peters' Half-Slope method (Figure 3.45). A tangent (Line 1) is drawn to the point of maximum slope and, using a right-angled triangle construction, a line (Line 2) with half the slope of the original tangent is constructed. Two further lines with the same slope as Line 2 are then drawn where they form tangents to the anomaly (Lines 3 and 4). The horizontal distance, d, between these two tangents is a measure of the depth to the magnetic body (see Box 3.8).

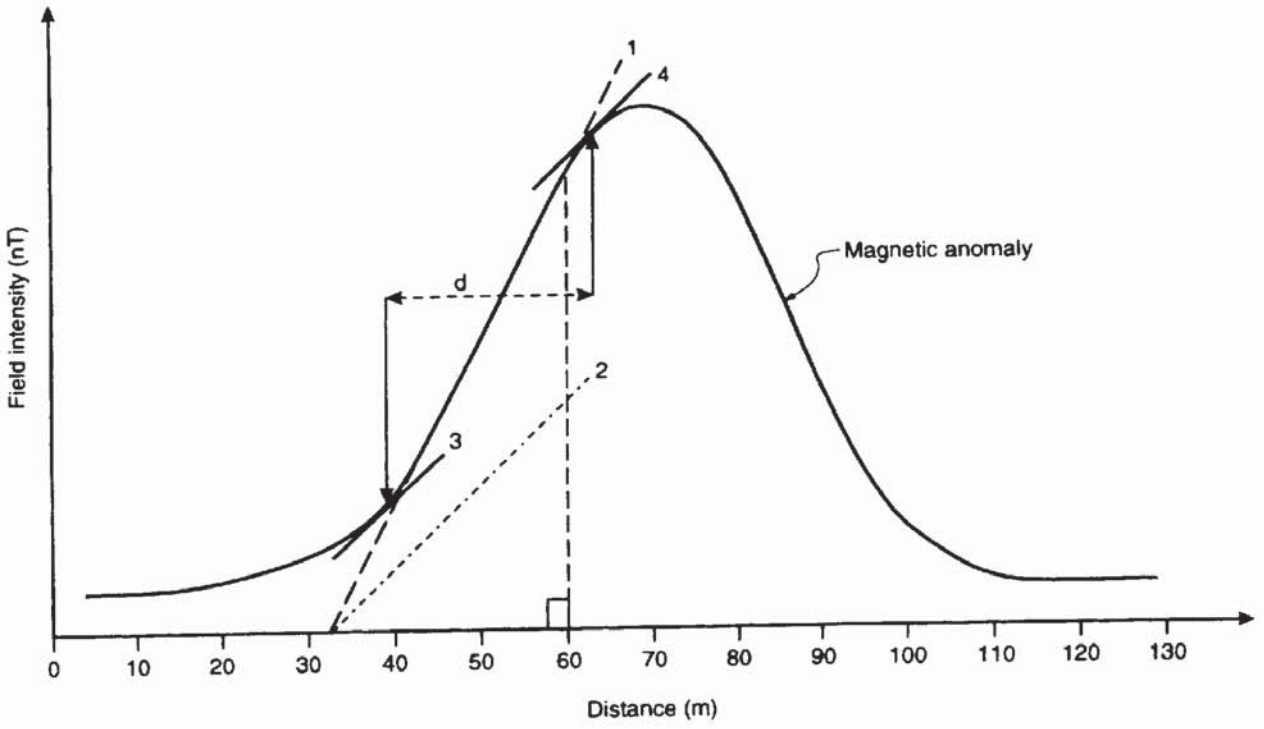

Figure 3.45 Peters' Half-Slope method of determining the depth to the top of a magnetised dyke (see text for further details)

Box 3.8 Peters' Half-Slope method of depth determination (see Figure 3.45)

The depth (z) to the top of the magnetised body is:

$$z = (d \cos \alpha)/n$$

where d is the horizontal distance between half-slope tangents; $1.2 \leqslant n \leqslant 2$, but usually $n = 1.6$; α is the angle subtended by the normal to the strike of the magnetic anomaly and true north.

Example: If $d = 24$ m, $n = 1.6$ and $\alpha = 10°$, then $z \approx 15$ m.

Parasnis (1986) derived alternative methods of depth determination for a magnetised sheet of various thicknesses and dips using the anomaly shape as well as amplitude. Given an asymmetric anomaly (Figure 3.46) over a dipping dyke of known latitude, dip and strike directions, the position of, and the depth to, the top of the dyke can be determined from the anomaly shape. If the maximum and minimum *numerical* values are denoted δF_{max} and δF_{min} respectively (i.e. irrespective of sign), the position of the centre of the top edge of the dyke is

located at the position of the station where the anomaly amplitude equals the sum of the maximum and minimum values (taking note of their respective signs, positive or negative) and which lies between the maximum and minimum values. For example, if $\delta F_{max} = 771\,nT$ and $\delta F_{min} = -230\,nT$, the position of the centre of the dyke would be located where $\delta F = 771 - 230\,nT = 541\,nT$. Expressions from which the depth to the top of the dipping sheet can be derived (see Box 3.9) relate the amplitudes of the minimum and maximum values and their respective separations. Expressions for thick dipping sheets and other models are much more complicated

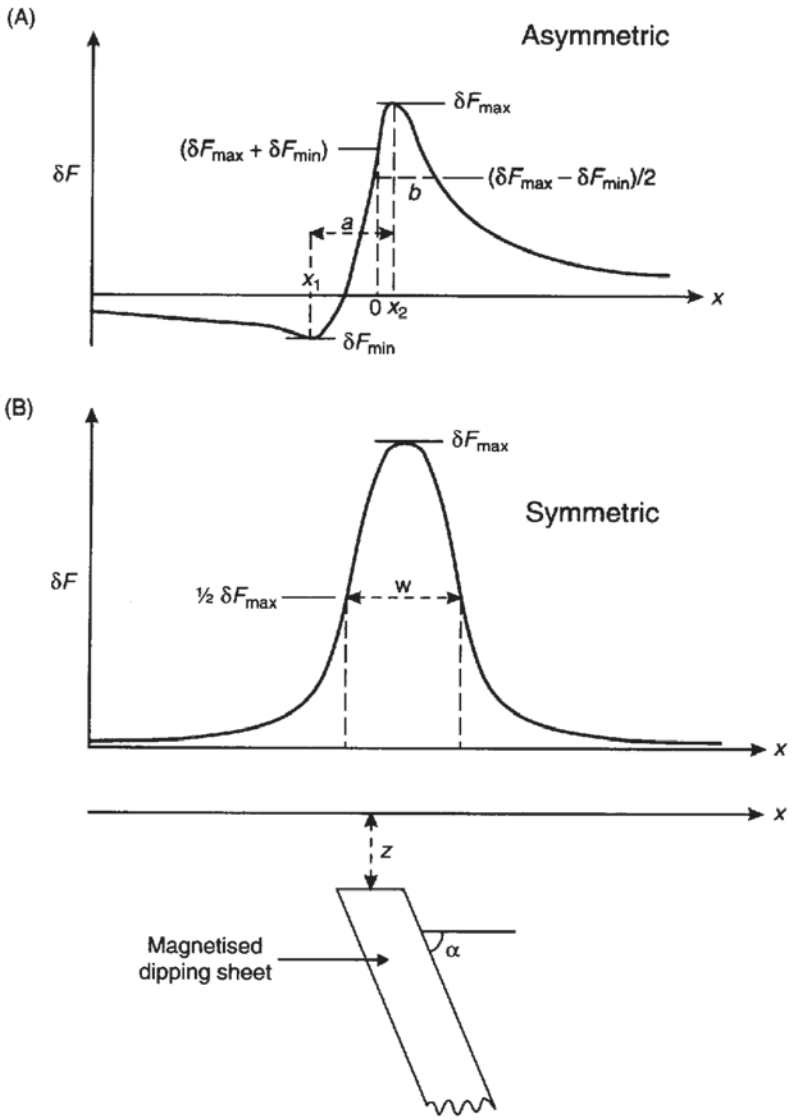

Figure 3.46 Parasnis' method of determining the position of the centre of, and the depth to the top of, a magnetised thin sheet. (A) An asymmetric profile, and (B) a symmetric profile

to calculate and are not discussed further here. Derivations of mathematical expressions and full descriptions of methods to determine shape parameters for a variety of dipping sheet-like bodies have been given by Gay (1963), Åm (1972), Parasnis (1986) and Telford *et al.* (1990), for example. Manual calculation of parameters has been largely superseded by the ease with which computer methods can be employed.

Box 3.9 Depth estimations (see Figure 3.46 for definitions of parameters)

Thin sheet (depth to top of body z)

Asymmetric anomaly:

$$z = (-x_1 . x_2)^{1/2} (x_1 \text{ or } x_2 \text{ is negative})$$

$$\text{and } z = (a^2 - b^2)^{1/2} . |C|/2.(1 + C^2)^{1/2}$$

where $1/C = \tan(I + i - \alpha)$; $|C|$ is the magnitude of C; I = inclination of the Earth's magnetic field; i = inclination of any remanent magnetisation; and α = angle of dip of the sheet.

Symmetric anomaly:

$$z = w/2$$

where w = anomaly width at $\delta F_{max}/2$.

3.8.3 Modelling in two and three dimensions

Manual calculations of depths to the top of a particular magnetised body may provide an approximate figure provided an individual anomaly can be isolated from the background adequately. One common problem is when two magnetised bodies are so close to each other spatially that their magnetic anomalies overlap to form a complex anomaly (Figure 3.47). Sometimes such an anomaly may be misinterpreted as being due to a much thicker body with lower susceptibility than the actual cause, and so gives rise to an erroneous interpretation. Geological control may help, but having the ability to generate models quickly by computer is a great boon. 'What if...?' models can be constructed to test to see what anomaly results if different configurations of magnetised bodies are considered. A basis for many computer programs was provided by Talwani *et al.* (1959) and Talwani (1965). In essence, two-dimensional modelling requires that the body being modelled has a lateral extent at least 20 times its width so that the end effects can be ignored. For many geological features this restriction is adequate and anomalies from such bodies can be analysed successfully. In

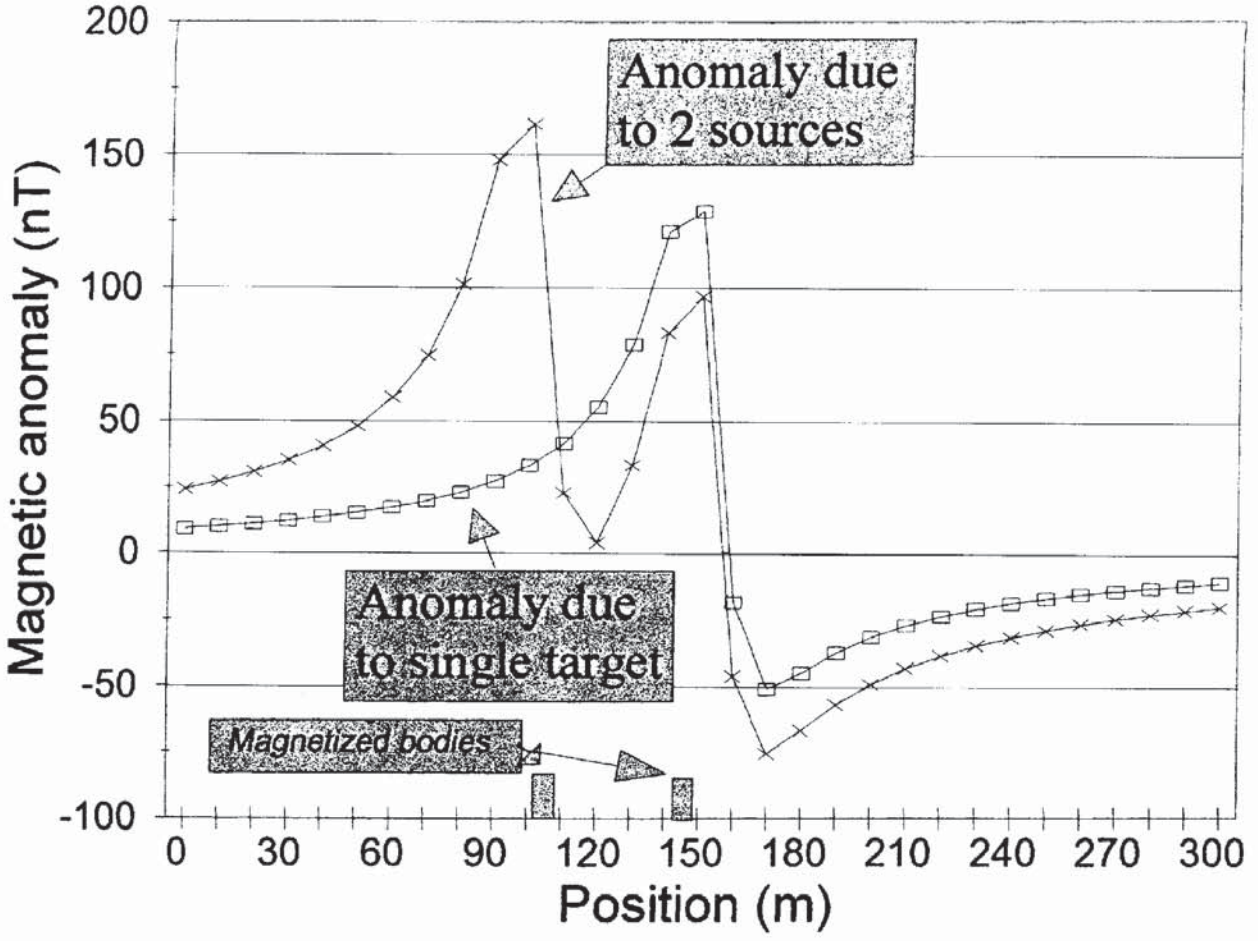

Figure 3.47 Total magnetic anomalies over two identical 5 m wide vertical dykes whose centres are separated by 45 m (their locations are indicated), and in contrast, the magnetic anomaly arising from just one of the dykes (at position 145 m), ignoring the other

many other cases, it is necessary to use more sophisticated computer methods.

With any set of profile data and the analysis of anomalies, it is absolutely essential that there be sufficient data to image the correct shape of the anomaly. Too few data leads either to incorrect evaluation of amplitude maxima or minima (consider the effects on simple depth determinations if the peak positions are not adequately defined), or in more extreme cases to severe aliasing (see Chapter 1). Limitations can be caused by too few field data values and/or by computer models producing too few point values at too large a station interval. It is therefore essential that, if computer methods are to be employed, the user is aware of what the software is actually trying to do and how it does it, and that adequate field data, both in number of values and data quality, are used.

A wide variety of computer methods exist, ranging from simple two-dimensional packages that can be run on low-cost personal

computers and laptops, up to extremely sophisticated 2.5-dimensional and three-dimensional modelling packages on more powerful workstations. Two-and-a-half dimensional modelling is an extension of two-dimensional modelling but allows for end effects to be considered (e.g. Busby 1987). Some packages provide a statistical analysis on the degree of fit between the computer-generated anomaly and the observed data. Others allow successive iterations so that each time the software completes one calculation it generates better input parameters automatically for the next time round, until certain quality parameters are met. For example, a computer program may run until the sum of the least-squares errors lies within a defined limit.

One other factor that needs to be borne in mind with magnetic modelling is that some software packages compute the anomaly for each body and then sum them arithmetically at each station. This ignores the fact that adjacent magnetised bodies will influence the magnetic anomalies of the other bodies. Consequently, the computed anomalies may be over-simplifications; and even if statistical parameters of the degree of fit are met, the derived model may still be only a crude approximation. In the majority of cases involving small-scale surveys in archaeology or site investigations, these problems are not likely to be as significant.

Modelling in three dimensions permits the construction of irregularly shaped bodies made up of a stack of magnetised polygons and takes into account edge effects. An example of three-dimensional interpretation of magnetic (and gravity) data is given in Section 3.9.1.

In addition to the spatial modelling, another method of assisting interpretation is the use of spectral analysis. The magnetic field is expressed by Fourier analysis as an integral of sine and/or cosine waves each with its own amplitude and phase. In this, the amplitude or power spectrum is plotted as a function of wavelengths (from short to long), expressed in terms of wavenumber (1/wavelength). A number of methods exist to determine the power spectrum (e.g. Spector and Parker 1979; García-Abdeslem and Ness 1994). They attempt to isolate the regional field so that the residual anomalies can be identified. Once the frequency of the residuals has been determined, the dataset can be filtered to remove the regional field, thus facilitating the production of anomaly maps on which potential target features may be highlighted. It is also possible to produce susceptibility maps from this type of analysis. From the form of the Fourier spectrum, estimates of depth to the magnetised bodies can be made (Hahn *et al.* 1976). The power spectrum yields one or more straight-line segments, each of which corresponds to a different magnetised body. A recent example of such an analysis of aeromagnetic data associated with the Worcester Graben in England has been described by Ates and Kearey (1995). Further analysis of magnetic data in the wavenumber domain has been discussed by Xia and Sprowl (1992), for example.

3.8.4 Recent developments

There have been two important developments in the display and processing of magnetic data. Where a large dataset exists for a regional aeromagnetic survey, say, the data have been displayed conventionally as a contoured anomaly map. With the advent since the 1970s of image processing using computers, it is possible to digitise and process data recorded previously in analogue form. Instead of contouring, the area covered is divided into rectangular cells each of which is assigned a total field strength value. These cells are manipulated and displayed as individual pixels. The resultant display is a colour image with blue indicating negative anomalies and red the positive anomalies. Shades of colour indicate intensities, so dark red indicates a high-amplitude positive anomaly while deep blue a high-amplitude negative anomaly. Image-processing software analogous to that used to process satellite image data, such as Landsat, is used to analyse the aeromagnetic (or indeed gravity) data (Figure 3.48).

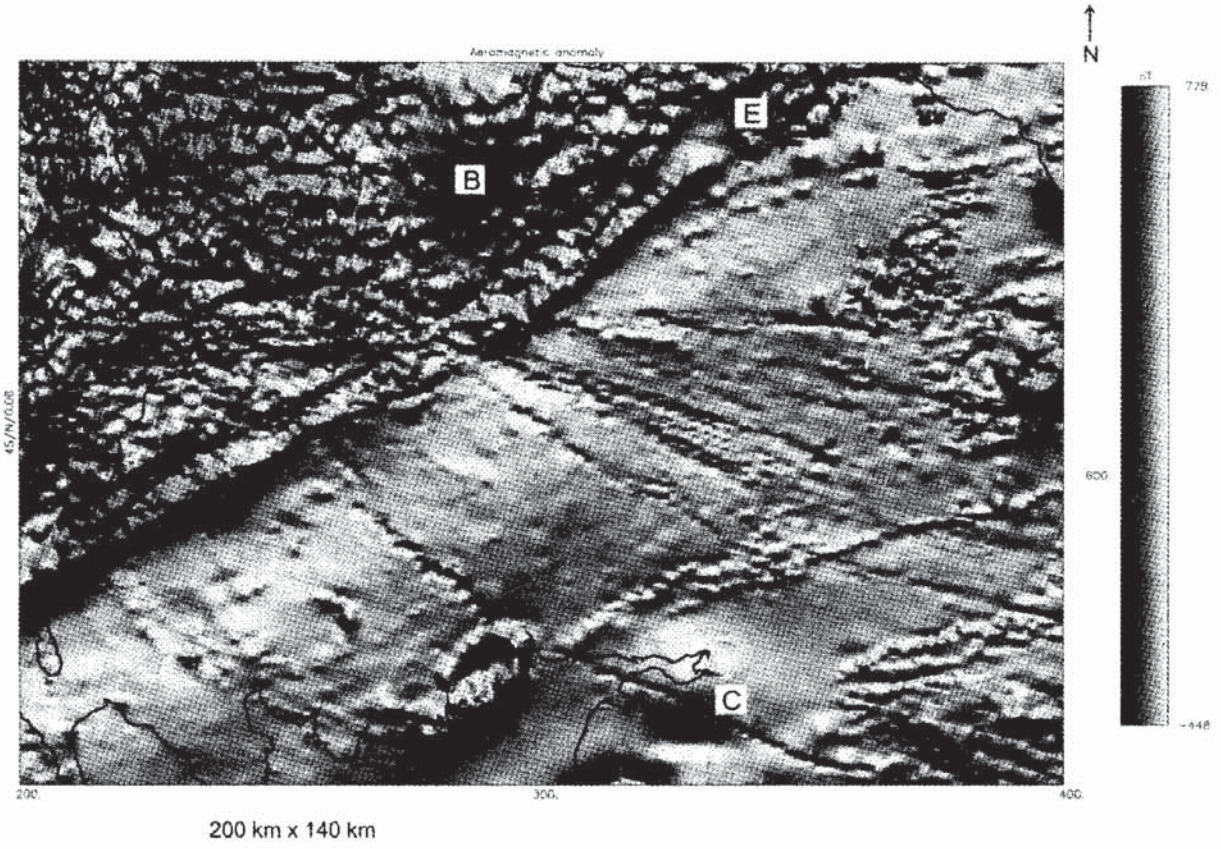

Figure 3.48 This image shows total field aeromagnetic data collected over an area of 200 km × 140 km of the Southern Uplands, Scotland (B: Bathgate; C: Carlisle; E: Edinburgh). The data were acquired in analog form along flight lines spaced approximately 2 km apart with tie lines about 10 km apart and with a mean terrain clearance of 305 m. The data were digitised, interpolated to a square grid of mesh size 5.0 km and displayed as a greyscale shaded-relief image. Sun illumination azimuth and inclination are N and 45° respectively. East–west lineations through the high-amplitude Bathgate anomaly are related to quartz-dolerite Permo-Carboniferous dykes. Numerous Teritiary dykes can be mapped trending NW–SE across the Southern Uplands. For comparison, see Figure 2.35. Image courtesy of Regional Geophysics Group, British Geological Survey

Lineaments suggestive of faults can be identified using edge filters. Spatial filters can be applied to resolve the data into regional and residual datasets and zoom facilities allow the accurate expansion of subsets of data for high-resolution analysis of much smaller areas, thus permitting the identification of any low-amplitude anomalies. Green (1983), for example, has discussed digital image processing in detail.

Image-processing methods need not be restricted to datasets covering very large areas. The only prerequisite for image processing to be possible is that there must be a large enough dataset. Dataloggers attached to magnetometers and memory-backed magnetometers or gradiometers can also be used for ground surveys where very high spatial discrimination is required (Sowerbutts and Mason 1984). Scollar *et al.* (1986) have reviewed the various data processing and display methods used in archaeology where very high resolution is also required.

Sowerbutts (1987) mapped the largely concealed Butterton Dyke in central England using a microcomputer-based fluxgate gradiometer. More than 16 800 magnetic measurements were made in one day by one person. Data were recorded at 0.5 m intervals along 317 parallel traverses 1 m apart and the results plotted as a contour map and as an isometric display (Figure 3.49). The lines of the olivine dolerite dykes are obvious. The survey produced an extremely accurate map of the dyke, which was totally concealed in the area of the survey, and demonstrated that the dyke was not terminated by a fault, as previously thought, but died out naturally.

Calculating depths to magnetic features is still the most significant aspect of magnetic surveys. Since Peters' classic paper in 1949 there has been a steady stream of publications describing new or modified methods of depth determination. In the 1980s, one technique, known as the Euler Deconvolution method, was developed to process magnetic data and convolve them to a point source at depth (Thompson 1982). The method operates on the data directly and provides a mathematical solution without recourse to any geological constraints. This has the advantage that the Euler-derived interpretation is not constrained by any preconceived geological ideas and thus can be used critically to appraise geological, and particularly structural, interpretations.

Euler's method utilises the magnetic field strength at any point in terms of the gradient of the total magnetic field, expressed in Cartesian coordinates. Furthermore, these gradients are related to different magnetic sources by a function termed the Structural Index, N. Euler's equation is given in Box 3.10. Considering the equation asterisked, a series of seven equations can be determined from observed data by evaluating this equation in at least seven places within a window placed on the data. This provides seven equations to solve for three unknowns using a least-squares procedure. The output

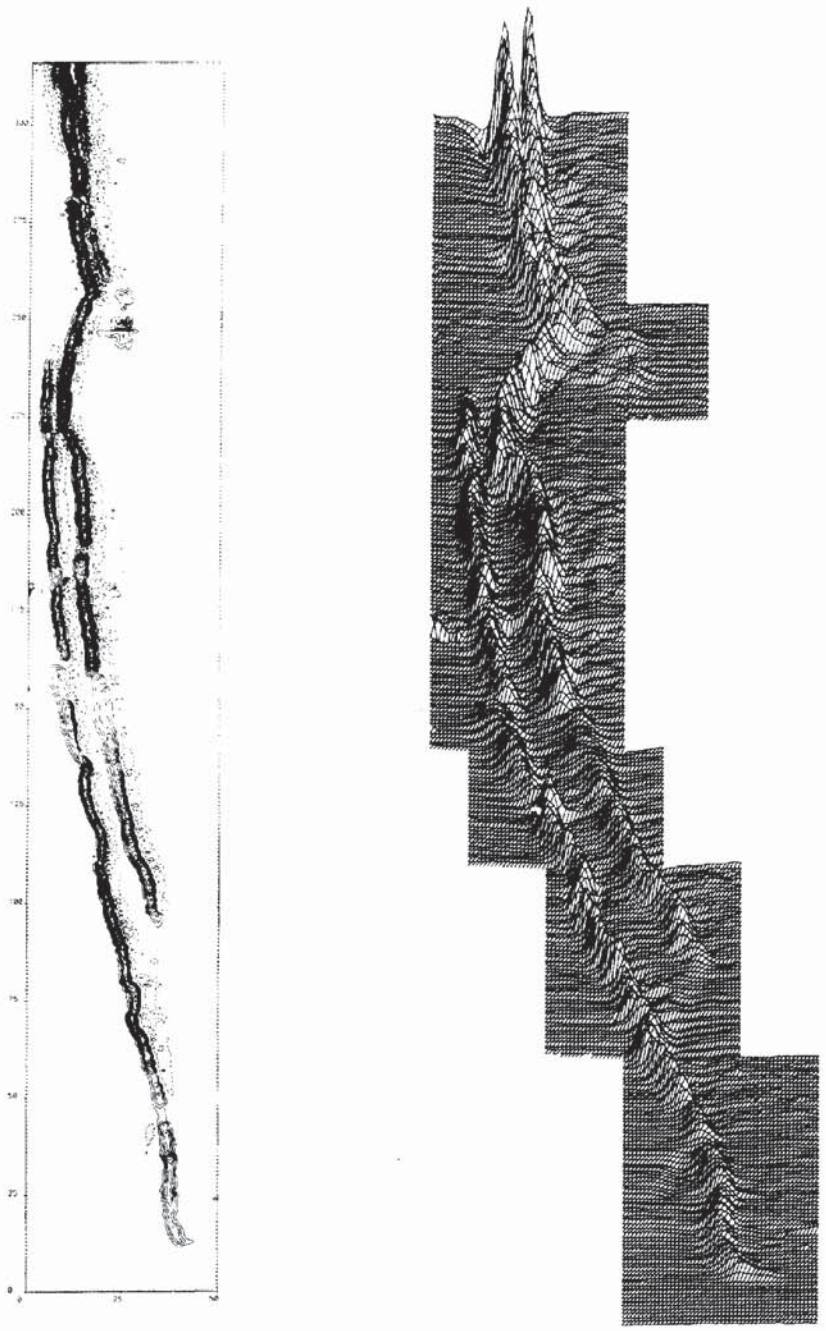

Figure 3.49 Butterton Dyke anomalies displayed as a magnetic gradient contour map with a contour interval of 20 nT/m (positives values, solid; negative values, dashed). From Sowerbutts (1987), by permission

consists of determinations of the depth to the magnetic body (z_0) producing the anomaly which can be plotted on a map as a circle, the increasing size of which indicates greater depth. Solutions that lie outside predetermined statistical bounds are rejected, thus constraining the possible number of solutions.

Box 3.10 Euler's equation

$$(x - x_0)\frac{\delta T}{\delta x} + (y - y_0)\frac{\delta T}{\delta y} - z_0\frac{\delta T}{\delta z} = N(B - T)$$

where x_0, y_0, z_0 are the coordinates of a magnetic source whose total field intensity T and regional value B are measured at a point (x, y, z); N is the degree of homogeneity and referred to as the Structural Index.

For two dimensions (x, z), Euler's equation reduces to:

$$x_0\frac{\delta T}{\delta t} + z_0\frac{\delta T}{\delta z} + NB = x\frac{\delta T}{\delta x} + NT\,(*)$$

The only unknowns are x_0, z_0 and N; gradients of T with respect to x and z can be derived from the measured magnetic data; $\delta T/\delta y$ is assumed to be equal to zero.

Structural indices N:

Vertical geological contact	Edge of large tank	0–<0.5
Infinite sheet		0
Thick step		0.5
Irregular sill	Metal sheet	1
Vertical cylinder	Well/drum	2–2.25
Cylinder with unknown orientation	Drum	2.5
Horizontal cylinder	Pipeline/drum	2–2.75
Point dipole		3
Sphere	Tank	3

Reid *et al.* (1990) have used Euler's method to aid the interpretation of an area in south-central England. A simplified geological map of the survey area is given in Figure 3.50 with the aeromagnetic survey data. The Euler solutions have been plotted in Figure 3.50C which has been interpreted to form a structural map shown in Figure 3.50D. The Euler display has picked out the two north–south striking boundary faults marking the central block. Depth solutions for the Eastern Boundary Fault were within 0.3 km of those derived by other means. The magnetic anomalies over the central block yield very few

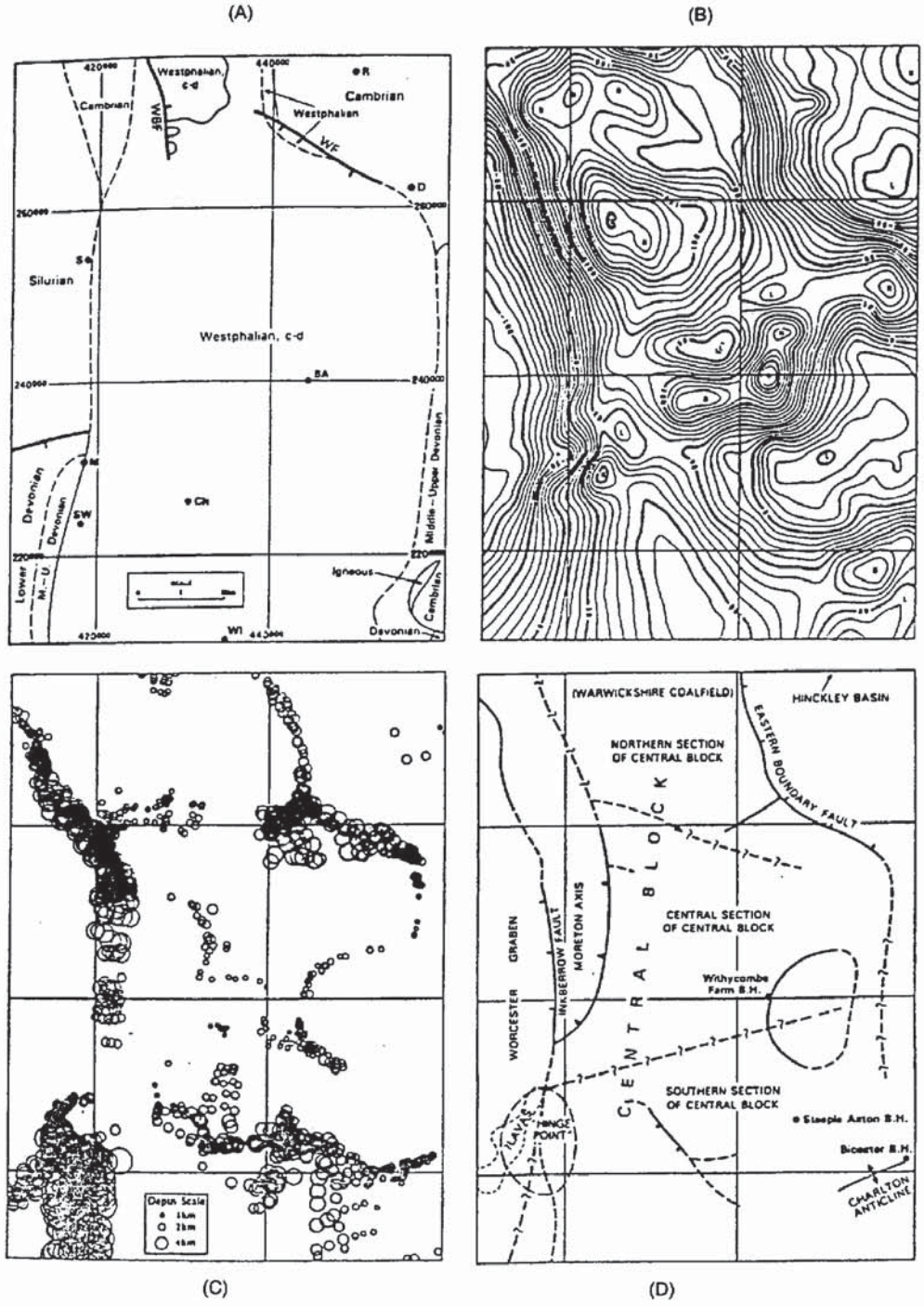

Figure 3.50 (A) Simplified geological map of the south-central part of England. (B) Aeromagnetic map of the area shown in (A). (C) Euler solutions derived from the aeromagnetic data calculated for a structural index of 1. (D) structural interpretation of the Euler solutions. From Reid *et al.* (1990), by permission

Euler solutions and this may be due to overlapping anomalies making Euler solutions statistically unacceptable and so have been rejected. Alternatively, there are insufficient data to represent the area adequately. In the south-west corner, there is a strong cluster of solutions with large depth values. This has been interpreted as being due to a magnetic body intruded at a depth of about 10 km. The main benefit of using the Euler method appears to be the delimitation of lineaments due to faults or major linear intrusions, and these features are best imaged by the Euler solutions if they are dipping, rather than vertical. The technique offers a method of independent interpretation which can be used to appraise existing geological models.

Euler's method has been incorporated into commercially available software (GRIDEPTH [Registered trademark of the Simon–Robertson Group plc] Geosoft Ltd) and has been demonstrated to be applicable to the location of near-surface utilities (pipes, drums, etc.) in addition to regional structural features. Examples of the use of the method in locating buried man-made targets have been given by Yaghoobian *et al.* (1992). They have described a detailed magnetic survey carried out at the Columbia Test Site, University of Waterloo, Canada, and corresponding Euler analysis. The results are shown in Figure 3.51. This example is perhaps too contrived to demonstrate the effectiveness in a real situation with a typical amount of background noise, but it does serve to show that the method works. Where there is a significant background noise problem, accurate depths and/or locations may be hard to achieve, especially if the measured data yield only weak signals. With careful analysis and selection of processing parameters (especially the Structural Index and GRIDEPTH window size) best-possible solutions may be obtained. It is also important that the field data be of as high quality as can be achieved and that appropriate filtering to remove obvious noise is undertaken before Euler analysis.

In addition to Euler analysis, increasing attention is being paid to the use of three-dimensional analytic signals (Nabighian 1984; Roest *et al.* 1992; MacLeod *et al.* 1993). The general principle behind the method is illustrated schematically in Figure 3.52. Given a magnetic anomaly (in the case illustrated, this arises from a square prism magnetised in an arbitrary direction), the three derivatives can be obtained from which the analytic signal is derived (Box 3.11). The amplitude of the three-dimensional analytic signal of the total magnetic field produces maxima over magnetic sources irrespective of their magnetisation direction (MacLeod *et al.* 1993; Parlowski *et al.* 1995). The three-dimensional analytic signal can be calculated readily from an accurately gridded dataset. A 3×3 filter can be applied to obtain the horizontal gradients ($\delta T/\delta x$ and $\delta T/\delta y$). A fast Fourier transform (FFT) can be used to obtain the vertical gradient ($\delta T/\delta z$). Alternatively, if a gradiometer has been used to acquire the data, the vertical gradient is a measured parameter.

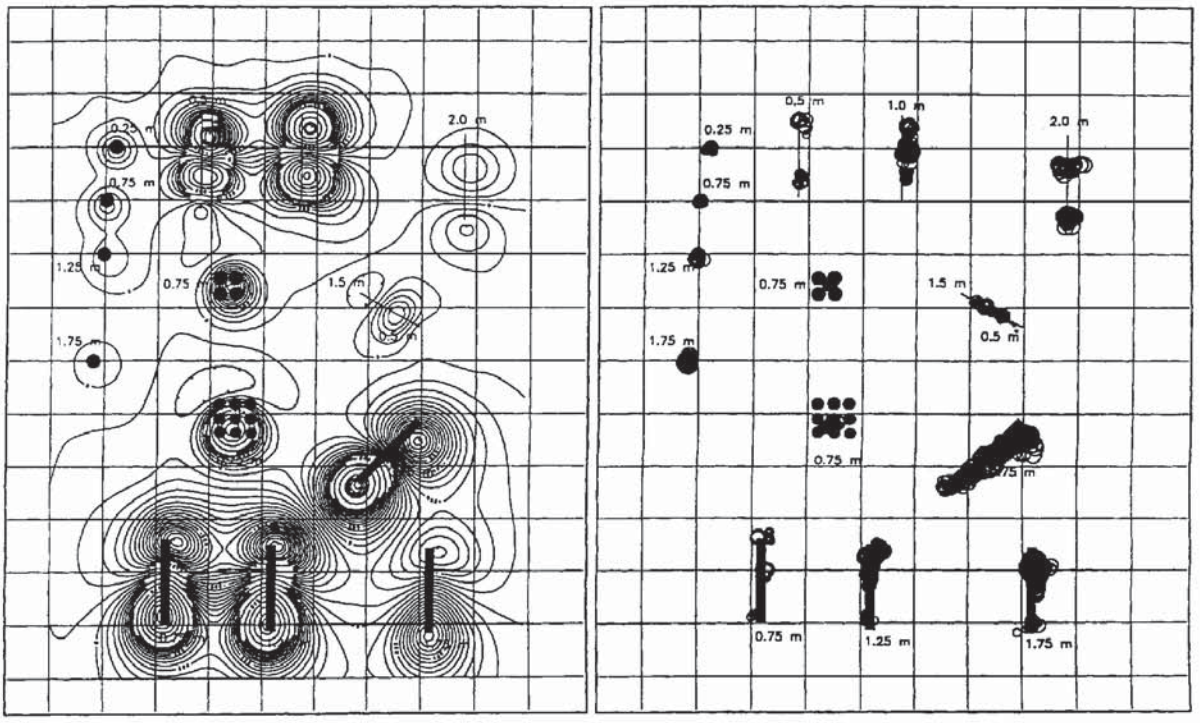

Figure 3.51 (A) Total magnetic field anomaly map over the Columbia Test Site, University of Waterloo, Canada, with the known depths to the various targets listed. (B) The Euler solutions calculated from (A). From Yaghoobian *et al.* (1992), by permission

From the form of the resultant analytic signal, solutions are obtained as to the location (x, y, z) of the source. These are shown graphically as circles, much the same as from Euler solutions. The distance between the inflection points of the analytic signal anomaly is directly proportional to the depth to the top of the magnetic source. It has been demonstrated that both Euler and analytic solutions can be used to produce an integrated model of the causative magnetised structure: the analytic signal can be used to delineate the magnetic contrasts and give estimates of their approximate depths, while the Euler solution yields more detailed interpretation at depth (Roest *et al.* 1992; Parlowski *et al.* 1995). It should be noted that the use of analytic signals can also be applied to gravity data or a combination of potential-field data.

Box 3.11 The amplitude of the three-dimensional analytic signal (MacLeod et al. 1993)

The amplitude of the analytic signal ($|A(x, y)|$) at any location (x, y) is given by:

$$|A(x, y)| = [(\delta T/\delta x)^2 + (\delta T/\delta y)^2 + (\delta T/\delta z)^2]^{1/2}$$

where T is the measured field at (x, y).

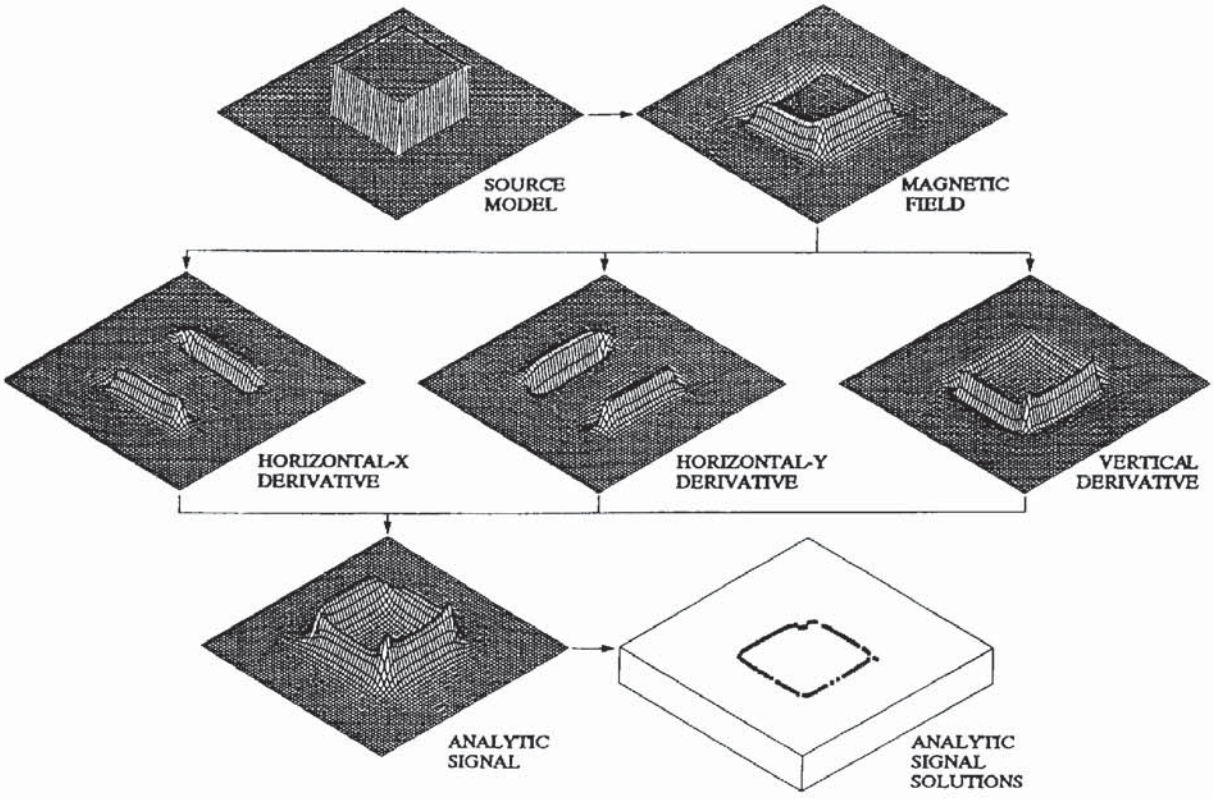

Figure 3.52 Schematic outline of the analytic signal method. Horizontal and vertical derivatives are calculated from the total field anomaly over a square prism and combined to yield the absolute value of the analytic signal. The locations of the maxima and the shape of this signal can be used to find body edges and corresponding depth estimates. From Roest *et al.* (1992), by permission

In shallow environmental applications, sources at very shallow depth (< 1 m) give rise to extremely high frequency signals which are difficult to resolve using these techniques. It is probably more cost-effective to dig with a shovel on the position of magnetic anomalies to locate the target source than to go through the analytic procedures outlined above. However, as soon as the depth is beyond easy excavatability, the value in the use of analytic solutions increases. Accuracies in depth determination are of the order of 30% of the target depth. This figure is one that may be improved upon in time with future developments and experience.

3.9 APPLICATIONS AND CASE HISTORIES

3.9.1 Regional aeromagnetic investigations

An aeromagnetic survey over the Lizard Peninsula in Cornwall, which was interpreted in conjunction with gravity data (Rollin 1986), provides an example of three-dimensional interpretation. The Lizard Complex comprises what is thought to be an ophiolite suite made up of a lower tectonic sheet of hornblende schists and metasediments and

structurally overlain by peridotite and gabbro. This upper sheet shows lateral variation from harzburgite peridotite, gabbro and a dyke complex in the east to therzolite peridotite and cumulate complex to the west. Comparison of the simplified geological map with the corresponding aeromagnetic map (Figure 3.53) demon-

Figure 3.53 (A) Simplified geological map of the Lizard Peninsula, south Cornwall, and (B) the corresponding aeromagnetic map. From Rollin (1986), by permission

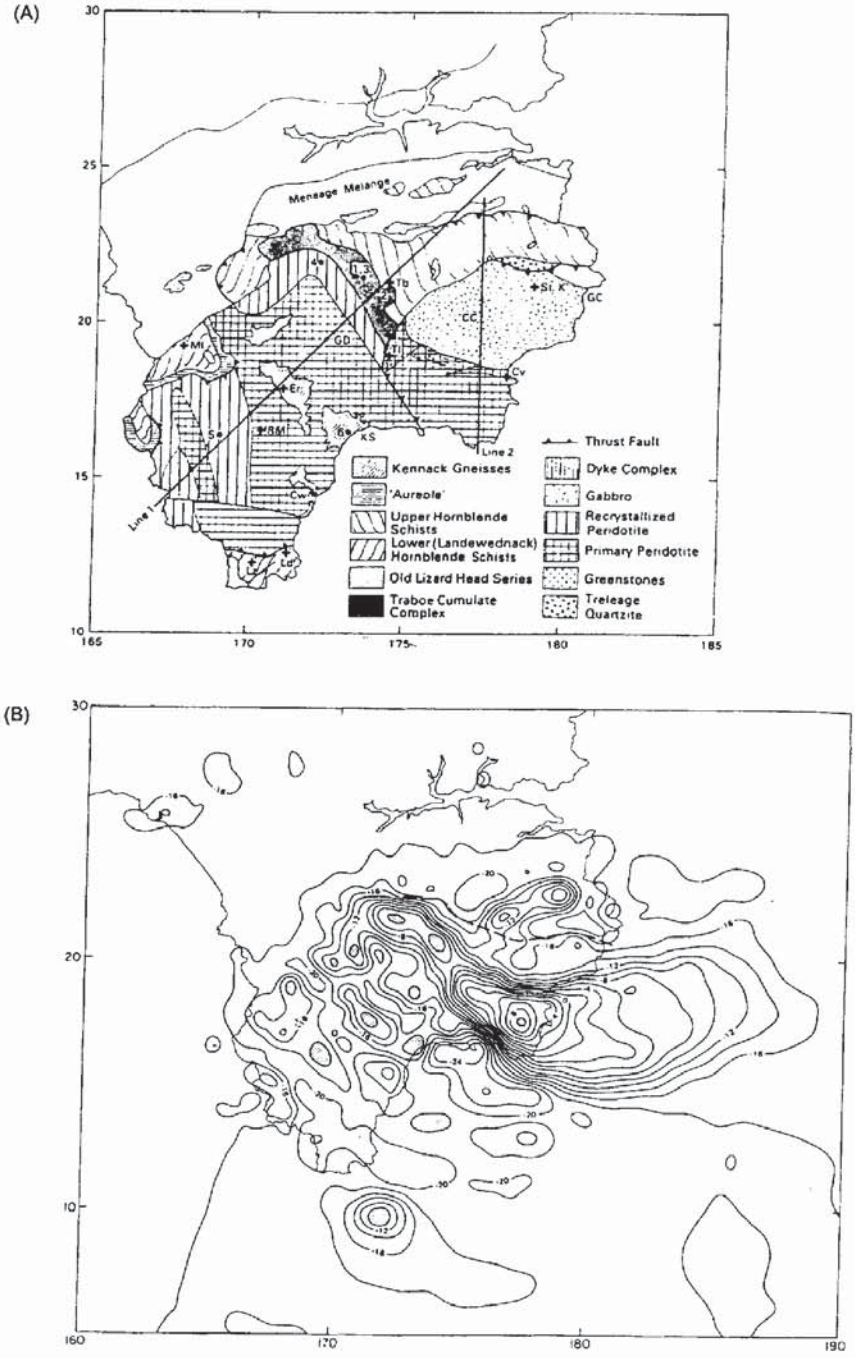

strates the correlation of the most prominent magnetic feature, a magnetic high which extends offshore to the east, onshore across the harzburgite peridotite south of Coverack north-westwards with diminishing amplitude over the Traboe Cumulate Complex. Western Lizard is characterised by small localised anomalies over the western peridotite. These features correlate with small outcrops of interlayered basic gneiss. A summary of the tectonic units and their respective schematic geophysical responses are shown in Figure 3.54. From this it can be seen that the lherzolite peridotite has a much smaller magnetic effect than the harzburgite peridotite while they both have comparable effects on the gravity field. It was found that the harzburgite peridotite was depleted particularly in TiO_2 compared with the lherzolite peridotite. Low concentrations of titanium in these rocks are indicative of complex geochemical processes which affected the formation of magnetite during serpentinisation.

When modelling these aeromagnetic anomalies, Rollin found that it was necessary to investigate the remanent magnetisation which is

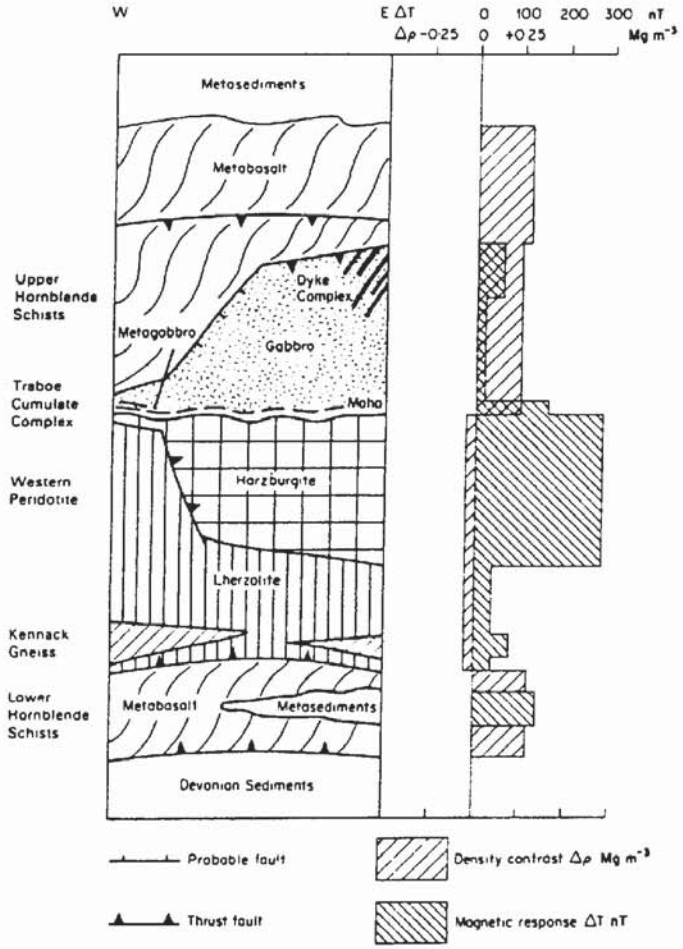

Figure 3.54 Tectonics units of the Lizard and a schematic representation of their geophysical responses. From Rollin (1986), by permission

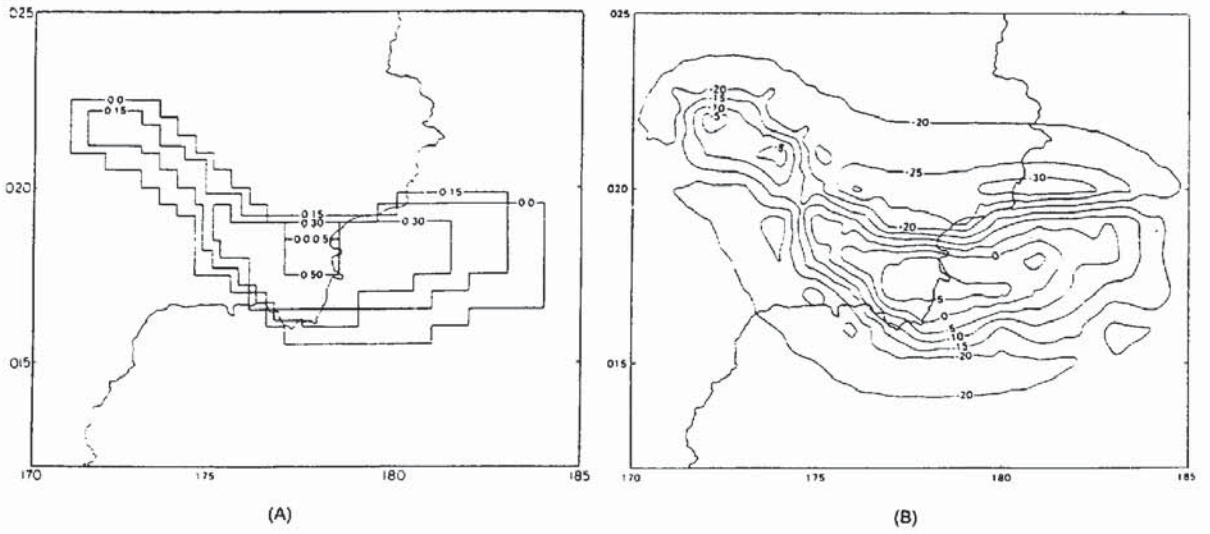

significant, as might be expected for such a suite of rocks. On the basis of field and laboratory measurements, the overall Königsberger ratio (remanent:induced magnetisation) was taken to be 0.43 with a declination and inclination of the remanent magnetisation of 286° and 75° respectively, with a resultant magnetisation up to 220 nT and a mean susceptibility of 0.0774 (SI). A simple three-dimensional model comprising stacked horizontal polygons was then constructed for the eastern area, which produced a calculated anomaly (Figure 3.55)

Figure 3.55 Three-dimensional modelling of the south-east part of the Lizard. (A) Stacked horizontal polygons, and (B) the resulting calculated magnetic anomaly. From Rollin (1986), by permission

Figure 3.56 Aeromagnetic and gravity anomaly profiles along Line 2 (Figure 3.53A) across the south-eastern part of the Lizard. From Rollin (1986), by permission

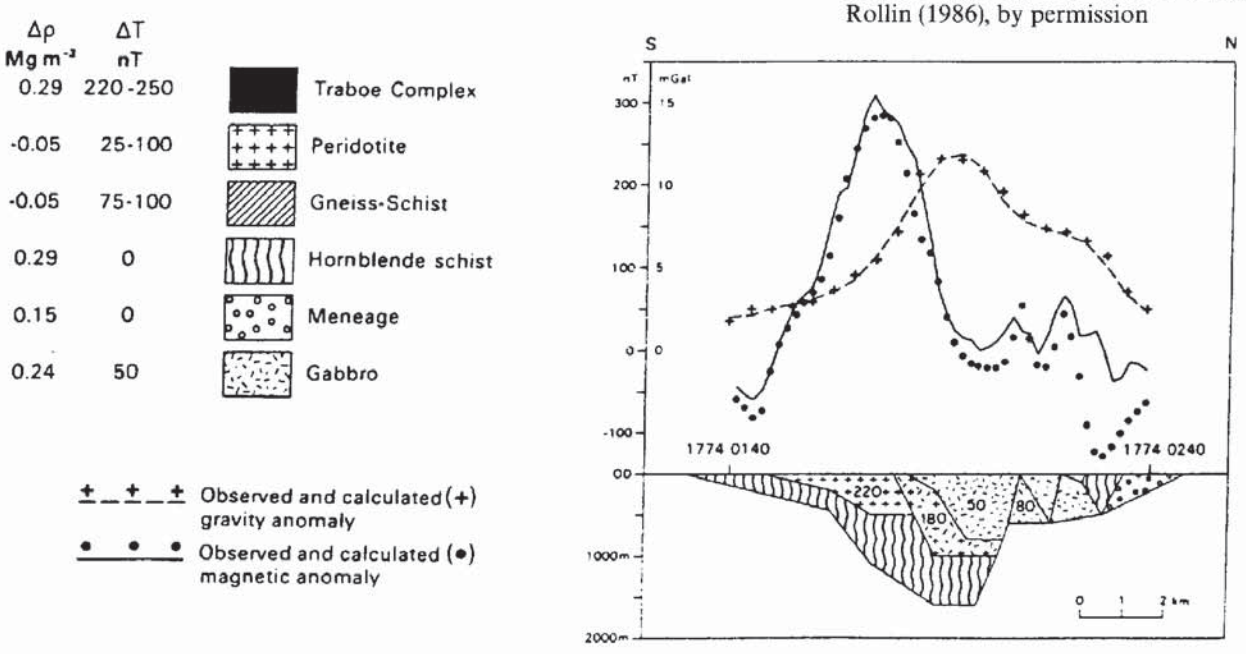

comparable to the observed aeromagnetic anomaly. The magnetic interpretation indicated that the Traboe Complex has a thickness of only 150 m while the eastern harzburgite peridotite is about 500 m thick (Figure 3.56). Independent gravity modelling gave the thickness of the eastern peridotite as 560 m, which is in reasonable accord with the magnetic interpretation.

3.9.2 Mineral exploration

In Finland, in regions of Pre-Cambrian basement comprising black graphite-schists, the location of sulphide ores is becoming increasingly difficult. The easy-to-find ores have already been identified. The more difficult ones, such as pyrrhotite-rich black schists and associated mineralisation, have been more easily eroded by glacial ice than the surrounding rocks and have become buried beneath a veneer of overburden, commonly up to 30 m thick. The overburden is characterised by high resistivities so the relatively conductive ore zones can be located using electrical methods. However, this is not always practicable so magnetic methods have also been used in conjunction with geochemical surveys. Furthermore, it is difficult to discriminate between the geophysical anomalies produced by economic sulphide mineralisation and those caused by the black schists and other rocks. Consequently, the identification of copper ores is particularly difficult.

The Saramäki orebody, located about 370 km north-east of Helsinki, forms a compact copper mass with some cobalt, and occurs in geological complexes comprising serpentinites, dolomites, skarns, quartzites and black schists, in a country rock of mica schist. The exploration strategy has been discussed in detail by Ketola (1979). The whole mineralised complex can be traced using aerogeophysical methods for over 240 km. The specific orebody, which was located in 1910 by drilling, is 4 km long, 200–400 m wide and extends down to about 150 m. Average copper content is 3.8% with 0.2% cobalt.

Problems with identification of the orebody can be seen by reference to Figure 3.57. The electrical resistivity (SLINGRAM) anomalies are caused by the black schists. The whole skarn zone forms a denser block (0.23 Mg/m^3 higher) compared with the country rock and so the sub-units within the mineralised zone cannot be differentiated using gravity. Susceptibility measurements made using the boreholes suggested that the mineralised zone was magnetised heterogeneously and that its upper part influenced the magnetic anomaly. In addition it was found by two-dimensional modelling that the main magnetised zones had significant remanent magnetisation. If remanence is ignored, the dip of the two main zones is inconsistent with the known dips, derived from drilling, even though the computed anomaly fits the observed one very well (Figure 3.58A). By incorporating remanence, with inclination 45° and declination 90° (compared

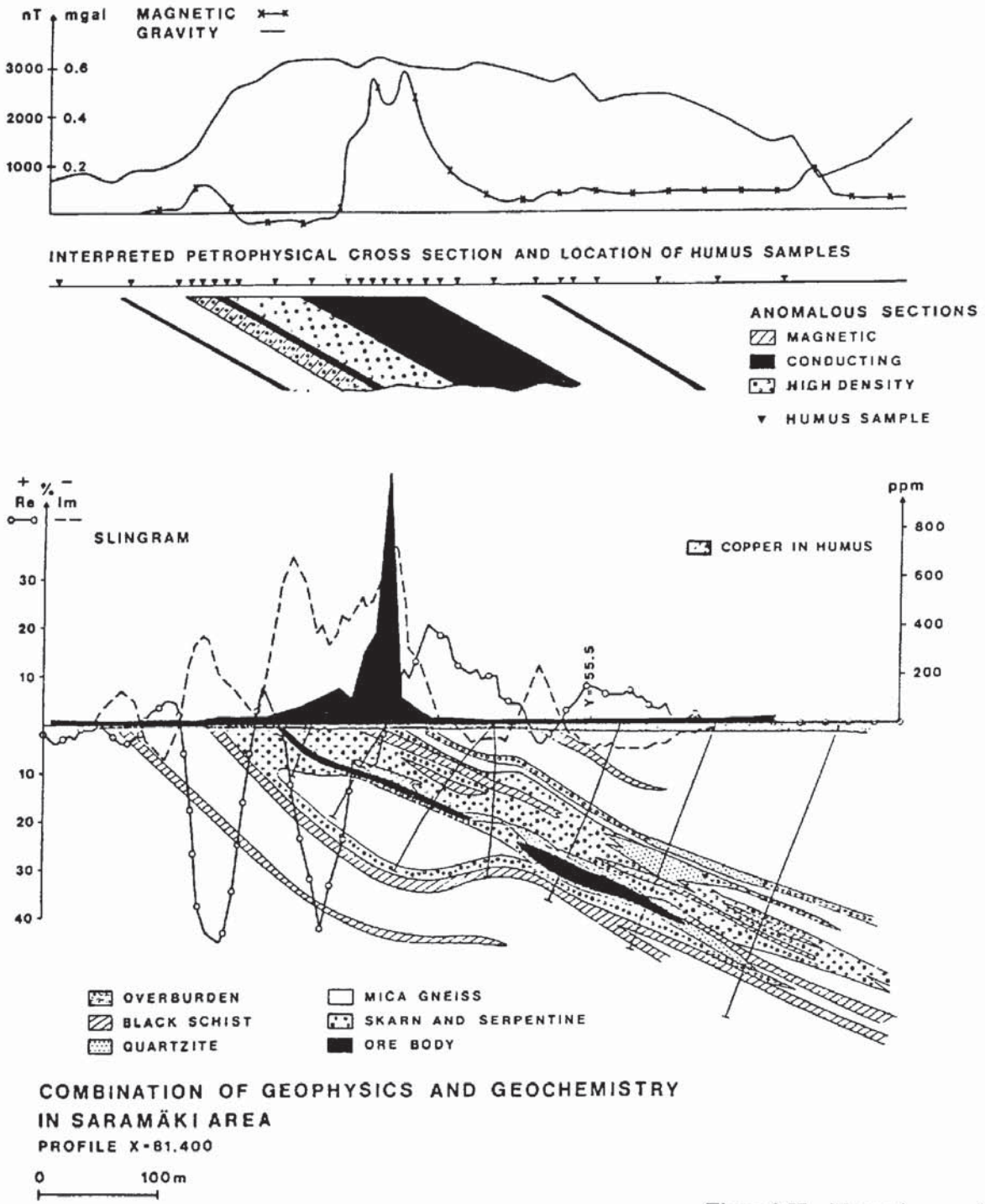

Figure 3.57 Magnetic, gravity and SLINGRAM electrical data with a geological cross-section for the Saramäki orebody, Finland. From Ketola (1979), by permission

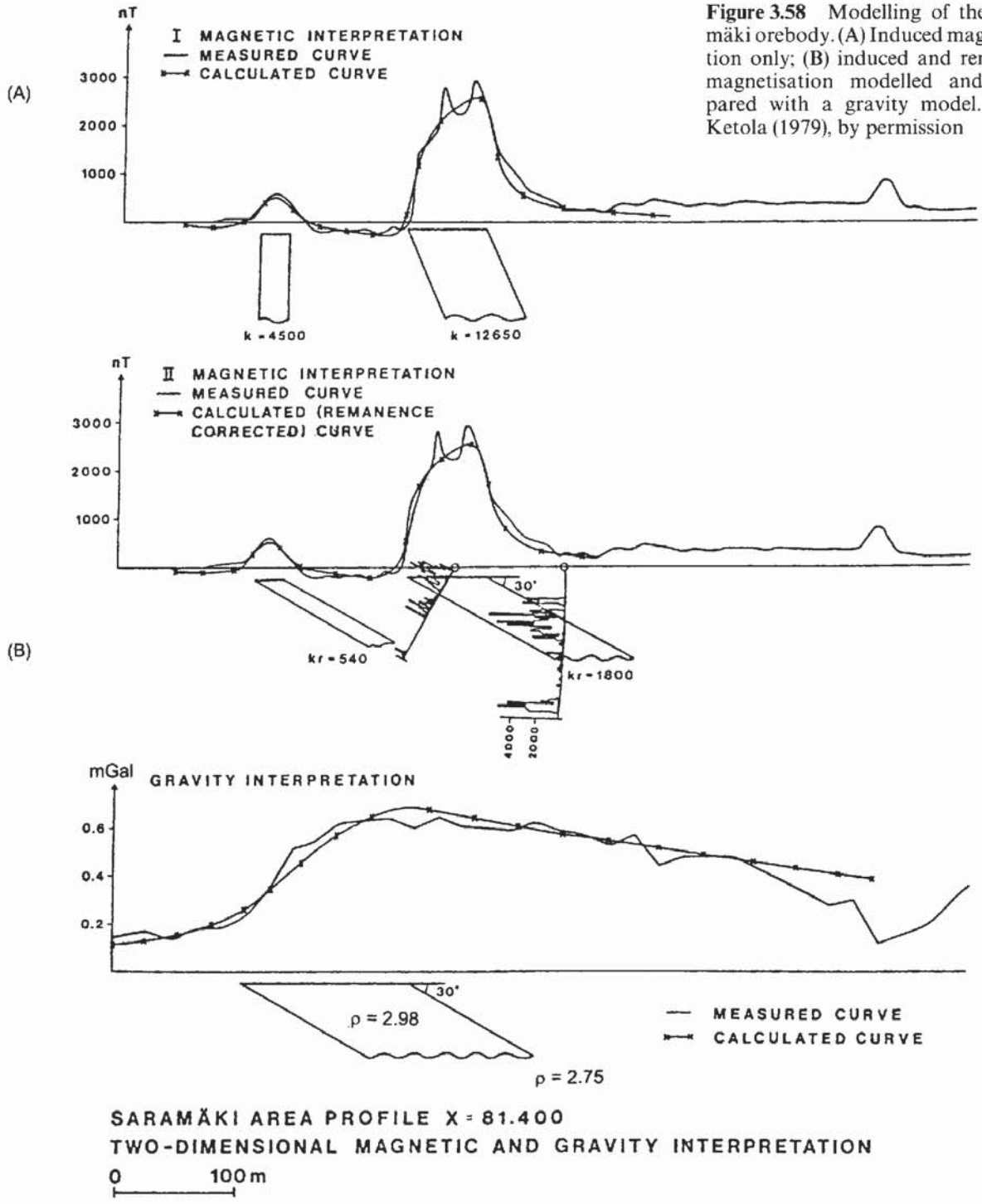

Figure 3.58 Modelling of the Saramäki orebody. (A) Induced magnetisation only; (B) induced and remanent magnetisation modelled and compared with a gravity model. From Ketola (1979), by permission

with 75° and 7°, respectively for the Earth's field), geologically compatible models were then produced which were also in accord with those used in the gravity modelling (Figure 3.58B).

Ketola concluded from this and other similar examples in Finland that geophysical or geochemical methods alone were insufficient to resolve these complex orebodies. It was necessary to use a wide variety of geophysical and geochemical techniques together, in conjunction with drilling, to provide a successful differentiation of the sub-surface geology.

Other illustrations of magnetic anomalies over mineralised bodies have been shown in Figure 1.9D, for a lode at Wheel Fanny, north-west Devon, where the course of the lode is picked out clearly by the linear magnetic anomalies. Figure 3.32 illustrates a ground magnetometer profile over sulphide mineralisation at Sourton Tors, north-west Dartmoor, Devon.

3.9.3 Engineering applications

3.9.3.1 Detection of underground pipes

Sowerbutts (1988) has provided a clear example of how high-resolution magnetic gradient surveys can identify not only the location of underground metal pipes but also the position of joints between individual sections of pipe. If joints can be located remotely, the amount of excavation required to examine and repair a pipe can be minimised, saving time, money and inconvenience.

The magnetic anomaly along a pipe consists of a series of smaller anomalies each of which corresponds to an individually cast segment of pipe which behaves like a magnetic dipole. For a pipe buried close to the surface and away from extraneous magnetic sources, a clear repetition of anomalies can be identified (Figure 3.59A). In the case illustrated, the pipe had a diameter of 0.5 m and was made of ductile iron in 6.3 m long sections and buried at a depth of 0.5 m. Magnetic highs, with gradients up to 4000 nT/m, are centred between 0.5 m and 1.0 m along from the socket end. For a pipe orientated east–west, a typical negative (north) and positive (south) anomaly doublet is produced along a profile aligned north–south in the northern hemisphere (cf. Figure 3.37A). A magnetised body orientated north–south produces a more symmetric positive-only or negative-only anomaly, and this is also seen in pipes orientated north–south (Figure 3.59B). For a smaller 76 mm diameter pipe (Figure 3.59C) this anomaly doublet effect is clearly repeated along the line of this north–south orientated pipe. In an urban environment, identifying the anomalies associated specifically with the buried pipe can be very difficult. Other magnetic materials are likely to be nearby and this can obscure or defocus the pipeline anomaly (Figure 3.59D). In the last case, the pipe was 0.15 m diameter and buried about 1.5 m down. Local metal grids

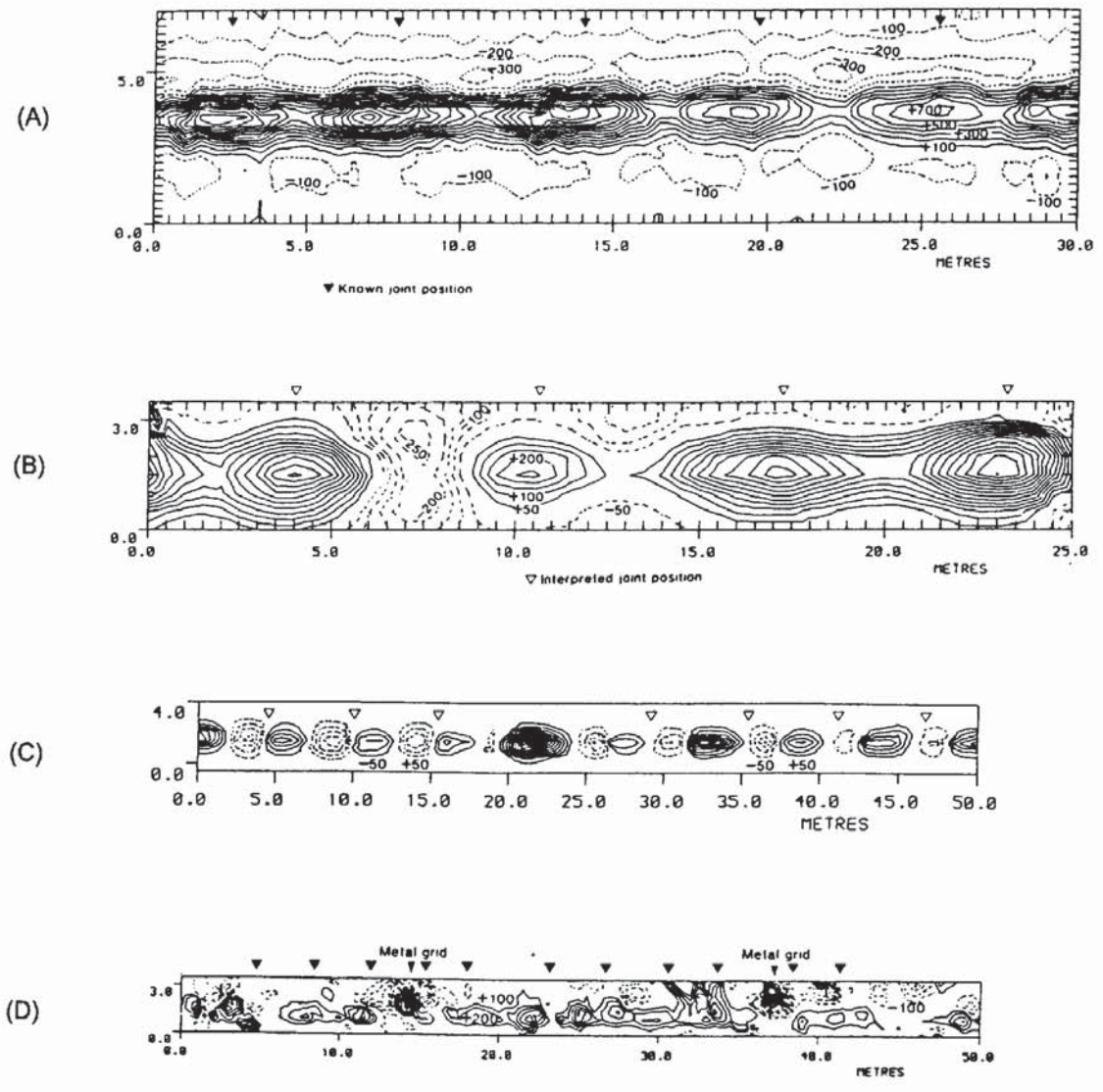

Figure 3.59 Magnetic gradiometer anomalies over buried pipelines: (A) Ductile iron pipe, diameter 0.5 m buried at 0.5 m depth, E–W trend of pipe; contour interval 200 nT/m. (B) Cast iron pipe, N–S trend of pipe; contour interval 50 nT/m. (C) 76 mm diameter cast iron gas pipe trending N–S. (D) 0.15 m diameter pipe, buried about 1.5 m down, in an urban environment with extraneous magnetic anomalies caused by adjacent metal grids. From Sowerbutts (1988), by permission

produce large magnetic anomalies. The anomaly pattern associated with this pipe is now irregular and complex, and it is not possible to identify pipe joints. Even seamless steel pipes with welded joints can be identified in areas with a quiet magnetic background.

A further example of the use of magnetometry to locate near-surface pipes has been given by Geometrics Inc., who acquired data over a test site at Stanford University, USA, using a caesium magnetometer. The data were contoured and displayed as both a map and an isometric projection which are shown with a map of the utilities in Figure 3.60. The correlation between buried objects and the corresponding magnetic anomalies is obvious.

(A)

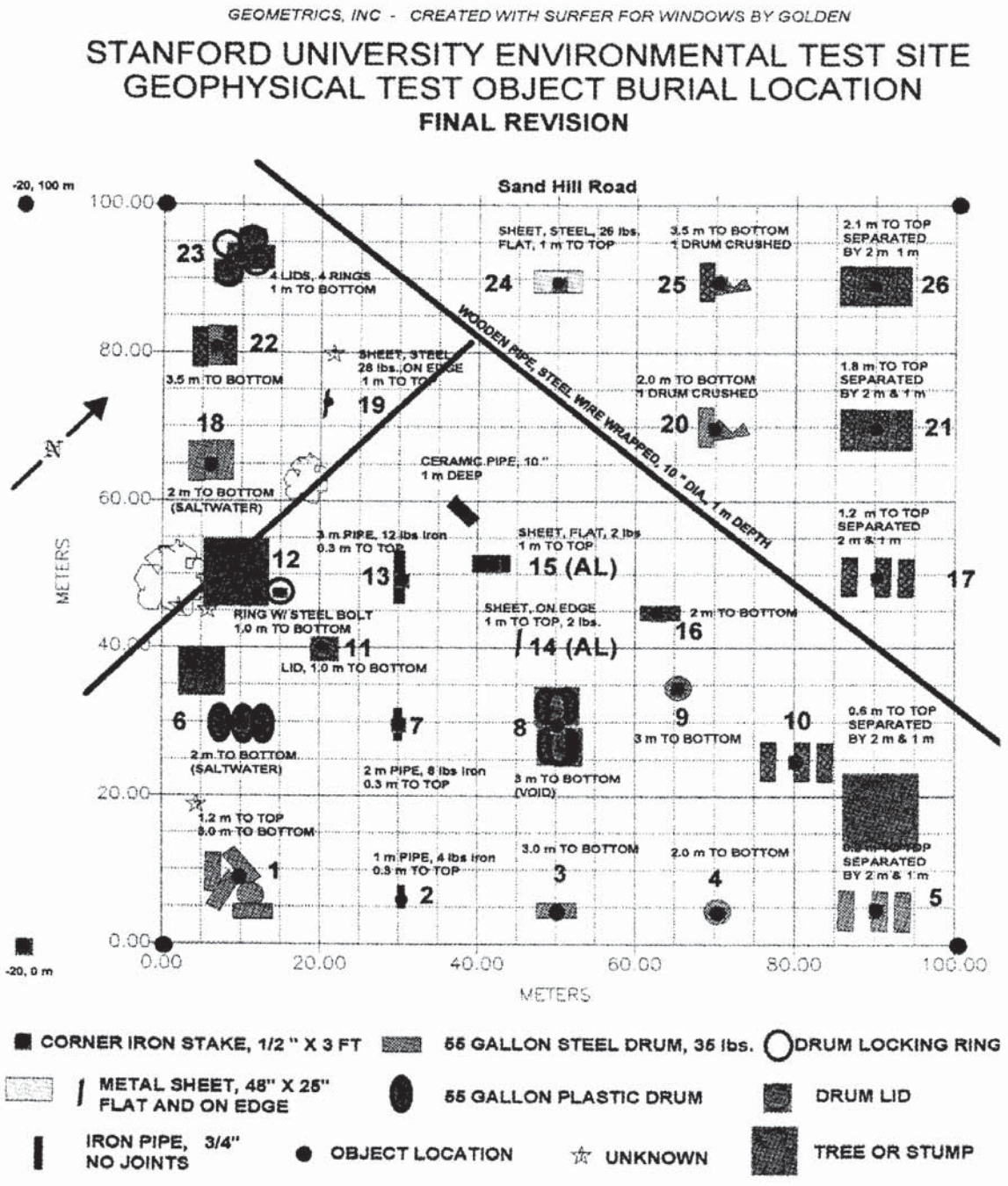
GEOMETRICS, INC - CREATED WITH SURFER FOR WINDOWS BY GOLDEN
STANFORD UNIVERSITY ENVIRONMENTAL TEST SITE
GEOPHYSICAL TEST OBJECT BURIAL LOCATION
FINAL REVISION
Sand Hill Road
WOODEN PIPE, STEEL WIRE WRAPPED, 10" DIA, 1 m DEPTH
-20, 100 m
-20, 0 m
100.00
80.00
60.00
40.00
20.00
0.00
0.00
20.00
40.00
60.00
80.00
100.00
METERS
METERS
23
4 LIDS, 4 RINGS
1 m TO BOTTOM
24
SHEET, STEEL, 26 lbs.
FLAT, 1 m TO TOP
25
3.5 m TO BOTTOM
1 DRUM CRUSHED
26
2.1 m TO TOP
SEPARATED
BY 2 m 1 m
22
3.5 m TO BOTTOM
SHEET, STEEL
26 lbs., ON EDGE
1 m TO TOP
19
18
2 m TO BOTTOM
(SALTWATER)
CERAMIC PIPE, 10"
1 m DEEP
20
2.0 m TO BOTTOM
1 DRUM CRUSHED
21
1.8 m TO TOP
SEPARATED
BY 2 m & 1 m
12
3 m PIPE, 12 lbs iron
0.3 m TO TOP
13
SHEET, FLAT, 2 lbs
1 m TO TOP
15 (AL)
17
1.2 m TO TOP
SEPARATED
2 m & 1 m
RING W/ STEEL BOLT
1.0 m TO BOTTOM
SHEET, ON EDGE
1 m TO TOP, 2 lbs.
14 (AL)
16
2 m TO BOTTOM
11
LID, 1.0 m TO BOTTOM
6
2 m TO BOTTOM
(SALTWATER)
7
2 m PIPE, 8 lbs iron
0.3 m TO TOP
8
5 m TO BOTTOM
(VOID)
9
3 m TO BOTTOM
10
0.6 m TO TOP
SEPARATED
BY 2 m & 1 m
1.2 m TO TOP
3.0 m TO BOTTOM
1
1 m PIPE, 4 lbs iron
0.3 m TO TOP
2
3.0 m TO BOTTOM
3
2.0 m TO BOTTOM
4
SEPARATED
BY 2 m & 1 m
5
CORNER IRON STAKE, 1/2 " X 3 FT
55 GALLON STEEL DRUM, 35 lbs.
DRUM LOCKING RING
METAL SHEET, 48" X 25"
FLAT AND ON EDGE
55 GALLON PLASTIC DRUM
DRUM LID
IRON PIPE, 3/4"
NO JOINTS
OBJECT LOCATION
UNKNOWN
TREE OR STUMP
SALTWATER IS 2.5 lbs. ROCKSALT PER 55 GALLONS WATER - OBJECT SIZES NOT TO SCALE

(B)

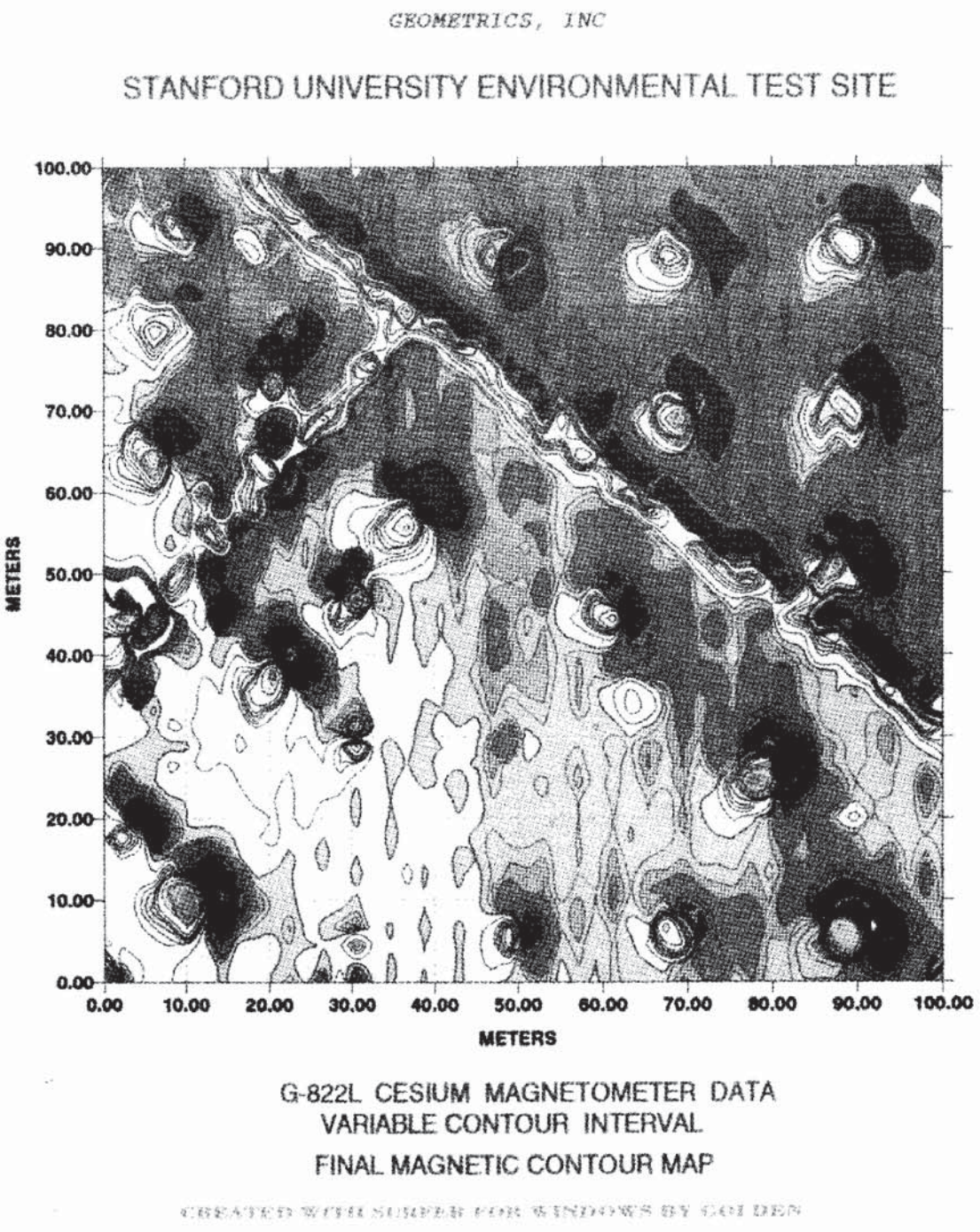
GEOMETRICS, INC
STANFORD UNIVERSITY ENVIRONMENTAL TEST SITE
100.00
90.00
80.00
70.00
60.00
50.00
40.00
30.00
20.00
10.00
0.00
METERS
0.00
10.00
20.00
30.00
40.00
50.00
60.00
70.00
80.00
90.00
100.00
METERS
G-822L CESIUM MAGNETOMETER DATA
VARIABLE CONTOUR INTERVAL
FINAL MAGNETIC CONTOUR MAP

(C)

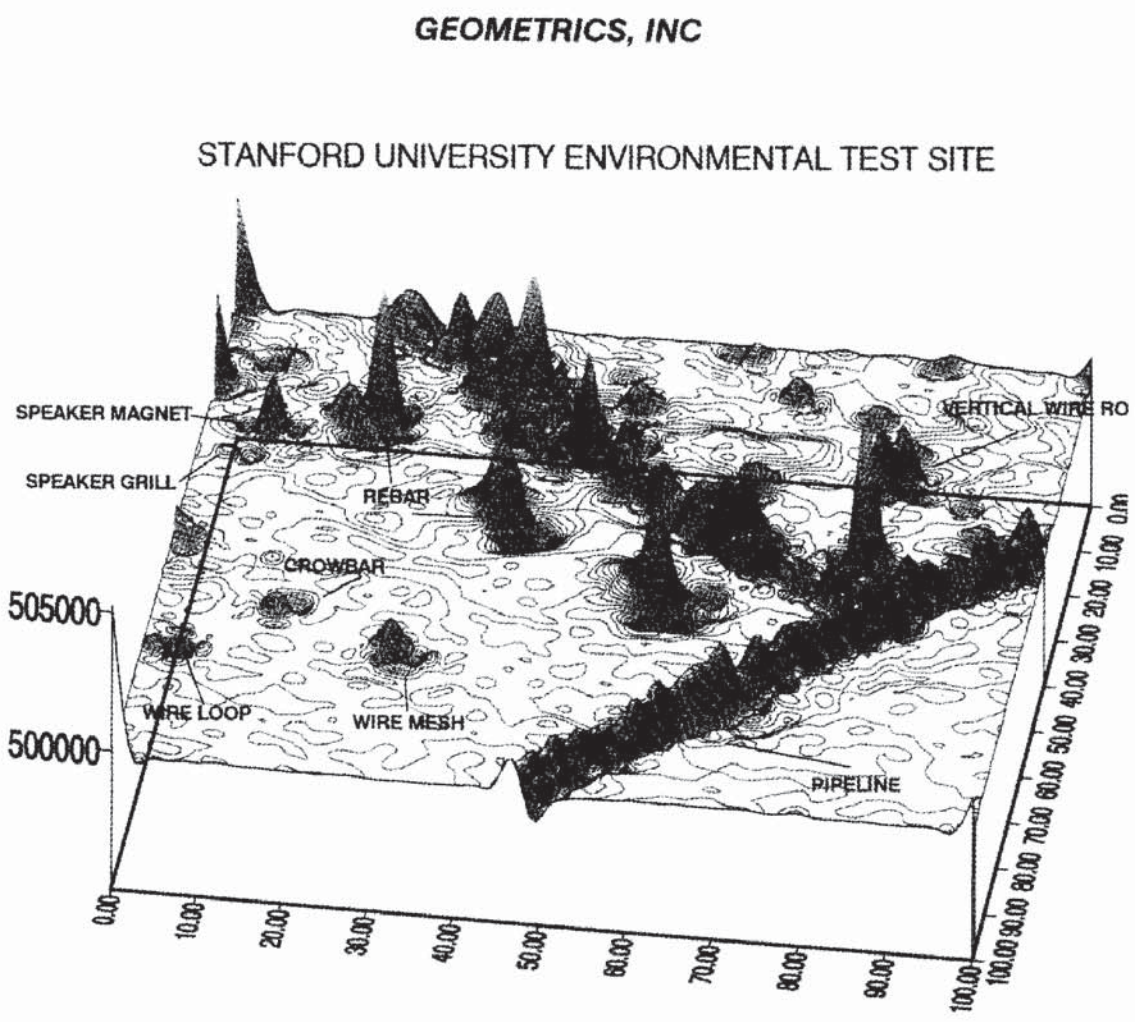
GEOMETRICS, INC
STANFORD UNIVERSITY ENVIRONMENTAL TEST SITE
SPEAKER MAGNET
SPEAKER GRILL
REBAR
CROWBAR
WIRE LOOP
WIRE MESH
PIPELINE
VERTICAL WIRE RO
505000
500000
0.00
10.00
20.00
30.00
40.00
50.00
60.00
70.00
80.00
90.00
100.00
0.0m
G-822L CESIUM MAGNETOMETER DATA
20 GAMMA CONTOUR INTERVAL
INTERSECTING PIPELINES
CREATED WITH WINSURF BY GOLDEN

Anomalies have been produced which have been characteristic of induced magnetisation in many cases, but what has not been considered is that pipes acquire a permanent magnetisation on cooling during manufacture. It may be necessary to examine the orientation of the pipes as they cool at their respective foundries (hence determine the inclination and declination of permanent magnetisation). Having ascertained the permanent magnetisation, and knowing where these pipes have been buried, it should then be possible to determine more accurately the magnetic anomaly due to each segment of pipe.

Figure 3.60 (*previous pages*) (A) Map of the Stanford University, USA, environmental test site showing the details of the various buried targets. (B) Magnetic anomaly map produced using a caesium magnetometer sampling at 10 readings per metre along survey lines at 2 m spacings. (C) Isometric projection of the data in (B). Courtesy of Geometrics Inc.

3.9.3.2 Detection of buried infill

In areas where clay infills hollows in bedrock such as chalk, the slight contrast in magnetic susceptibility can still be sufficient for magnetic survey methods to be useful.

In many engineering investigations, an arbitrary spacing or grid of boreholes is used that in all too many cases is inadequate to indicate the actual variation on ground conditions. To drill holes at small enough separations may be prohibitively expensive as well as being unnecessarily intrusive. In such cases, geophysical methods can be used to image the ground variability.

McDowell (1975) has provided an example of how magnetic mapping of magnetic anomalies with only 15 nT amplitudes provided a clearer picture of a clay with flints cover over chalk in Upper Enham, Hampshire. A magnetic anomaly map (Figure 3.61A) of the site shows the possible clay infill and clearly demonstrates that the inter-borehole separation was far too large to provide a representative impression of ground conditions. Should a contractor have started excavations on the basis of ground conditions predicted by the borehole data, a claim for compensation could have justifiably been made to recompense the additional work required to cope with the unexpected variations in ground conditions. The cost of the claim probably would have exceeded that of the geophysical survey in the first place! The magnetic profile across the clay pipe, which is orientated north–south, shows a form similar to that illustrated in Figure 3.41 but with opposite polarity, as the clay with flints has the slightly higher magnetic susceptibility than the chalk.

3.9.4 Detection of buried containers

There are many situations where it is imperative that potentially harmful objects, such as bombs or drums of toxic waste, be located passively. Drilling holes to locate drums of poisonous waste, or using electromagnetic signals to detect hidden bombs, could have devastating consequences. As both types of object will produce a magnetic anomaly, it is possible to use magnetic methods to locate them without risk. The amplitudes of magnetic anomalies detectable for

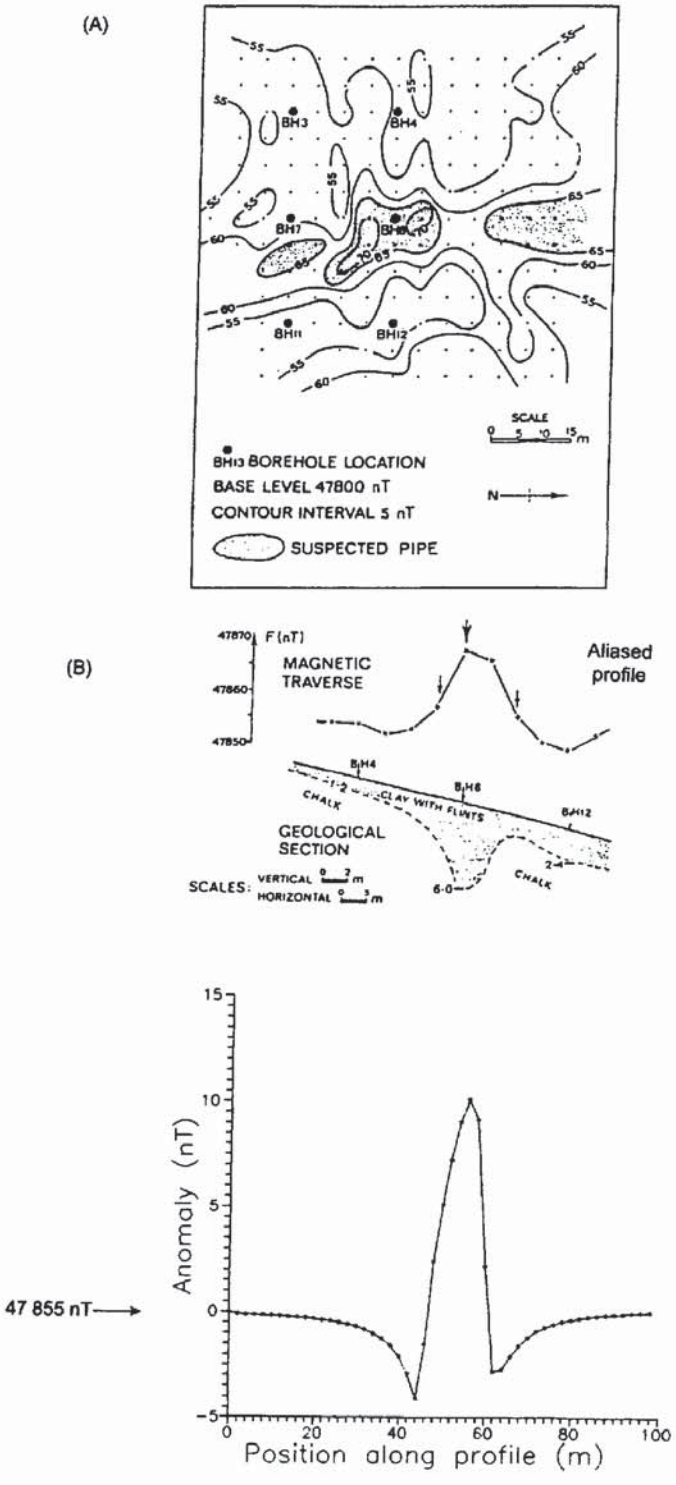

Figure 3.61 Megnetic anomalies over a clay-with-flints infill over chalk at Upper Enham, Hampshire, showing (A) how the magnetic survey resolved the variable ground conditions far better than the inadequately spaced boreholes, and (B) the shape of the profile across the clay pipe infill, which trends N–S, compared with a modelled anomaly (cf. Figure 3.41). (A) and (B) from McDowell (1975), by permission

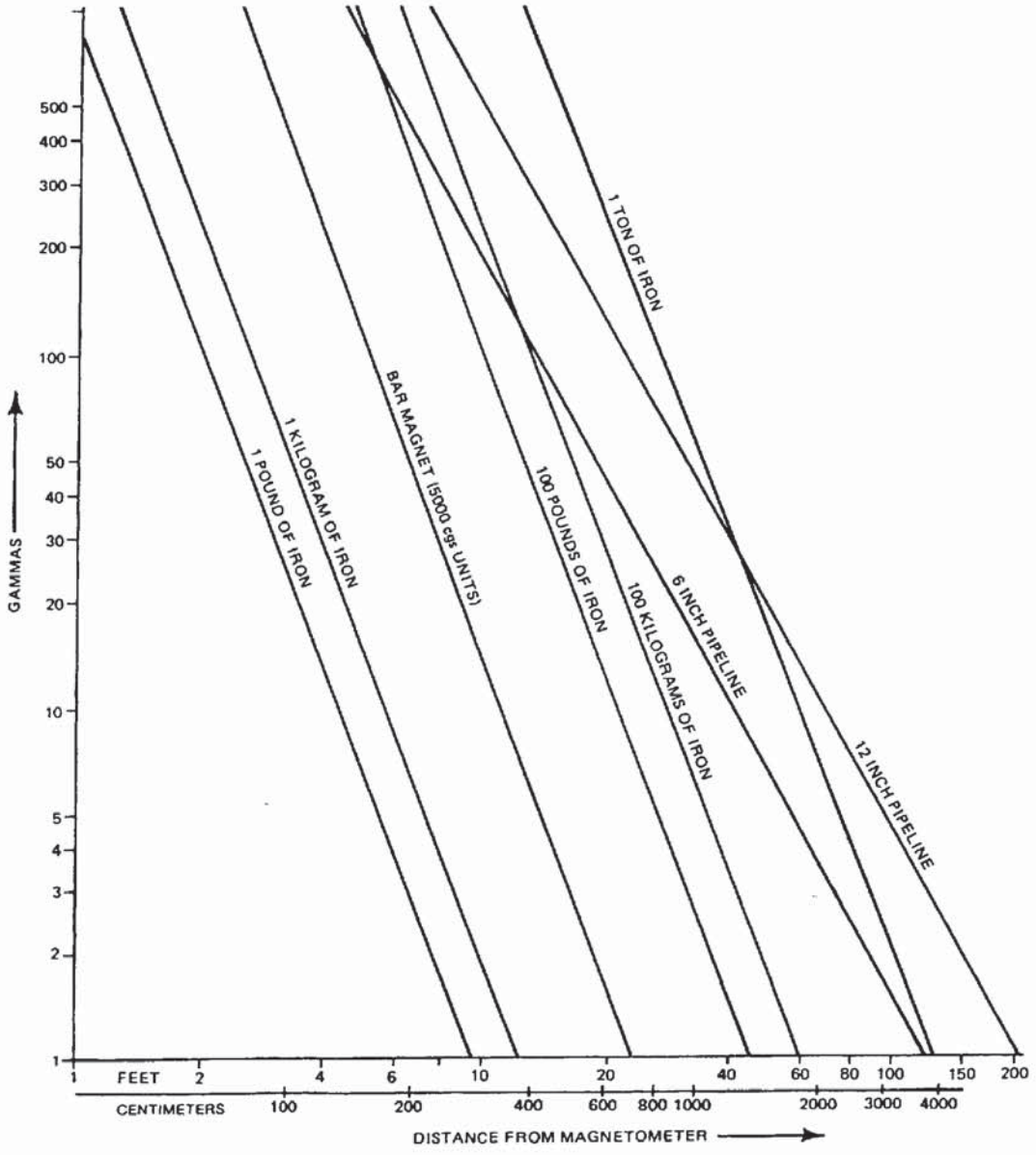

Figure 3.62 Minimum detectable anomaly amplitudes for different types of ordnance at various depths of burial. Note that the distances cited are those between the sensor and the target, not the depth below ground of the target. From Breiner (1981), by permission

various types of ordnance of different size and depth of burial are illustrated in Figure 3.62, assuming a maximum detectability of 0.1 nT. However, in practice, the smallest anomaly likely to be discernible above background noise is likely to be around 1 nT. This means that it would technically be possible to detect a 1000 lb bomb buried at a depth of 22 m.

Metal drums also give rise to strong magnetic anomalies and, if dumped together in a random way, will produce large-amplitude but highly variable anomalies that will stand out from background noise. An example of the kind of anomaly produced is shown in Figure 3.63.

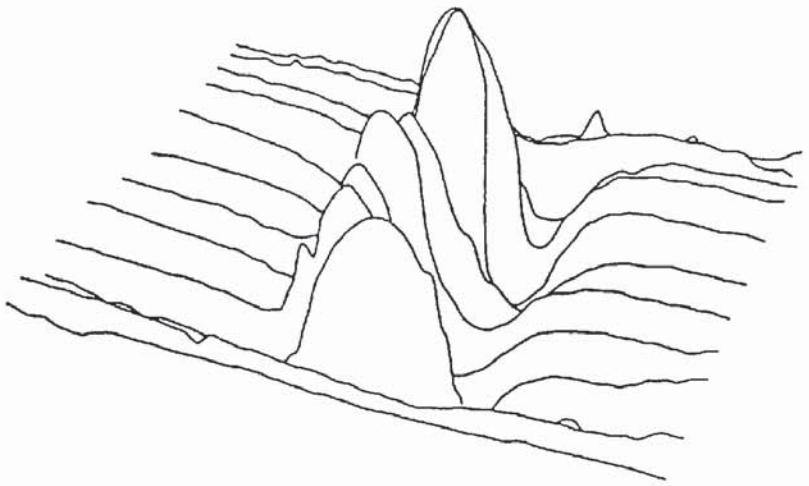

Figure 3.63 Magnetic anomaly over a trench containing metal drums of waste. From Evans (1982), by permission

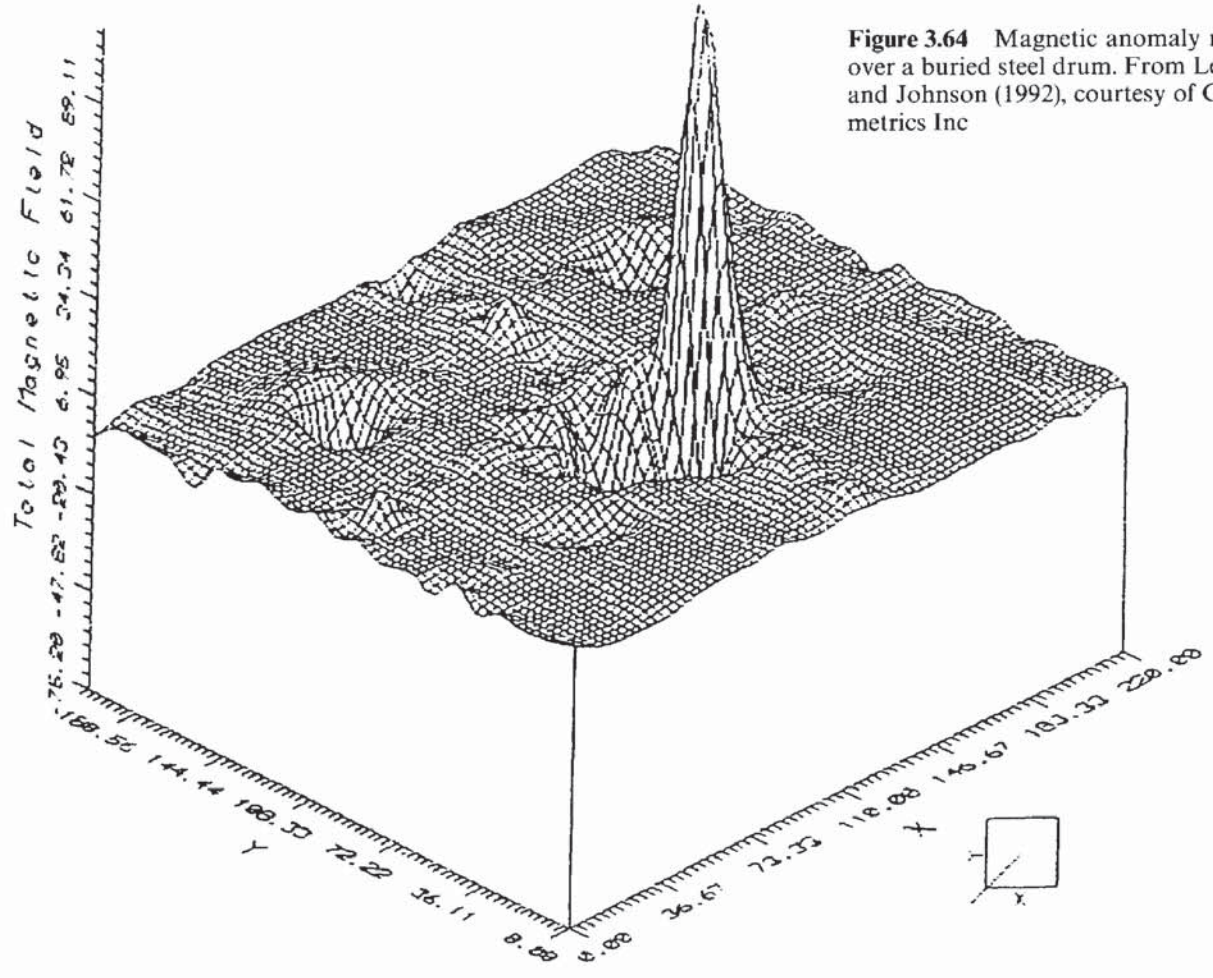

Figure 3.64 Magnetic anomaly map over a buried steel drum. From Leech and Johnson (1992), courtesy of Geometrics Inc

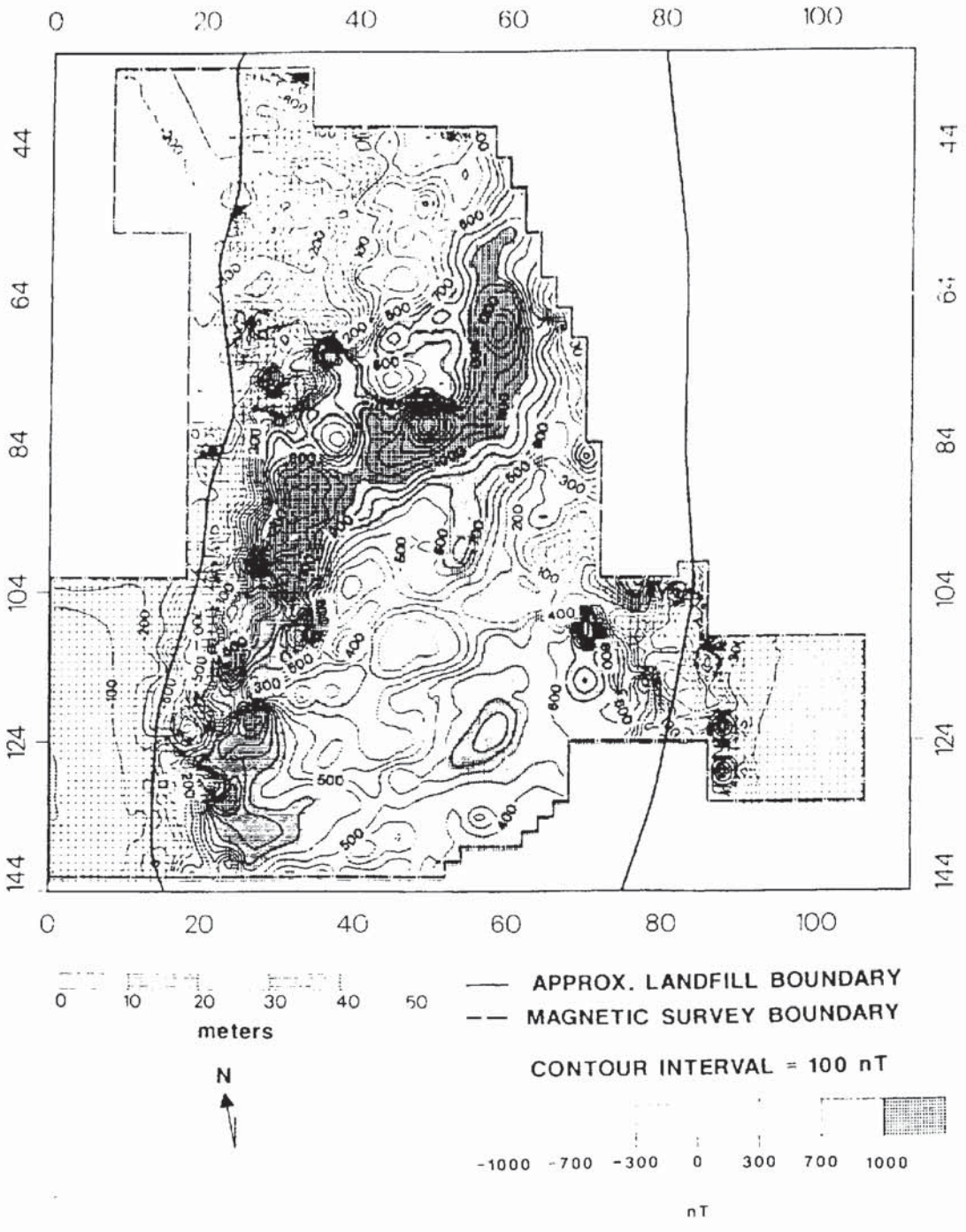

Figure 3.65 Contour map of total field magnetic intensity data measured at 1 m height, at the Thomas Farm landfill site, USA. From Roberts *et al.* (1990), by permission

To resolve the number of drums and their possible size, it may be preferable to use a gradiometer survey and datalogger so that the anomalies can be imaged with greater resolution. The magnetic anomaly over a buried steel drum is shown in Figure 3.64, from which it can be seen that local anomaly amplitudes are as high as several thousand nanoteslas, and field gradients several thousand nanoteslas per metre (Leech and Johnson 1992). The main difficulty with locating illegally buried drums of toxic waste is that they are usually dumped in ground with other rubbish which would help to mask their anomalies. However, by careful analysis of the anomaly shapes, amplitudes, orientations and overall characteristics, it should be possible to differentiate between various buried objects, if not actually identify them.

3.9.5 Landfill investigations

One of the aspects of landfills is that they are likely to contain large amounts of ferrometallic debris deposited at irregular angles. Consequently, a magnetic anomaly map produced over a former landfill will show a considerable amount of high-frequency noise from near-surface ferrometallic objects. There is perhaps a tendency to think that such noise is likely to dominate the magnetic anomaly map to produce a highly chaotic and largely unhelpful anomaly map.

One aspect of old closed landfills is that their previous tipping history may have been lost, or was never recorded. It might be useful to be able to obtain some idea as to whether a site has had different tipping sequences, such as periods of waste of a similar character being tipped and then having another type of waste with different magnetic properties. Consequently, the magnetic method lends itself to the rapid surveying of closed landfills in order to assess previous tipping histories and the zonation of waste types within a site.

An example of a magnetic survey over the Thomas Farm landfill in the USA has been given by Roberts *et al.* (1990). The site was surveyed on a 2×2 m grid with a sensor height at 1 m above the ground. Roberts and co-workers demonstrated that, by careful data processing, the high-frequency noise could be filtered out to reveal longer-wavelength anomalies more closely associated with broad types of waste. An example of one of their maps is given in Figure 3.65. In this case, the lateral extent of the landfill was already known. The magnetic anomaly map reveals several zones with quite distinctive magnetic anomaly characters. For example, note the band of strong magnetic anomalies (> 1000 nT) orientated NE–SW. To the south-east of this the magnetic anomalies are broader in wavelength and have low positive amplitudes, whereas those anomalies found north-west of this band are slightly higher frequency but predominantly negative. The actual wastes were domestic refuse in the north-west and brush, wood-cuttings and construction debris in the southern part.

Section 2
APPLIED SEISMOLOGY